

New insights into the evolution of portunoid swimming crabs (Portunoidea, Heterotremeta, Brachyura) and the brachyuran axial skeleton

Dennis Hazerli (✉ dennis-haz@web.de)

Universität Rostock Mathematisch-Naturwissenschaftliche Fakultät: Universität Rostock Mathematisch-Naturwissenschaftliche Fakultät
<https://orcid.org/0000-0001-5180-0559>

Christoph Gert Höpel

Universität Rostock Mathematisch-Naturwissenschaftliche Fakultät: Universität Rostock Mathematisch-Naturwissenschaftliche Fakultät

Stefan Richter

Universität Rostock Mathematisch-Naturwissenschaftliche Fakultät: Universität Rostock Mathematisch-Naturwissenschaftliche Fakultät

Research Article

Keywords:

Posted Date: April 28th, 2022

DOI: <https://doi.org/10.21203/rs.3.rs-1587578/v1>

License:   This work is licensed under a Creative Commons Attribution 4.0 International License. [Read Full License](#)

Abstract

Portunoidea (Heterotremata) represents a morphologically disparate taxon of true crabs (Brachyura), best-known for many of its representatives being considered as “swimming crabs”. This term, however, sometimes refers to a distinct taxon (traditionally to Portunidae within Portunoidea), but sometimes also to a certain morphotype, with the 5th pereopod (P5) having the shape of a specific swimming leg. We herein use the term “P5-swimming crab” or “P5-swimmer”, not only to restrict it to the morphotype, but also to distinguish it from other kinds of swimming in Brachyura. The evolution of P5-swimming crabs is still poorly investigated. For example, it is not known, whether the morphotype evolved several times independently in different lineages of Portunoidea or if it evolved only once and had been lost in several lineages.

We here present the first approach combining molecular with morphological data resulting in a new phylogenetic hypothesis of Portunoidea. For the first time, the latter involve data from the axial skeleton and extrinsic musculature. Morphological examinations revealed that axial skeleton and extrinsic musculature in P5-swimming crabs were more diverse than previously thought, except for the origin of the P5 anterior coxa muscle origin at the median plate, which was present in all P5-swimmers. Ancestral state reconstructions based on parsimony revealed that the stem species of Portunoidea already showed the morphotype of a P5-swimming crab, but with a long merus which probably resulted in a less effective P5-swimming ability compared to that of extant P5-swimming crab species with short merus. Several other extant taxa represent a reversal of the P5-swimmer morphotype with variable degree, with some extant species showing a complete reversal of unambiguous P5-swimming crab character states, like for example the common shore crab *Carcinus maenas*. Finally, a missing connection of interosternite 7/8 to the sella turcica (the secondary loss of the “brachyuran sella turcica”) in the stem species of Heterotremata, resulting in a junction plate forming a cavity that offered room and attachment sites for the P5 extrinsic musculature is uncovered as preadaptation to the P5-swimmer morphotype in Heterotremata, which is missing in “Podotremata” and Thoracotremata, the other two traditional main taxa of Brachyura.

1 Introduction

Brachyuran crabs of the taxon Portunoidea display a wide range of morphological disparity. It is well-known for its representatives showing a typical swimming crab morphotype, in which the 5th pereopod (P5) has the shape of a swimming leg, enabling these crabs to perform a special mode of swimming (see for example Kühl 1933, Schäfer 1954, Hartnoll 1971, Schmidt et al. 2020). This is what we call **P5-swimming** herein, since other modes of swimming are documented in crabs that show no swimming modifications of their pereopods or have different morphological modifications for swimming (Hartnoll 1971, Steudel, 1998). Accordingly, we here refer to the morphotype as **P5-swimming crab** (or **P5-swimmer**) **morphotype** while referring to its P5 as **swimming leg**. However, many portunoid taxa do not belong to this morphotype. For example, representatives of *Carcinus* and *Chaceon* are typical walker that lack any swimming ability, while others like *Thia* and *Portumnus* show morphological features considered to represent primarily adaptations to a burying mode of life (Garstang 1897a, b, Schäfer 1954, Hartnoll 1971, Bellwood 2001, Hazerli & Richter 2020). Representatives of portunid Thalamitinae are known to live in symbiotic relationships to other marine organisms, with some having the P5 modified for grasping (Stephenson & Rees 1968, Hay et al. 1989, Spiridonov 1999, Caulier et al. 2013, Evans 2018).

The morphology and evolution of portunoid crabs is still poorly examined. Hartnoll (1971) characterized the external features of the P5-swimming crab morphotype/ swimming leg based on statements by Herter (1932) regarding *Liocarcinus holsatus*. They include (1) a significantly shorter P5 merus than in a walking leg, (2) a P5 propodus and dactylus being much broader than in a walking leg and paddle-like, (3) a rotation of the P5 thoraco-coxal articulation axis of about 90° compared to a hypothetical ancestor (i. e. a subdorsal P5 coxa position) and (4) an increased range of motion in the P5 coxal-basi-ischial and meral-carpal articulations. According to Kühl (1933), it also includes (5) a carpal-propodal articulation axis that lies on the longitudinal propodus axis (instead of oblique to it like in a walking leg; see also Hazerli & Richter 2020). Schäfer (1954) emphasizes the meaning of (6) relatively long setae arranged in dense fringes along P5 podomere margins for P5-swimming. However, if a short merus really should be included to characterize a P5-swimmer is a matter of debate. Steudel (1998) found several portunoid genera to show all the typical P5-swimming crab features mentioned above except for a short merus. One of them – *Carupa* – was anecdotally reported to swim, but with no details on the swimming technique. It was concluded, that these genera are generally able to perform the same swimming movements as “real” P5-swimmers, but not as fast and effectively. Nevertheless, this hypothesis was never corroborated by behavioural observations or kinematic studies. As crucial for the swimming performance of a P5-swimming crab is considered the ability to bend the swimming leg in antero-dorsal direction over the carapax (Kühl 1933, Schäfer 1954, Hartnoll 1971, Steudel 1998, Schmidt et al. 2020).

As in other Brachyura, information concerning the inner anatomy is lacking in most taxa of Portunoidea. Here, features concerning the inner skeleton, which is formed by infoldings of the exoskeleton (Secretan 1980, 1998, 2002, Guinot et al. 2013, Davie et al. 2015a) are especially interesting, because in the P5-swimmer *Liocarcinus depurator* (which is morphologically very similar to *L. holsatus*) this endophragmal system shows significant differences to non-swimmers like *Cancer pagurus* and *C. maenas* (Hazerli & Richter 2020). These differences are associated with a particularly enlarged P5 extrinsic musculature in the P5-swimmers, together with altered muscular attachment sites. In general, it is a combination of these inner morphological traits, together with external features (particularly those of the swimming leg) that enable P5-swimming, which thus can be used to characterise the P5-swimming crab morphotype (Hazerli & Richter 2020). Schmidt et al. (2020) also found an increased range of motion in the thoraco-coxal articulation, which matches findings by Hazerli & Richter (2020) in which a larger thoraco-coxal arthrodival cavity is present in *L. depurator* compared to *C. maenas* and *C. pagurus*. However, the latter has to be confirmed in other P5-swimmers, together with features concerning the endophragmal system and extrinsic musculature. So, the first aim of this study is to examine, describe and 3D-visualize the axial skeleton (= endophragmal system + pleurum + sternum; for more information on the terminology used here, see Hazerli & Richter 2020) and P5 extrinsic musculature of various portunoid taxa (together with some

outgroup taxa), which will represent the most comprehensive work on these structures in Portunoidea. Consequently, this study will test if the traits (morphemes) found in *L. depurator* are also present in other P5-swimmers.

The main goal of the present study is to deduce the transformations of morphological character evolution in Portunoidea, testing whether the P5-swimmer morphotype evolved several times independently or if it appeared only once and was lost in some lineages. To answer this question, a robust phylogenetic hypothesis is necessary, which to date, has not been achieved. Previous phylogenetic analyses of Portunoidea are still controversially, at least in parts (Karasawa et al. 2008, Schubart & Reuschel 2009, Spiridonov et al. 2014, Evans 2018, Spiridonov 2020). In the present study, a new phylogenetic hypothesis is deduced by combing available gene sequences (with some new data of species in which to date, sequences were missing) with new morphological data of inner anatomy, together with newly conceptualized characters of external structures, which for the most part is based on Karasawa et al. (2008). Statements by Evans (2018) and Spiridonov (2020) is also considered in our character conceptualization. To understand the evolution of morphological traits, the ancestral states of characters are reconstructed based on parsimony (Swofford & Maddison 1996, Rieppel 1999, Schuh 2000).

2 Material & Methods

2.1 Taxon sampling, provision of voucher material

Several species of Portunoidea are chosen to represent the ingroup (Table 1). The taxon sampling represents the morphological disparity (especially with respect to the locomotive apparatus, which involve pereopods 2–5) in putative monophyletic groups within Portunoida, with typical P5-swimming crabs represented in each group. Based on the criteria mentioned by Herter (1932), Kühl (1933), Schäfer (1954) and Hartnol (1971), typical P5-swimmers are *Liocarcinus depurator*, "*Polybius*" *henslowii*, *Macropipus rugosus*, *Necora puber* and *Parathranites orientalis* (all six Carcinidae *sensu* Evans 2018), *Ovalipes ocellatus* (Geryonidae), *Callinectes sapidus* and *Portunus inaequalis* (both Portunidae). Outgroup taxa are *Sternodromia monodi* representing Dromiidae of Podotremata (which may be paraphyletic, see for example Luque et al. 2019), *Eriochier sinensis* and *Varuna litterata* as representatives of Thoracotremata, the putative sister taxon to Heterotremata, and *Medorippe lanata* (Dorippidae, Dorripoidea) as putative basal heterotreme species, (Jamieson & Tudge 1990, Guinot et al. 2013; Davie et al. 2015). Several other non-portunoid taxa of Heterotremata are also added to represent the outgroup, with *Cancer irroratus* and *Cancer pagurus* being chosen as representatives of Cancroidea, while *Corystes cassivelaunus* and *Telmessus cheiragonus* represent Corystoidea, both putative sister taxa to Portunoidea (Schubart & Reuschel 2009). *Ashtoret lunaris* (Matutidae) was added as having comprehensive morphological modifications for swimming and/or burying, but does not fit all the criteria by former authors for a P5-swimmer. *Calappa granulata* represents Calappidae, the potential sister taxon to Matutidae (both Calappoidea; Ng et al. 2008, Kim et al. 2019, Lu et al 2020). Altogether, representatives of 34 species were examined.

Table 1
Taxa used in this study, with their voucher codes, references and GenBank accession numbers.

Taxa examined for morphological characters	Voucher ID (morphological characters)	Taxa examined and combined as OTUs for the genetic data set	Voucher ID (genetic data set)	Reference	16S	CO1	NADH1	H3
<i>Ashtoret lunaris</i>	SMF 19731, ZSRO no ID	<i>Ashtoret lunaris</i>	unknown	Tan et al. 2014	LK391941	LK391941	LK391941	
		<i>Matuta planipes</i>	ZRC2009.0753	Tsang et al. 2014				KJ133142
<i>Bathynectes maravigna</i>	ZMH-K 34625 & 34205	<i>Bathynectes maravigna</i>	MNHN-B31441	Schubart & Reuschel 2009	FM208770		FM208770	FM208814
			JSDUKdeep_47	da Silva et al. 2011		JQ305964		
<i>Calappa granulata</i>	ZSRO 347	<i>Calappa granulata</i>	ZMS:6832	unpublished	KU206591			KU206702
			JSDAz218	da Silva et al. 2011		JQ306054		
		<i>Calappa bilineata</i>	unknown	Lu et al. 2020			MN562587	
<i>Callinectes sapidus</i>	ZMH-K 2217 & 2218	<i>Callinectes sapidus</i>	unknown	Place et al. 2005	AY363392	AY363392	AY363392	
			ULLZ3895	Schubart & Reuschel 2009				FM208798
<i>Cancer pagurus</i>	ZSRO no ID	<i>Cancer pagurus</i>	SMF-32764	Schubart & Reuschel 2009	FM207653		FM207653	FM208806
			JSDUK10	da Silva et al. 2011		JQ306000		
<i>Cancer irroratus</i>	ZMH-K 656	<i>Cancer irroratus</i>	ULLZ 3843	Schubart & Reuschel 2009	FM207654			FM208807
			L195AR2-01	Radulovici et al. 2009		FJ581562		
<i>Caphyra loevis</i>	AMS P.17124, SMF 6353	<i>Caphyra loevis</i>	NMMBCD 4090	Evans 2018	KT365592	KT365697		KT425009
<i>Caphyra rotundifrons</i>	ZMH-K 2565 & 2566	<i>Caphyra rotundifrons</i>	UF:4079	Evans 2018	KT365530	KT365698	KT365530	KT424989
<i>Carcinus maenas</i>	ZSRO no ID	<i>Carcinus maenas</i>	SMF-32757	Schubart & Reuschel 2009	FM208763		FM208763	FM208811
			L174AR1-07	Radulovici et al. 2009		FJ581597		
<i>Carupa tenuipes</i>	SMF ZMG 832	<i>Carupa tenuipes</i>	MNHN-B31436	Schubart & Reuschel 2009	FM208758		FM208758	FM208789
			UF16184	Evans 2018		KT365703		
<i>Catoptrus nitidus</i>	ZMH-K 3136	<i>Catoptrus nitidus</i>	MNHN-B31435	Schubart & Reuschel 2009	FM208755		FM208755	
		<i>Catoptrus aff. nitidus</i>	UF1024	Evans 2018		KT365706		
<i>Chaecon mediterraneus</i>	SMF 29486	<i>Chaecon granulatus</i>	SMF-32762	Schubart & Reuschel 2009	FM208775		FM208775	FM208827
			unknown	unpublished		AB769383		

Taxa examined for morphological characters	Voucher ID (morphological characters)	Taxa examined and combined as OTUs for the genetic data set	Voucher ID (genetic data set)	Reference	16S	CO1	NADH1	H3
<i>Coelocarcinus foliatus</i>	UF 050654	<i>Coelocarcinus foliatus</i>	UF: 40056	Evans 2018	KT365601	KT365724		KT425058
		<i>Coelocarcinus sp.</i>	UF 27553	Evans 2018			KT365545	
<i>Corystes cassivelaunus</i>	ZMH-K 4887 & 27128	<i>Corystes cassivelaunus</i>	SMF-32770	Schubart & Reuschel 2009	FM208781		FM208781	FM208801
			JSDUK23	da Silva et al. 2011		JQ306005		
<i>Eriocheir sinensis</i>	ZMH-K 24504	<i>Eriocheir sinensis</i>	unknown	Li et al. 2016	KP064329	KP064329	KP064329	
		<i>Eriocheir japonica</i>	MSLKHC-EjapHK	Tsang et al. 2014				KJ133099
<i>Libystes alphonisi</i>	ZMH-K 3143	<i>Libystes nitidus</i>	MNHN-B31438	Schubart & Reuschel 2009	FM208762		FM208762	
			UF12587	Evans 2018		KT365728		
<i>Liocarcinus depurator</i>	ZSRO no ID,	<i>Liocarcinus depurator</i>	MNHN-B31439	Schubart & Reuschel 2009	FM208767		FM208767	FM208819
			JSDUK052-08	da Silva et al. 2011		JQ306013		
<i>Liocarcinus navigator</i>	ZSRO no ID, SMF 10662 & 45835	<i>Liocarcinus navigator</i>	SMF-32775	Schubart & Reuschel 2009				FM208821
			SMF < DEU>:44087	Plagge et al. 2016	KU560476	KP795939	KU560476	
<i>Lissocarcinus orbicularis</i>	SMF 19738	<i>Lissocarcinus orbicularis</i>	unknown	Schubart & Reuschel 2009	FM208757		FM208757	FM208791
			UF15741	Evans 2018		KT365732		
<i>Macropipus tuberculatus</i>	ZSRO 262	<i>Macropipus tuberculatus</i>	MNHN-B31440	Schubart & Reuschel 2009	FM208769		FM208769	FM208815
			FCFOPC041-33	da Silva et al. 2011		JQ306218		
<i>Medorippe lanata</i>	ZSRO 189	<i>Medorippe lanata</i>	ZRC	Sin et al. 2009	EU636950	EU636981		
		<i>Dorippe quadridens</i>	ZRC2008.0064	Tsang et al. 2014				KJ133093
<i>Necora puber</i>	ZSRO no ID, SMF 4906	<i>Necora puber</i>	SMF-32749	Schubart & Reuschel 2009	FM208771		FM208771	FM208813
			unknown	Sotelo et al. 2009		FJ755619		
<i>Ovalipes ocellatus</i>	SMF 22191 & 7326	<i>Ovalipes punctatus</i>	MNHN-B31442	Schubart & Reuschel 2009				FM208824
			FKU63_mgp01	unpublished	MH802052	MH802052	MH802052	
<i>Parathranites orientalis</i>	SMF 30810	<i>Parathranites orientalis</i>	NTOU B00090	Tsang et al. 2014	KJ132616			KJ133173
<i>Pirimela denticulata</i>	ZMH-K 6780 & 6781	<i>Pirimela denticulata</i>	SMF-32767	Schubart & Reuschel 2009	FM208783		FM208783	FM208808

Taxa examined for morphological characters	Voucher ID (morphological characters)	Taxa examined and combined as OTUs for the genetic data set	Voucher ID (genetic data set)	Reference	16S	CO1	NADH1	H3
<i>Polybius henslowii</i>	ZMH-K 26238 & 2631	<i>Polybius henslowii</i>	SMF-32759	Schubart & Reuschel 2009	FM208765		FM208765	FM208816
			JSDUK74	da Silva et al. 2011		JQ306293		
<i>Portumnus latipes</i>	ZSRO 195, SMF 43553, ZMH-K 2616	<i>Portumnus latipes</i>	SMF-32758	Schubart & Reuschel 2009	FM208764		FM208764	FM208812
<i>Portunus inaequalis</i>	ZSRO 193 & 225	<i>Portunus inaequalis</i>	SMF-32754	Schubart & Reuschel 2009	FM208752		FM208752	FM208795
		<i>Portunus pelagicus</i>	unknown	Meng et al. 2016		KR153996		
<i>Raymanninus schmitti</i>	UF 9676	<i>Raymanninus schmitti</i>	UF:9676	Evans 2018	KT365560		KT365560	
<i>Sternodromia monodi</i>	ZSRO 354	<i>Lauridromia dehaani</i>	AMSP67928	Ahyong & O'Meally 2004	AY583899			
			unknown	Sin et al. 2009		EU636986		
			NTOU B00006	Tsang et al. 2014				KJ133125
			C20191207LD	Yang et al. 2020			MT038417	
<i>Telmessus cheiragonus</i>	ZMH-K 4952	<i>Telmessus cheiragonus</i>	SMF:22475	Schubart & Reuschel 2009	FM207656		FM207656	FM208802
			CIB213	Castelin et al. 2016		KX039796		
<i>Thia scutellata</i>	ZSRO 363	<i>Thia scutellata</i>	SMF-32769	Schubart & Reuschel 2009	FM208782		FM208782	FM208810
			MT04558	Raupach et al. 2015		KT209396		
<i>Varuna litterata</i>	SMF-10002, ZSRO 100	<i>Varuna litterata</i>	unknown	Wang et al. 2021	MW125542	MW125542	MW125542	
			MZUF:2503	Schubart & Cuesta 2010				FN434060
<i>Xaiva biguttata</i>	ZMH-K 29763	no data						

Specimens used in morphological examinations were provided by the collections of the Senckenberg Research Institute and Natural History Museum in Frankfurt, Germany (SMF), the Zoological Museum of the Center of Natural History (CeNak) in Hamburg, Germany (ZMH-K), the Florida Museum of Natural History, University of Florida in Gainesville, USA (UF), the Australian Museum in Sydney, Australia (AMS) and our own collection of the Institute of Zoology in Rostock (ZSRO), Germany. For more information on the material, see Table 1. Freshly collected specimens in 2019 of *Cancer pagurus*, *Carcinus maenas*, *Liocarcinus depurator*, *Liocarcinus navigator* from the waters near Gullmarn, Sweden, were considered in morphological examinations as well.

2.2 Micro-computed tomography (μ CT), 3D reconstruction

Specimens of at least one female and one male per species (if available) were used for X-ray imaging using a XRadia Versa 410 x-ray microscope (ZEISS, Oberkochen, Germany) and the program Scout and Scan v.11 (Table 1). In species of which only one sex was represented in the voucher material, then at least two specimens of the same sex (if available) were used. If extrinsic pereopod musculature was barely visible in μ CT scan images, the respective specimen was bathed in alcoholic Lugol's iodine solution for several days to improve the visibility of the musculature during μ CT scans. Processing of digital image stacks obtained via μ CT were conducted using the 3D reconstruction software Amira 6.4/6.5/6.6/6.7 (by FEI). Depending on the quality of the scan and the condition of the extrinsic musculature, scans for 3D reconstruction of the axial skeletons and P5 extrinsic musculature were chosen.

Extrinsic musculature of pereopods 2–4 (P2-P4) were checked in μ CT scan image stacks whether differences can be found between species. Some of these muscles were reconstructed in 3D models as well. Remaining scans were used to check (and optionally, the axial skeleton and extrinsic musculature roughly reconstructed) if there were differences between specimens of the same or the respective other sex in each species (if available). Some μ CT scans, 3D models and photographs of the specimens were used to produce images and drawings using CorelDraw 2020 and common graphics programs.

2.3. Terminology

The Terminology concerning morphology is basically the same as in Hazerli & Richter (2020), with some adjustments in details of the term endophragma (pl. endophragmata). In Hazerli & Richter (2020), we adopt the definition of endophragma used by Guinot et al. (2013) as infoldings of the axial skeleton being “composed of two layers that are confluent with their cuticle at its outer margin (being “technically inseparable at moult”)”. However, we found that in many species, large parts of axial skeleton infoldings generally defined as endophragmata consist of two separate, clearly distinguishable layers of cuticular infoldings, which especially concerns large areas of the junction plate and median plate. In fact, the wall of the junction plate cavity always appears to be formed by only one layer of cuticular infolding. Plus, in many of the species with interosternite 4/5, 5/6, and/or 6/7 connected to the median plate, the two layers of median infoldings connected to interosternites are predominantly not confluent at their outer margin. Strictly speaking, these infoldings are no true endophragmata by the definition used by Hazerli & Richter (2020). However, we here prefer a less strict definition of the term endophragma, simply defining the median plate and interosternites as median and lateral sternal infoldings and interopleurites as pleural infoldings which together with the junction plate and sella turcica are referred to as endophragmata herein.

2.4 Molecular data set, phylogenetic analysis and ancestral state reconstruction

We created a combined dataset containing 2142 characters, comprising 59 newly conceptualised morphological characters and 2081 nucleotide sites. Sequences were obtained from GenBank and derived from 63 vouchered specimens listed in Table 1. The final molecular data set comprises 34 operational taxonomic units (OTUs). When sequence data were not available for a certain species analysed for morphology, OTUs were concatenated of the species morphologically studied and sequence data of closely related species (see Table 1). This data set combines fragments of 16S rRNA, CO1, NADH1, and H3 data from 90 sequences. The sequences of all four gene fragments were separately aligned in Geneious Prime 2021.0.3 (Biomatters Limited) and concatenated to a single molecular data set with a total amount of 2083 nucleotides (16S: 671 Bp, CO1: 657 Bp, NADH1: 427 Bp, H3: 328 Bp). Published sequences were mostly drawn from Schubart & Reuschel (2009), da Silva et al. (2011) and Evans (2018). The dataset was analysed using Maximum parsimony (MP) and Bayesian inference (BI). For BI analyses, the best fit model of evolution was determined by the implemented model test in MEGA X. The MP analyses were performed in TNT (Goloboff et al. 2008). BI analyses were performed with MrBayes 3.2.7a (Ronquist et al. 2012) on CIPRES Science Gateway (Miller, Pfeiffer, & Schwartz 2010). The GTR + G + I Model was applied. Each Bayesian analyses included four runs with four differentially heated chains and 6×100 generations, sampled every 5,000 generations. The first 10% were discarded as burn-in. Resulting trees were visualized with FigTree v.1.4.2 (Rambaut 2014) and Corel Draw 2020 and common graphics programs. In all analyses, *Sternodromia monodi* was set as most basal outgroup.

Ancestral state reconstructions were traced using the software Mesquite (build 927) by Maddison and Maddison (2008). It was based on the phylogenetic tree deduced from MP analysis by choosing the parsimony model ‘unordered’ as the most conservative option for optimizing character states.

3 Results And Discussion Of Morphological Characters

3.1 Character conceptualization

We here follow Hennig (1966; see also Grant & Kluge 2004, Wirkner & Richter 2010, Richter & Wirkner 2014, Göpel & Wirkner 2018) with assigning character states belonging to a certain transformation series (which represents the character). We further treat the assignment of the same state to different taxa as “character state identity hypothesis”, while the assignment of two (or more) different states to the same character represents one (or more) “transformational hypothesis” (or “hypotheses”). Both types of hypotheses can be seen as homology hypothesis of some kind (for a discussion of the term “homology”, see for example Hennig 1966, Szuchcich & Wirkner 2007, Wagner 2014, Richter 2017). Characters are phrased as suggested by Sereno (2007). Character dependencies are expressed by the state “inapplicable (-) if” followed by the state(s) of the character(s), which make(s) the present character inapplicable for a certain taxon. This work focuses on characters concerning the axial skeleton, extrinsic musculature of pereopods 2-5 (P2-P5) and external morphology of the 5th pereopod (representing the extensively modified swimming leg in P5-swimmers), which are discussed in detail herein. With respect to remaining external features, characters are only briefly discussed and conceptualized mainly considering statements by Karasawa et al. (2008) and Spiridonov (2020).

3.1.1 Characters concerning the axial skeleton and extrinsic musculature of pereopods 2-5

Shape and proportion of overall axial skeleton. An overview of axial skeleton morphology (including some 3D data) in most of the taxa is given in Figures 1-6. High resolution 3D models of these species’ axial skeletons including some of the pereopodal extrinsic musculature are supplied in the appendix. The axial skeleton in all taxa consists of a ventral sternum, a left and right latero-dorsal pleurum, as well as infoldings deriving from them. Interosternites and interopleurites are pairwise sternal and pleural infoldings between thoracomeres, respectively. Those of each lateral body side are fused to build the two junction plates of the endophragmal system, of which the two lateral halves are connected by the sella turcica, which also separates the cephalothorax from the pleon. Most species have a median plate, which is a medially uprising endophragma of the sternum (for more information on the terminology of morphemes, see Hazerli & Richter 2020). Examples on the states with respect to the axial skeleton proportion (character 1) are shown in

Fig. 7 A-D. The degree of dorsoventral sternal curving, which is conceptualized as two discrete states herein (character 2), can be seen in Fig 7 E-L. Characters concerning proportions of the sternum (character 3) and its shape (character 4) are shown in Fig 8. Characters 1-3 are conceptualized with respect to thoracomeres 5-8 only, since the shape of thoracomere 4 depends on the size of the cheliped, which is not included here. *Ashoret* is the only taxon, in which the pleurites of thoracomeres 5, 6 and 8 are noticeably expanded in medial direction, with interpleurites (=infoldings of the pleurum) 5/6 and 6/7 almost reaching the median plane of the axial skeleton. Although, this is restricted to a single taxon, we conceptualize this as a character here (character state 5(1); Fig. 9). A minor medial expansion of pleurite 8 is also present in P5-swimming crabs (Fig. 9 D, F, H). However, we here do not conceptualize this as a character state, since variation of this morphological feature is very high between species, with a more or less distinct medial expansion of pleurite 8 being also present in several non-P5-swimmers (Fig. 9 A, C, I).

1. (Fig. 7 A-D) **Thoracomeres 5-8, axial skeleton, maximum height relative to maximum width:** higher than wide or about as high as wide (0); wider than high (1).
2. (Fig. 7 E-L) **Thoracomeres 5-8, sternum, dorsoventral curving:** distinct (0); indistinct (1).
3. (Fig. 8) **Thoracomeres 5-8, sternum, maximum length relative to maximum width:** longer than wide (0); wider than long (1).
4. (Fig. 8) **Thoracomeres 5-8, sternum, shape:** more or less straight anterior-posteriorly (0); narrowing anterior-posteriorly (1); widening anterior-posteriorly (2).
5. (Fig. 9) **Thoracomeres 5-6 and 8, pleurum, medial margin, shape:** rather straight (0); with prominent expansions (1).
6. (Fig. 7 E-L) **Thoracomeres 5-8, pleurum, gill openings, number and positions:** 4 in pleurites 5-8 (0); 2 only in pleurites 5-6 (1).

Extension and shape of median plate. In the outgroup taxon *Sternodromia monodi*, a median plate is absent (Fig. 1 A), which is also the case in *Medorippe lanata* (Fig. 3) which differs from all other taxa by the males having medially uprising sternal infoldings in thoracomeres 5, 6 and 7 to 8 (not connected to the sella turcica), which are absent in female specimens. The reason for that lies in the males having a narrower sternum than females, with the P2 and P3 ventral basi-ischium muscles originating at the medial sternal infoldings, while in females, the broad sternum offers an area large enough to serve as an attachment site for these muscles alone. In all other taxa, the median plate is present in thoracomere 8 of both female and male specimens, and posteriorly connected to the sella turcica (extending with variable extension in anterior direction; see for example Fig. 1-6). Therefore, we here consider the median sternal infolding in *Medorippe* males (termed "median plate" by Guinot et al. 2013) not to be homologous to the median plate in the remaining taxa (i.e. the median plate in *Medorippe* scored as absent; character state 7(0)). Character 8 refers to the maximal extension of the median plate in anterior direction, not considering a further anterior extension ("anterior process") due to the shape of the anterior margin of the median plate (character 9, 10; Fig. 11 B, D, F). Depending on how far the median plate extends in anterior direction, its dorsal margin may differ in its shape. In taxa that share a median plate reaching interosternite 4/5 (character state 8(0); 10 B-E, 11 E) it may be concave and without indentations and/or gaps (character state 11(0); 10 C, D) or of irregular shape, with indentations and/or gaps between thoracomeres (character state 11(2); Fig. 10 E, 11 E). Taxa with a median plate reaching interosternite 5/6 (character state 8(1); Fig. 10 A, 11 A, C, F) can have a margin being more or less convex and entire (character state 11(1); Fig. 11 A, F) or irregularly shaped as well (with indentations and/or gaps; character state 11(2); Fig. 10 A, 11 C). Only in taxa with a median plate extending up to interosternite 6/7, the median plate margin is always convex without indentations and/or gaps between thoracomeres (character states 8(2), 11(1); Fig. 10 F, 11 B, D). In several taxa with the median plate reaching interosternite 5/6 (character state 8(1)) together with a median plate having a convex dorsal margin (character state 11(2)), and interosternite 6/7 not connected to the median plate (character state 15(1); see below), there is a transverse sternal ridge from the lower medial edge of interosternite 6/7 directed to the anterior end (not considering the anterior process that is present in some species) of the median plate (character 12; Fig.12).

7. **Sternum, median plate:** absent (0); present (1).
8. (Fig. 10, 11) **Sternum, median plate, maximal anterior extension:** up to or further than interosternite 4/5 (0); up to interosternite 5/6 (1); up to interosternite 6/7 (2); inapplicable (-) if 7(0).
9. (Fig. 10, 11) **Sternum, median plate, anterior process:** absent (0); present (1), inapplicable (-) if 7(0) or 8(0).
10. (Fig. 11 B, D, F) **Sternum, median plate, anterior process, length:** overlapping up to one thoracomere (0) overlapping more than one thoracomere (1); inapplicable (-) if 7(0) or 9(0).
11. (Fig. 10, 11) **Sternum, median plate, dorsal margin, shape:** concave, without indentations and/or gaps between thoracomeres (0); more or less convex, without indentations and/or gaps between thoracomeres (1); irregular, with indentations and/or gaps between thoracomeres (2); inapplicable (-) if 7(0).
12. (Fig. 12) **Sternum, transverse sternal ridge from interosternite 6/7 to anterior end of median plate:** absent (0); present (1); inapplicable (-) if 7(0), 8(0), 8(2), 8(3) and/or 15(0).

Connection of interosternites to the median plate and distance to median plane. Taxa may differ in which interosternites are connected to the median plate (Fig. 1-6, 10, 11; in several species, interosternites lack any connection). In species with the median plate just reaching interosternites 5/6 or 6/7 (character states 8(1), 8(2); Fig. 10 A, F, 11 A-D, F), interosternite 4/5 can never be connected to the median plate (and character 13 thus scored as inapplicable). The same is true for interosternite 5/6 (character 14) in species with the median plate just reaching interosternite 6/7 (character state 8(2);

Fig. 10 F, 11 B, D). In several taxa distance between the medial edge of interosternite 7/8 to the median plane is greater than that of interosternite 6/7 (character state 17(1); Fig. 13). In taxa, in which interosternite 7/8 is connected to the median plate (character state 16(0); Fig. 10 A-E, 11 C, E), distance of interosternal 7/8 medial edge to the median plane is obligatorily similar as in interosternite 6/7 (and thus, character 17 scored as inapplicable).

13. (Fig. 10, 11) **Sternum, interosternite 4/5, connection to median plate:** present (0); absent (1); inapplicable (-) if 7(0), 8(1) or 8(2).

14. (Fig. 10, 11) **Sternum, interosternite 5/6, connection to median plate:** present (0); absent (1); inapplicable (-) if 7(0) or 8(2).

15. (Fig. 10, 11) **Sternum, interosternite 6/7, connection to median plate:** present (0); absent (1); inapplicable (-) if 7(0).

16. (Fig. 10, 11) **Sternum, interosternite 7/8, connection to median plate:** present (0); absent (1); inapplicable (-) if 7(0).

17. (Fig. 13) **Sternum, interosternite 7/8, distance of medial edge to median plane:** similar as in interosternite 6/7 (0); greater than in interosternite 6/7 (1); inapplicable (-) if 7(0) or 16(0).

Medial margins of interosternites 4/5 to 6/7. The medial margin of an interosternite is characterised by an upper, medially directed interosternal expansion we herein term “interosternal process” (Fig. 14; for more information on the terminology of morphemes, see Hazerli & Richter 2020). As it is difficult to conceptualize the morpheme variability seen in the different taxa into distinct character states, we here only distinguish between three discrete states, which are not prone to subjective perception (character 18; Fig. 14). In all cases, the distinctiveness of processes successively decreases from interosternite 4/5 to 6/7. That is why the character is conceptualized by the process shape of interosternite 4/5 only.

18. (Fig. 14) **Sternum, interosternite 4/5, medial margin, shape:** transversal with interosternal process being most medial (0); almost perpendicular (1); transversal with lower margin being most medial, but not touching (2); transversal with lower margin being most medial and touching (3).

Connection of interosternite 7/8 to sella turcica and interosternal process of interosternite 7/8. In non-heterotreme outgroup taxa and *Medorippe*, interosternite 7/8 is directly connected to the sella turcica (character state 19(0); Fig. 15 A, B, D, E). Which we here consider as “interosternal process 7/8” is a medio-anteriorly directed process at the upper medial margin of interosternite 7/8, only present in all remaining taxa, in which interosternite 7/8 is not connected to the sella turcica (character state 19(1); Fig. 15 G, H). Its shape can be quite variable (and thus vulnerable to subjectivity): For example, it may be barely visible, like in *Thia* (Fig. 16 C, G), distinct and short like in *Bathynectes* and “*Polybius*” (Fig. 16 A, B, E, F) or very long like in *Portunus* (Fig. 16 D, H). However, in several species, the process touches interosternite 6/7, representing an intersubjective morphological feature that can be used to conceptualize a character (character 20; Fig. 16 E-H).

19. (Fig. 15 A, B, D, E, G, H, 15 A-D) **Sternum, interosternite 7/8, connection to sella turcica:** present (0); absent (1).

20. (Fig. 16 E-H) **Sternum, interosternite 7/8, interosternal process, contact to interosternite 6/7:** absent (0); present (1); inapplicable (-) if 19(0).

Shape of junction plate and sella turcica All ingroup taxa (with interosternite 7/8 being not connected to the sella turcica; character state 19(1); Fig. 15 G, H, 16 A-D) have each junction plate forming a cavity with variable anteriorad extension (Fig. 15 H, I, 17), which is absent in all non-heterotreme outgroup taxa (with interosternite 7/8 being connected to the sella turcica (character 19(0); Fig. 15 A-F). The shape of this “junction plate cavity” (for more information on the terminology of morphemes, see Hazerli & Richter 2020) is much variable between taxa, in most cases forming an anteriorly closed calyx with an asymmetrical posterior margin, of which the ventral part is more anteriorly situated than its dorsal part (Fig. 15 H, I, 17 A-C, E). In some taxa, the ventral part of the calyx is completely missing, with the junction plate cavity being more similar to a convex roof (Fig. 17 D). We here conceptualize the anteriorad extension of the junction plate cavity as a character with states representing which interosternites are overlapped by the anterior end of the cavity (character 22; Fig. 17). In *Sternodromia*, the sella turcica differs from that of all other taxa not only by being not directly connected with the two junction plates (character 21; Fig. 15 A, D, G, 16 A-D, 18 I-L), but also by being fused with interosternites 4/5 to 7/8 (Fig. 1 A). As borders between the elements of this fusion cannot be distinguished unambiguously, they shall rather be considered as diffuse transitions in 3D reconstructions, with the fusion reconstructed as being part of the sella turcica. The shape of the sella turcica is variable between taxa, making a character conceptualization difficult (Fig. 18 A-H). We here conceptualize its shape with only one unambiguous character expressing if the sella turcica covers the dorsal median plate margin (character 23; Fig. 18 A-H). In outgroup taxa *Eriochel*, *Varuna*, and *Medorippe*, the whole medial margin of interopleurite 7/8 is confluent with the sella turcica, while in all other taxa, its medial margin is not or only partly connected to the latter (character 24; Fig. 18 I-L).

21. (Fig. 15 A, B, D, E, G, H, 18 I-L) **Junction plate, connection to sella turcica:** absent (0); present (1).

22. (Fig. 17) **Junction plate cavity, maximal anterior extension:** overlapping interosternite 5/6 (0); overlapping interosternite 6/7(1); overlapping interosternite 7/8 (2); inapplicable (-) if 18(0) or 20(0).

23. (Fig. 18 A-H) **Sella turcica, covering of dorsal median plate margin:** present (0); absent (1); inapplicable (-) if 7(0)

24. (Fig. 18 I-L) **Pleurum, interopleurite 7/8, medial margin, degree of connection to sella turcica:** not or only partly connected (0); completely connected (1); inapplicable (-) if 21(0).

Extrinsic musculature of pereopods 1-4. In contrast to the extrinsic musculature of P5 (see below), in the taxa examined, differences in the origin positions of P1-P3 extrinsic musculature are limited to single terminals in most cases. We found no apparent differences in the P1 extrinsic musculature origins between species. In all taxa, the P2 anterior coxa muscle originates at interosternite 4/5, interosternite 5/6 and interopleurite 4/5 (character state

25(0); Fig. 19 A B), while the P3 anterior coxa muscle originates at interosternite 5/6, interosternite 6/7 and interopleurite 5/6 (Fig. 19 C). Only in *Ovalipes*, we found parts of the P2 anterior coxa muscle additionally originating at interopleurite 3/4 (character state 25(1); Fig. 19 D). In most of the species, the P2 and P3 anterior coxa muscles have a branch originating at interopleurite 4/5 and 5/6, respectively, with the branch running along (but not attaching at) the medial side of the junction plate (Fig. 19 A, C). This branch was not found in some of the taxa (*Sternodromia*, *Medorippe*, *Telmessus*, *Corystes*, *Ovalipes*, *Lissocarcinus*, *Catoptrus*), but since it is very thin and the musculature in the voucher material representing these taxa in parts poorly preserved, this might be artificial. We thus do not implement these findings in the character statements. *Telmessus* and *Corystes* both have the P2 posterior coxa muscle originating at interopleurite 4/5 and 5/6 (character state 26(1); Fig. 20 A), while *Libystes* is the only representative having the muscle originating at interosternite 6/7 in addition to interopleurite 5/6 (character state 26(2); Fig. 20 C). In all other species, it originates at interopleurite 5/6 alone (Fig. 20 B). The P2 dorsal basi-ischium muscle originates at interosternite 4/5 and 5/6 in all terminals, but only in *Thia* and *Ashtoret*, it additionally originates at the median plate, which here is conceptualized as a neomorphic character (character 27; Fig. 20 D, E) that is scored as inapplicable in taxa in which the median plate is absent or does not extend to pereiomere 2/thoracomere 5 (character states 7(0), 8(1) or 8(2)). In all taxa with the median plate reaching thoracomere 5, the P3 and P4 ventral basi-ischium muscle originates at the median plate and interosternites 4/5 and 5/6, respectively. However, *Thia* differs from the other taxa in that it lacks the P2 ventral basi-ischium muscle originating at interosternite 4/5 and the P3 muscle originating at interosternite 5/6 respectively (the anterior interosternite of the respective thoracomere; character state 28(1); Fig. 21 D). Interestingly, this is also the case in the outgroup taxon *Sternodromia* (character state 28(0); Fig. 21 A). Both species of *Cancer*, but also *Lybistes alphonsi* are the only taxa in which the P2 and P3 ventral basi-ischium muscles originate both at the anterior and posterior interosternites of the respective thoracomere (interosternites 4/5, 5/6 and 6/7), but not at interopleurite 5/6 and interopleurite 6/7, respectively, as in most other species (character states 28(3) and 28(4); Fig. 21 B, D). All taxa have a P3 posterior coxa muscle originating at interopleurite 6/7 (character state 29(0); Fig. 22 B). *Libystes* again is the only species having an additional branch originating at interosternite 6/7, remotely from the junction plate (character state 29(2); Fig. 22 C), while not only in *Libystes*, but also in *Corystes*, *Ashtoret*, *Macropipus* and *Bathynectes*, the P3 posterior coxa muscle also originates at interosternite 7/8 (character state 29(1); Fig. 22 A). A P3 dorsal basi-ischium muscle at interosternite 6/7 only is exclusive to *Sternodromia* (character state 30(0); Fig. 23 A). *Ashtoret* and *Thia* are the only taxa with the P3 dorsal basi-ischium muscle originating at the median plate, but with the muscle additionally originating at interosternite 5/6 only in *Ashtoret* and *Corystes* (character states 30(2), 30(3); Fig. 23 B, D). All the other taxa possess the muscle originating at interosternite 5/6 and 6/7, but not at the median plate (character state 30(1); Fig. 23 C). In these taxa, this muscle always originates at the junction plate, near interopleurite 5/6, sometimes with some fibre bundles attached to it. However, as this is ambiguous in many specimens of different species, these attachment sites are not included in the character statements. Origin positions of the P4 ventral basi-ischium muscle (character 31) in species with the median plate reaching interosternites 5/6 or 6/7 (character states 8(1) and 8(2)) largely depends on whether the whole median plate is occupied by the P5 extrinsic musculature, which is the case in all the typical P5-swimming crabs (assigned to the morphotype based on the criteria mentioned above, including a short merus; character state 31(2); Fig. 24 F) except for "*Polybius*". In the latter and all the other species with a median plate being present (character state 7(1)), part of the P4 ventral basi-ischium muscle also originates at the median plate (character state 31(1); Fig. 24 E). However, in "*Polybius*", only a small fringe of the median plate is covered by the muscle. *Thia* is the only ingroup taxon which lacks the origin at interosternite 6/7, which again it has in common with outgroup taxa *Sternodromia* and *Medorippe* (character state 31(0); Fig. 24 C, G). With respect to the P4 dorsal basi-ischium-muscle, a distinct anterior and posterior branch can be distinguished in all species. The anterior branch always originates at interosternite 6/7 only (character state 32(1); Fig. 24 B, F, H), with the exception of *Sternodromia* and *Medorippe*, in which it has an origin at the sternum (character state 32(0); Fig. 24 D) and *Thia*, in which it additionally originates at the median plate (character state 32(2); Fig. 24 H). In all taxa, the posterior branch originates at interosternite 7/8, in *Calappa*, *Ashtoret*, *Cancer pagurus* and *Corystes* additionally at the median plate (character state 33(1); Fig. 24 B) and in several species additionally at interopleurite 6/7 instead (character 33(2), Fig. 24 F). *Eriocheir* and *Varuna* have the posterior branch additionally originating at both the median plate and interopleurite 6/7 (character state 33(3); Fig. 24 A).

Extrinsic musculature origins at the junction plate are not considered in characters 25-33, because muscular attachment sites at the junction plate are ambiguous as it is a product of the fusion of interosternites and interopleurites, with no visible sutures.

25. Pereiopod 2, anterior coxa muscle, origin (Fig. 19): at interosternites 4/5 + 5/6 + interopleurite 4/5 (0); at interosternites 4/5 + 5/6 + interopleurites 3/4 + 4/5, (1).

26. Pereiopod 2, posterior coxa muscle, origin (Fig. 20 A-C): at interopleurite 5/6 (0); at interopleurites 4/5 + 5/6 (1); at interosternite 6/7 + interopleurite 5/6 (2).

27. Pereiopod 2, dorsal basi-ischium muscle, origin at median plate (additional to interosternites 4/5 & 5/6; Fig. 20 D, E): absent (0); present (1); inapplicable (-) if 7(0), 8(1), 8(2), 9(1) or 9(2).

28. Pereiopod 2, 3, ventral basi-ischium muscle, origin (Fig. 21): at sternum + posterior interosternite of respective thoracomere + pleurum (0); at sternum + median plate + posterior interosternite of respective thoracomere (1); at sternum + median plate + anterior interosternite of respective thoracomere, (2); at sternum + median plate (if extending up to respective thoracomere) + anterior interosternite of respective thoracomere + posterior interosternite of respective thoracomere, (3) at sternum + median plate (if present and extending up to respective thoracomere) + anterior interosternite of respective thoracomere + posterior interosternite of respective thoracomere, + posterior interopleurite of respective thoracomere, (4).

29. Pereiopod 3, posterior coxa muscle, origin (Fig. 22): at interopleurite 6/7 (0); at interosternite 7/8 + interopleurite 6/7 (1); at interosternite 6/7 + 7/8 + interopleurite 6/7 (2).

30. Pereiopod 3, dorsal basi-ischium muscle, origin (Fig. 23): at interosternite 6/7 + interopleurite 5/6 (0); at interosternites 5/6 + 6/7 (1); at median plate + interosternite 6/7 (2); at median plate + interosternites 5/6 + 6/7 (3).

31. Pereiopod 4, ventral basi-ischium muscle, origin (Fig. 24 C, E, F, G): at median plate (if present) + interosternite 7/8 (0); at median plate + interosternites 6/7 + 7/8 (1); at interosternites 6/7 + 7/8 (2).

32. Pereiopod 4, dorsal basi-ischium muscle, anterior branch, origin (Fig. 24 A, B, D, F, H): at sternum (0); at interosternite 6/7 (1); at median plate + interosternite 6/7 (2);

33. Pereiopod 4, dorsal basi-ischium muscle, posterior branch, origin (Fig. 24 A, B, D, F, H): at interosternite 7/8 (0); at median plate + interosternite 7/8 (1); at interosternite 7/8 + interopleurite 6/7 (2); at median plate + interosternite 7/8 + interopleurite 6/7 (3).

Extrinsic musculature of pereiopod 5. The P5 extrinsic musculature is especially interesting as it is responsible for moving the swimming leg in P5-swimmers. Remarkably, all P5-swimming crabs have the anterior coxa muscle originating at the median plate. Here, the branch originating at this structure contains considerably long muscle fibres because of a large distance between the insertion at the coxa and the origin at the median plate or its anterior process (which is present in all typical P5-swimmers assigned to the morphotype based on the criteria mentioned above; Fig. 25 D-F). Also with respect to the anterior coxa muscle, in some taxa, several distal fibre bundles can be distinguished having their origin at interopleurite 7/8 (character states 34(1), 34(3); Fig. 25 B, C, 26). However, the exact attachment positions vary between the species. They may be at the upper end of interopleurite 7/8 like in *Medorippe*, *Calappa* and *Ashtoret* (in which the fibre bundles form a considerably voluminous branch; character state 35(0); Fig. 26 B), in the middle of interopleurite 7/8 like in *Eriocheir* and *Varuna* (character state 35(1); Fig. 26 A), or at the lower end like in the other species (character state 35(2); Fig. 26 C). A ventral posterior coxa muscle originating at the median plate is present in all the taxa with a median plate being present (character state 36(0); Fig. 27 B, D) except for *Eriocheir* and *Varuna* (character state 36(1); Fig. 27 A). The volume of the ventral posterior coxa muscle significantly differs from that of the dorsal posterior coxa muscle in several species (character states 37(0), 37(2); Fig. 27 A-C). Most species have the ventral basi-ischium muscle originating at the sternum, the median plate and interosternite 7/8 (character state 38(3); Fig. 28 B). In *Thia* and *Ovalipes*, it solely originates at the sternum and the median plate (character state 38(2); Fig. 28 C), while in *Lybistes* and both species of *Caphyra*, it originates at the sternum and interosternite 7/8 only (character state 38(1); Fig. 28 D). In outgroup taxa lacking a median plate, it only originates at the sternum (character state 38(0); Fig. 28 A). With respect to the dorsal basi-ischium muscle, in all taxa but *Stemodromia* and *Medorippe*, two distinct branches can be distinguished (character 39; Fig. 29), with the dorsal branch always originating at the sella turcica and in some species at the sternum near the border between sella turcica and sternum (which is indistinct and thus not considered as a separate character state). Only in *Calappa* and *Ashtoret*, the dorsal branch also originates at the median plate (character state 40(1); Fig. 29 A). The ventral branch can originate at interosternite 7/8 only (character state 41(0); Fig. 29 A, D), at the median plate only (state 41(2); Fig. 29 E), and at both interosternite 7/8 and the median plate (state 41(4); Fig. 29 C). In *Lybistes*, it originates at the sternum and interosternite 7/8 (character state 41(3)), while in both species of *Caphyra*, it only originates directly at the sternum (state 41(1); Fig. 29 F).

In typical P5-swimming crabs (assigned to the morphotype based on the criteria mentioned above), the P5 extrinsic musculature is considerably more voluminous than in P2-P4. A considerably voluminous musculature is also present in *Ashtoret* and *Coelocarcinus*, though here, the musculature is similarly expanded in anterior and dorsal direction, while in the P5-swimmers, it is mainly anteriorly expanded. The expansion of musculature is associated with specific features of the axial skeleton, like the anteriorly expanding process of the median plate (characters 9 and 10) in P5-swimmers. The dimension of the P5 extrinsic musculature thus is not considered as an independent character here.

Like in the extrinsic musculature concerning P2-P4, origins at the junction plate are not considered in characters 34-41.

34. Pereiopod 5, anterior coxa muscle, origin (Fig. 25): at interosternite 7/8(0); at interosternite 7/8 + interopleurite 7/8 (1); at median plate + interosternite 7/8 (2); at median plate + interosternite 7/8 + interopleurite 7/8 (3).

35. Pereiopod 5, anterior coxa muscle, origin at interopleurite 7/8, position (Fig. 26): at upper end of interopleurite 7/8 (0); at the middle of interopleurite 7/8 (1); at lower end of interopleurite 7/8 (2); inapplicable (-) if 34(0) or 34(2).

36. Pereiopod 5, ventral posterior coxa muscle, origin at median plate (additional to sternum/sella turcica; Fig. 27): present (0); absent (1), inapplicable (-) if 7(0).

37. Pereiopod 5, ventral posterior coxa muscle, volume compared to that of dorsal posterior coxa muscle (Fig. 27): greater (0); about as similar (1); smaller (2).

38. Pereiopod 5, ventral basi-ischium muscle, origin (Fig. 28): at sternum (0); at sternum + interosternite 7/8(1); at sternum + median plate (2); at sternum + median plate + interosternite 7/8 (3).

39. Pereiopod 5, dorsal basi-ischium muscle, configuration (Fig. 29): without distinct branches (0); separated into a ventral and a dorsal branch (1)

40. Pereiopod 5, dorsal basi-ischium muscle, dorsal branch, origin at median plate (in addition to sternum/sella turcica; Fig. 29): absent (0); present (1); inapplicable (-) if 7(0) or 39(0).

41. Pereiopod 5, dorsal basi-ischium muscle, ventral branch, origin (Fig. 29): at interosternite 7/8 (0); at sternum (1); at median plate (2); at sternum + interosternite 7/8 (3); at median plate + interosternite 7/8 (4) inapplicable (-) if 39(0).

3.1.2 Characters concerning the external morphology of pereiopod 5

There is much variability in the pereiopod 5 external features between species. The occurrence and mode of long setae arrangement on P5 can be seen in Fig. 1-6 and Fig. 30 A, B. Most species have them arranged in dense fringes along podomere margins, which is also the case in a typical swimming leg (character state 43(0); Fig. 30 B). We here express the shortened merus of a typical swimming leg through a comparison to P5 propodus length (character state 44(1); Fig. 30 B). The latter was shown to be rather independent of merus length (Schmidt et al. 2020). An insertion of the propodus in the disto-dorsal carpus margin is associated with an altered position of the carpal-propodal articulation axis relative to longitudinal propodus axis (character state 45(1); Fig. 30 B; see also Kühl 1933, Hazerli & Richter 2020). This is present in all typical P5 swimmers, but also (with variable distinctness) in some other taxa.

With respect to P5 dactylus shape, we here prefer a character concept with fewer states than in Karasawa et al (2008), as its variability may be very high not only between species (Fig. 31), but also within a species, implying that it is prone to subjectivity. For example, we found with respect to the dactylus shape in *Carcinus*, that there were specimens that would rather be assigned to the state “ensiform” (Fig. 31 D) based on Karasawa et al. (2008), while others show a “lanceolate” dactylus shape (Fig. 31 E). That is why we here conceptualize a character with only two states representing an apparent, intersubjective difference, expressing a broad “paddle-shaped” dactylus through a P5 dactylus being broader than the P5 merus (character state 47(1); Fig. 30 B, 31 C, F, G). A second character regarding the dactylus shape concerns its proximo-ventral margin, which is associated with the fact, that in species with the margin being concave, the disto-ventral propodus area is not immersed in the arthrodial cavity, when adducted (character state 48(1); Fig. 30 B, E, F; see also Hazerli & Richter 2020). This is the case in all the broad, paddle-shaped dactyli, but also in some of the narrow ones (see below).

We do not conceptualize the P5 propodus and dactylus being generally broader than respective P4 podomeres as an additional character herein, which is not only the case in taxa with a broad “paddle-shaped” dactylus, but also in *Carcinus* (albeit only rudimentarily; Fig. 32 C; see also for example Hartnoll 1971, Hazerli & Richter 2020). This is because in P5-swimming crabs and other taxa with a paddle-like dactylus, the extreme broadening of the propodus takes place by a large lobe-like projection of the disto-ventral propodus margin (character state 46 (1); Fig. 30 B, 32 B, D), which is absent in *Carcinus*. Actually, in *Carcinus*, the broader propodus correlates with a relatively larger volume of the musculature inserting at the dactylus, while in taxa with the propodus projection, this is not the case; i.e., the dactylus musculature is small in relation to propodus width (Fig. 32 B, C, D). Furthermore, the P5 proximo-ventral dactylus margin in *Carcinus* is that of a normal walking leg, which means that the broader podomere is not associated with a concave dactylus margin (Fig. 30 C, D, 31 D, E). That is why we here consider the broader distal P5 podomeres in *Carcinus* not to be homologous to those in P5-swimmers (representing whether an identical character state nor different states of the same character, i.e., being no part of the same transformation series as suggested by Hartnoll 1971). Schäfer (1954) also mentioned the P5 carpus in *Carcinus* to be broader than that of the P4, which also turns out to be the consequence of a relatively more voluminous musculature inserting at the propodus (Fig. 32 C). It is interesting to note that we found rudimentarily broader distal P5 podomeres (less pronounced than in *Carcinus*) that are associated with a relatively more voluminous intrinsic musculature to be also present in *Eriocheir sinensis* and *Cancer irroratus* (Fig. 32 A). An examination of external morphological features in another species of *Eriocheir* (*Eriocheir japonica*) even showed distal P5 podomeres being similarly broadened as in *Carcinus* compared to P4 podomeres. (Fig. A1 in appendix).

Ashtoret, *Bathynectes*, *Liocarcinus navigator*, *Carupa* and *Lissocarcinus* have a paddle-like dactylus like typical P5-swimming crabs (character states 46(1), 47(1)), but with the merus being not as short (character state 44(0); Fig. 2 B, 4 A, J, 6 B, F, 32 B). *Coelocarcinus foliatus* is another species with a paddle-shaped dactylus, but it has a short P5 merus, too (character state 44(1); Fig. 4 C). However, the P5 merus is not significantly shorter than those of the other pereiopods (which are relatively short, too) and it lacks the long setae along P5 podomere fringes typical for a swimming leg. *Portumnus* and *Xaiva* are the only taxa with the P5 dactylus being about as broad as in P5-swimmers (in *Portumnus* broader than in *Xaiva*; character state 47(1)), but with the propodus having no ventral propodus projection (character state 46(0); Fig. 4 G, I, 32 E). In *Caphyra loevis*, the dactylus is narrow (character state 47(0)), but has a concave proximo-ventral dactylus margin (character state 48(1)), while its propodus has a (small) ventral lobe-like projection (character state 46(1); Fig. 6 F, 31 L). *Raymanninus* eventually has a P5 propodus and dactylus being not much broader than those of the P4, but the dactylus has a concave proximo-ventral margin, resembling the configuration of a paddle-shaped dactylus (character state 48(1); Fig. 5 C, 30 E, F, 31 I). A similar configuration is present in *Libystes* (Fig. 6 D, 31 K). All these taxa, but also *Varuna* (Fig. 1 C) have a P5 disto-dorsal carpus insertion receiving the propodus (like in typical P5-swimmers; character state 45(1); Fig. 30 B).

In *Sternodromia*, *Medorippe* and *Caphyra rotundifrons*, the P5 propodus and dactylus are forming a subchela (Fig. 1 A, 3, 6 A 31 A). However, its shape between species is significantly different and thus, not conceptualized as a united character (state) herein.

42. Pereiopod 5, long setae: present (0); absent (1).

43. Pereiopod 5, long setae, arrangement (Fig. 30 A, B): arranged in dense fringes along podomere margins (0); rather irregularly (1); inapplicable (-) if 42(1).

44. Pereiopod 5, merus, length relative to propodus (Fig. 30 A, B): longer (0); equal or shorter (1).

45. Pereiopod 5, carpus, disto-dorsal margin, propodus insertion (Fig. 30 A, B): absent (0); present (1)

46. Pereiopod 5, propodus, lobe-like expansion of postero-ventral margin (Fig. 30 A, B): absent (0); present (1).

47. Pereiopod 5, dactylus, maximum width in relation to maximum width of P5 merus (Fig. 30 A, B): smaller or equal (0); larger (1).

48. Pereiopod 5, dactylus, proximo-ventral margin, shape (Fig. 30): convex or straight (0); concave (1).

49. Pereiopod 5, dactylus, tip, shape (Fig. 30 A, B): pointed (0); rounded (1).

Remarks on some morpheme properties mentioned by Hazerli & Richter (2020). Some morphological differences found by Hazerli & Richter (2020; called "morpheme properties" there) in the axial skeleton and external P5 morphology of non-swimmers *Cancer pagurus* and *Carcinus maenas* and the P5-swimming crab *Liocarcinus depurator*, which were unambiguous in these species, were not implemented in our character conceptualization herein. The reason for that lies in the great morphological variety found in the larger taxon sampling of this work, which sometimes makes it difficult to determine discrete character states covering more than one species. This concerns the shape of the P5 basi-ischium, size of the P5 thorax-coxa arthrodial cavity, general volume of the P5 extrinsic musculature (see also section *Extrinsic musculature of pereiopod 5* in 3.1.1 *Characters concerning the axial skeleton and extrinsic musculature of pereiopods 2-5*), general thoracomere 8 width together with the presence of an aliform thoracomere 8 pleural expansion in *Liocarcinus depurator* (which is absent in *Cancer* and *Carcinus*), and distances between medial edges of interosternites 4/5 to 7/8 in longitudinal plane (see morpheme properties 3, 4, 5, 11, 13, 14 and 23 in Hazerli & Richter 2020). As mentioned above, we also do not conceptualize the general P5 propodus and dactylus broadening as an additional character (morpheme property 2 in Hazerli & Richter 2020), which is the case both in *Carcinus maenas* and *Liocarcinus depurator* (in *Carcinus* to a much lesser degree; for a detailed explanation, see 3.1.2 *Characters concerning the external morphology of pereiopod 5*). Measuring inclination of P5 meral-carpal articulation and that between P1 and P5 thorax-coxa joints (morpheme properties 6, 32) were beyond the scope of this work and thus, not implemented either.

An extrinsic P5 anterior coxa muscle originating at interopleurite 6/7 (morpheme property 26 in Hazerli & Richter 2020) is not considered in our conceptualization either, since borders between the junction plate, interopleurite 6/7 and the sella turcica in many taxa are not as apparent as in those examined by Hazerli & Richter (2020).

3.1.3 Other external characters

Several morphological features used in taxonomic approaches are not conceptualized as characters here because of its high variability between species which makes the distinction of discrete states covering more than one species difficult and of which a discussion is beyond the scope of this paper (for a detailed discussion with respect to many of these features, see Spiridonov 2020). This concerns the shape of the carapace front, the number of spines and fissures on the ventral orbit margin, the presence or absence of a spine or lobe at the inner angle of the dorsal orbit margin, the shape and number of anterolateral carapace spines, the presence or absence and configuration of carapace tubercles and ridges, the shape of the basal antenna article, the presence and shape of a "portunid lobe" of maxillipede 1 (which was already marginally examined by Steudel, 1998) and the overall shape of the male pleon. Thus, only a few of previously used characters concerning the external morphology are considered herein. Spiridonov et al. (2014) who considered morphological features of the Chelae as important character complex, detailly described them in many portunoid species, but deduced no character concepts. It should be mentioned that we found at least in *Carcinus* a high degree of morphological chela variety, with specimens having a variable degree of heterochely and heterodonty (Fig. A2 A, B in appendix). Homochelic specimens (homodontic or somewhat heterodontic) had been observed, too (Fig. A2 C in appendix). At least in *Carcinus maenas*, this can be explained by morphological plasticity (see for example Brian et al. 2006, Duarte et al 2013). As for most of the other species examined herein, data concerning intraspecific variety are missing, we did not implement the chela morphology into the character matrix, either.

Karasawa et al. (2008) not only distinguished between the distinctiveness of sutures between male pleomeres, but also between pleomere movability. As the movability was difficult to determine in conserved specimens, we here only conceptualize suture distinctiveness (character 53). We determined character states that were different from Karasawa et al. 2020 regarding the mode of connection of the basal antenna article to the suborbital region in *Caphyra loevis*, *Raymanninus schmitti* and *Macropipus rugosus* (character 54). The presence or absence of a subterminal spine on the first gonopod is adapted from Karasawa et al. (2008), if data for the species were available (character 58).

Although we do not claim to present an exhaustive list of external morphological characters, we nevertheless conceptualize a few other conspicuous morphological differences as characters herein. They involve a putative respiratory canal formed by the prolonged endopodite of maxillipede 1 (character state 55; Fig. A3 A-C in appendix), which occurs in *Ashtoret*, *Calappa* and *Medorippe* (representing a morphological feature that once was used to assign them to Oxysytomata, a taxon that nowadays is widely refused; Garstang 1897a, Brösing et al. 2007, Davie et al. 2015b), and the degree of maxillipede 3 obscuring the mandibles when adducted to cover the buccal cavern. The latter represents an apparent morphological difference separating the thoracotreme from podotreme and heterotreme taxa examined here (character 56; Fig. A3 E, F in appendix). With respect to external features of pereiopods 2-4, *Sternodromia* and *Medorippe* differ from all other taxa by having a P4 being less than half as long as P2 and P3 (with a coxa being situated subdorsally; character state 57(0)). Gonopore positions are finally conceptualized. and assigned to taxa based on statements by Guinot et al. (2013; character 59).

Images showing several of characters 50-59 and their states are supplied in appendix.

50. Carapace, maximum width in relation to maximum length: larger or equal (0); smaller (1).

51. Carapace, surface structure: smooth or only loosely covered with soft setae (0); velvety, densely covered with rigid setae (1).

- 52. Carapace, orbit, dorsal margin, surface structure (Fig. A4 in appendix):** with one fissure (0); with two fissures (1), with distinct spine (2); smooth (3).
- 53. Male pleon, distinctiveness of sutures:** with distinct sutures between all pleomeres (0) with indistinct or no sutures between pleomeres 3-5 (1); with interrupted suture between pleomere 3 & 4 (2).
- 54. Antenna, basal article, mode of connection to suborbital region and epistome:** articulated (0); confluent (1).
- 55. Maxillipede 1, endopodite (adducted), degree of closing exhalant aperture (Fig. A3 A-D in appendix):** not closing (0); completely closing except for small distal opening (1).
- 56. Maxillipede 3 (adducted), degree of covering mandibles (Fig. A3 E, F in appendix):** completely covered, mandibles not visible (0); not completely covered, mandibles visible (1).
- 57. Pereiopod 4, length:** less than half as long as P3 (0); similar as in P3 (1).
- 58. Gonopod 1, subterminal spines:** absent (0); present (1)
- 59. Gonopore, position:** coxal in females and males (0); sternal in females, coxal in males (1); sternal in both females and males (2).

4 Results And Discussion Of Phylogenetic Analysis

Both phylogenetic analyses of the combined data set (BI and MP) resulted in nearly the same topologies (Fig. 33). In both analyses, the Portunoidea are recovered as monophyletic, being composed of three distinct clades we herein name according to the classification system established by Evans (2018): Portunidae being the sister group to a taxon comprising the monophyletic Carcinidae and Geryonidae. The position of Portunidae is a main difference to the phylogenetic hypothesis by Evans (2018), in which Geryonidae is the sister group to Carcinidae and Portunidae.

In our analysis, *Parathranites orientalis* is part of the Portunidae, being sister taxon to the remaining portunid representatives. In Evans (2018), this species was assigned to Carcinidae, although, it was already noted that this is not well supported. The position within Portunidae is consistent with our morphological data showing that all representatives of Portunidae have a median plate extending up to interosternite 5/6 (character state 8(1)), including a transverse sternal ridge from interosternite 6/7 to the anterior end of the median plate (character state 12(1); Fig. 12). The only other species with this combination of character states not assigned to Portunidae was *Macropipus tuberculatus* (Carcinidae in both our analyses and that of Evans 2018; see below). We further recovered monophyletic Thalamitinae (represented by *Caphyra loevis*, *Caphyra rotundifrons* and *Lissocarcinus orbicularis*) and monophyletic Carupinae *sensu lato* (represented by *Carupa tenuipes*, *Catoptrus nitidus* and *Lybistes nitidus*) following the nomenclature of Evans (2018). Only the positions of *Callinectes sapidus* and *Portunus inaequalis* differ between our analyses (Fig. 33).

In accordance with Evans (2018), the Geryonidae of our taxon sampling include *Chaceon*, *Ovalipes* and *Raymanninus*, with differing relationships between them, depending on the analysis (Fig. 33). Within Carcinidae, the status of *Carcinus maenas* and *Portumnus latipes* as sister taxa is consistent with previous molecular-based phylogenies (Schubart & Reuschel 2009, Spiridonov et al. 2014, Evans 2018). The position of carcinid *Pirimela denticulata* being more closely related to *Coelocarcinus foliatus* is unexpected, as *Pirimela* was robustly identified to be the sister taxon to the *Carcinus-Portumnus* clade (Schubart & Reuschel 2009, Spiridonov et al. 2014, Evans 2018). Actually, the phylogenetic placement of *Coelocarcinus* repeatedly made problems due to their unusual external morphology ("*unusual portunid crab*" – Ng 2002; "*certainly not a portunid*" - Karasawa et al. 2008), but Evans (2018) placed *Coelocarcinus* as basal carcinid taxon based on molecular data. Interestingly, identifying *Coelocarcinus foliatus* as sister taxon to carcinid *Xaiva* herein was solely based on morphological data, since for *Xaiva biguttata* as rare European species, no genetic data were available. However, *Coelocarcinus* lacks the P5 anterior coxa muscle originating at interopleurite 7/8 (character states 34(1), 34(3); Fig. 25), which is present in all other taxa of the *Carcinus-Portumnus-Pirimela-Coelocarcinus-Xaiva* clade, and finally, it is the only species of this clade not native to Europe (Ng 2002). *Liocarcinus navigator*, *Liocarcinus depurator* and "*Polybius*" *henslowii* are forming a monophyletic clade, but with *Liocarcinus depurator* being more closely related to "*Polybius*" than to *Liocarcinus navigator*, which is consistent with former findings uncovering the genus *Liocarcinus* to be polyphyletic (Schubart & Reuschel 2009, Plagge et al. 2016, Evans 2018). In accordance with Evans (2018), *Macropipus tuberculatus* and *Thia scutellata* form a monophyletic clade within Carcinidae (Fig. 33). Interestingly, for a species of Carcinidae, both taxa have an unusual axial skeleton configuration, with *Macropipus* having the transverse sternal ridge from interosternite 6/7 to the anterior end of the median plate (character state 12(1); Fig. 12), otherwise only present in Portunidae, and *Thia* having a median plate extending further than interosternite 4/5 (character state 8(0)), with all interosternites connected to the median plate (character states 13(0), 14(0), 15(0), 16(0); Fig. 11 E), a configuration that otherwise was only present in the heterotrematan outgroup. The latter was represented by a clade comprising all non-portunoid Heterotrema, but not *Medorippe lanata* (Fig. 33) which is positioned as sister to a clade comprising Heterotremata as well as Thoracotremata (not as heterotreme taxon as suggested by Jamieson & Tudge 1990). However, this and the position of *Ashtoret lunaris* as sister taxon to all remaining Heterotremata (Fig. 33; instead of being sister to *Calappa*; Lu et al. 2020) should be considered with caution due to the limited outgroup taxon sampling.

5. Discussion On The Evolution Of The P5-swimming Crab Morphotype

5. 1 Characterising the P5-swimming crab morphotype

Based on our analysis, the P5-swimming crab morphotype characterisation by Herter (1932), Kühl (1933), Schäfer (1954) and Hartnoll (1971) can now be evaluated by determining the character states that all P5-swimmer species in our taxon sample share. Character states occurring in all P5-swimming crabs are summarised in Fig. 34 and table 2 (the character matrix involving the entire taxon sampling is included in the appendix). It is interesting to note that P5-swimmers only occurred in Portunoidea. With respect to how merus length (character 44) should be interpreted, Steudel (1998) noted that species showing the P5 swimming leg with a long merus were generally able to perform the same swimming movements as P5-swimmers with a short merus, which is in accordance with findings by Schmidt et al. (2020), discovering that theoretical ranges of motion in P5 articulations in *Carupa tenuipes* with a long merus were similar to those of P5-swimming crabs with a short merus. In *Liocarcinus pusillus*, a species morphologically similar to *Liocarcinus depurator*, but with a longer merus, swimming movements were principally the same as in *L. depurator* (although somewhat less effective; see high-speed recordings of video 1, 2, 3 in appendix). *Liocarcinus navigator* with a merus being even longer also showed a swimming similar to that of typical P5-swimmers, even though it was not as fast and agile (personal observation). In all these species, the P5 anterior coxa muscle originates at the median plate, which was also the case in all typical P5-swimmers with a short merus (character state 34(2)) corroborating the hypothesis by Hazerli & Richter (2020) that this is crucial for P5-swimming. Consequently, we do not consider a short merus mandatory to identify a swimming leg, although we are well aware that with variable merus length, there may be high morphological variation in species assigned to the morphotype, which presumably results in a high variation in the effectiveness of P5-swimming ability. However, with respect to the interpretation on how the morphotype evolved, we consider this to be less important (see below). In summary, P5-swimming crabs can unambiguously be identified by the character states shown in Fig. 35, but with the merus length (character 44) representing a state that “merely” influences the effectivity of P5-swimming. A subdorsal position of the P5 coxa (see for example Hartnoll 1971) without doubt also influences P5-swimming effectivity, but was not considered here because of the difficulty to conceptualise discrete character states due to high interspecific variability. We further consider *Xaiva biguttata* (albeit unusual) P5-swimmer, since it has the swimming leg with a long merus, including the P5 anterior coxa muscle originating at the median plate, even though unlike in all other P5-swimmers, it additionally originates at interpleurite 7/8 (like in, but not homologous to *Thia*; character state 34(3); Fig. 25 C, 35). It should eventually be mentioned that with the merus length, the dactylus width (character 47) also varies between species. (Fig. 4-6), and with *Raymanninus schmitti* and *Caphyra loevis* there were even species that had all unambiguous P5-swimmer states mentioned above except for a broad paddle-like dactylus. In *Raymanninus*, however, the P5 anterior coxa muscle originating at the median plate has to be confirmed in other specimens, because the musculature was poorly preserved in the only specimen available.

Hazerli & Richter (2020) identified morphological features characterising the P5-swimming morphotype based on muscular and axial skeleton, but also external features of *Liocarcinus depurator*. However, the greater taxon sampling of our study revealed that especially many axial skeleton features mentioned by Hazerli & Richter (2020) differ between P5-swimmer taxa, namely the shape and configuration of the interosternite 7/8 process (character 20; morpheme 25 in Hazerli & Richter 2020), the presence and extension of the median plate process (characters 9, 10; morpheme property 18 in Hazerli & Richter 2020), and the distance of interosternite 7/8’s medial edge to the median plane (character 17; morpheme property 22 in Hazerli & Richter 2020). However, it should be mentioned that at least all P5-swimmer taxa with a short merus have the same character states with regard to the latter two characters. Apart from that, it is conspicuous that all unambiguous P5-swimming crab character states shown in Fig. 35 solely refer to features of the P5, including the P5 anterior coxa muscle originating at the median plate.

Table 2. Character states present in all P5-swimming crabs.

5.2. Ancestral state reconstructions and evolutionary transformations of P5-swimmer character states

Fig. 35 shows ancestral state reconstructions and transformations of character states that unambiguously characterise P5-swimmers (raw Mesquite data that show transformations of all morphological character states are supplied in the appendix). The most important finding is that the P5 swimming morphotype (with a long merus) already evolved in the stem species of Portunoidea (Fig. 35). Starting from this condition, evolutionary transformations proceeded into two general directions. One direction represents the evolution into a more efficient P5-swimmer with a short merus. Based on our data, this happened several times independently within Portunoidea (at least twice each in Portunidae and Carcinidae, once in Geryonidae). The second direction is characterised by the loss of P5-swimming crab character states of variable degree. A complete reversal of the swimming leg into a walking leg occurred independently in *Chaceon*, *Carcinus*, and *Pirimela* (given that the position of *Pirimela* as sister taxon to the clade *Coelocarcinus-Xaiva* is correct; see “4 Results and discussion of phylogenetic analysis”), from ancestors that had already “lost” one or several P5-swimming leg states (Fig. 35). *Catoptrus* evolved a P5 walking leg, but retained the anterior coxa origin at the median plate and interosternite 7/8 (typical for P5-swimmers; character state 34(2)) from an ancestor that had already “lost” its short merus and broad dactylus (Fig. 35). Generally, within Portunidae, P5-swimmer character states were reversed with variable degree, but noticeably, in all taxa except for *Libystes alphonsi* (which has a significantly smaller median plate), this anterior coxa muscle configuration is retained.

It is interesting to note that a broad paddle-like dactylus (character state 47(1); Fig. 30 B) is always associated (=coherent) with a carpal propodus insertion (character state 45(1); Fig. 30 B) and a concave proximo-ventral dactylus margin (character state 48(1); Fig. 30 B, F), but not vice versa (Fig. 35). Furthermore, if a paddle-like dactylus (character state 47(1); Fig. 30 B) evolved back to a slender dactylus (state 47(0); Fig. 30 A), while the carpal propodus insertion is retained (state 45(1); Fig. 30 B), a concave proximo-ventral dactylus margin (state 48(1); Fig. 30 B, F) is retained, too (which also represents some sort of coherence). This is the case in the common ancestor of both *Caphyra* species, the common ancestor of *Catoptrus* and *Libystes*, and in *Raymanninus schmitti* (Fig. 35). *Caphyra rotundifrons* with its P5 propodus and dactylus proximo-ventral margins forming a subchela is an exception.

Character	State	Statement
11	1	Sternum, median plate, dorsal margin, shape: more or less convex, without indentations and/or gaps between thoracomeres.
15	1	Sternum, interosternite 6/7, connection to median plate: absent.
16	1	Sternum, interosternite 7/8, connection to median plate: absent.
18	2	Sternum, interosternite 4/5, medial margin, shape: transversal with lower margin being most medial, but not touching.
23	0	Sella turcica, covering of dorsal median plate margin: present.
34	2 OR 3	Pereiopod 5, anterior coxa muscle, origin: at median plate + interosternite 7/8 OR at median plate + interosternite 7/8 + interopleurite 7/8
43	0	Pereiopod 5, long setae, arrangement: arranged in dense fringes along podomere margins.
45	1	Pereiopod 5, carpus, disto-dorsal margin, propodus insertion: present.
46	1	Pereiopod 5, propodus, lobe-like expansion of postero-ventral margin: present.
47	1	Pereiopod 5, dactylus, maximum width in relation to maximum width of P5 merus: larger.
48	1	Pereiopod 5, dactylus, proximo-ventral margin, shape: concave.
50	0	Carapace, maximum width in relation to maximum length: larger or equal.

The origin of the P5 anterior coxa muscles is certainly one of the key characters in the evolution of P5 swimming. Its evolution is, however, difficult to interpret. Our data show that the conditions typical for a P5-swimmer (origin at median plate and interosternite 7/8; state 34(2); Fig. 25 D, E, F) is the plesiomorphic state in Portunoidea (Fig. 35), but it is ambiguous, from which state it evolved (Fig. A5 in appendix), either from an origin at interosternite 7/8 only (state 34(0); Fig. 25 A) or from an origin at both interosternite 7/8 and interopleurite 7/8 (state 34(1); Fig. 25 B, 26). In this case, assuming that an alteration in the muscle origin during the course of evolution took place by a gradual shift of one (or several) muscle fibre(s) in its proximal attachment site(s), for an interpretation of muscle origin transformations, the connection of interosternite 7/8 to the median plate has to be considered in evolutionary scenarios. It is well thinkable that a shift in the fibres originating at interosternite 7/8 to the median plate could take place as long as interosternite 7/8 was connected to the median plate (character state 16(0)). Consequently, even if based on our ancestral state reconstruction, the state of this character is ambiguous for the ground pattern of Heterotremata (Fig. A6 in appendix), we prefer a scenario, in which interosternite 7/8 is connected to the median plate in the heterotrematan stem species. A reversal of the P5 anterior coxa muscle origin at both the median plate and interosternite 7/8 (state 34(2); Fig. 25 D, E, F) back to an origin at interosternite 7/8 (state 34(0); Fig. 25 A) or at interosternite 7/8 and interopleurite 7/8 (state 34(1); Fig. 25 B, 26) in taxa with an interosternite 7/8 connection to the median plate being absent is imaginable assuming a degeneration of the muscle fibres attached to the median plate. This must have happened in the stem species of the *Carcinus-Portumnus-Pirimela-Coelocarcinus-Xaiva* clade (Fig. 35). Indeed, *Xaiva* regained a P5 anterior coxa muscle origin at the median plate, but its phylogenetic position should be considered carefully, as it is only based on morphological data.

Until now, few hypotheses on the evolution of P5-swimming crabs exist. Hartnoll (1971) and Steudel (1998) were the first to formulate explicit hypotheses, but not based on phylogenetic relationships. Hartnoll (1971) suggested a transformation series to swimming crabs based largely on one single morphological feature, the dactylus width of pereiopods 2-5. As far as we understand it (Hartnoll 1971 was rather imprecise in his statements), *Carcinus* was considered a "basal" genus, with its rudimentarily broader P5 podomeres compared to those of the P4 being interpreted as a plesiomorphic

character state. With its pereopods 2-4 considered to be modified for swimming, "*Polybius henslowii*" is considered by Hartnoll (1971) as more advanced P5-swimmer compared to those with only the P5 being modified, presumably assuming that the former evolved from the latter (which is well possible considering our data; Fig. 35). Concerning *Carcinus*, in accordance with previous phylogenies, our combined analysis identified it as highly derived taxon within Portunoidea (Fig. 33, 35; Karasawa et al. 2008, Schubart & Reuschel 2009, Evans 2018). We consider the P5 podomere broadening in *Carcinus* not to be homologous to those in P5-swimmers and other taxa with a paddle-like dactylus (see also 3.1.2 *Characters concerning the external morphology of pereopod 5*).

Steudel (1998) distinguished between several swimming crab morphotypes (termed "*Konstruktionstypen*" there) denoted after distinct genera, namely the *Liocarcinus* type, *Polybius* type, *Ovalipes* type and *Portumnus* type, but already recognised that only the former three types were capable of the typical P5-swimming movements. However, it was assumed that the *Ovalipes* type evolved from the *Portumnus* type, independently from the *Liocarcinus* and *Polybius* type, an assumption that mainly was based on the sternum shape (see character state 4(1) herein; Fig. 8 B, E). In contrast, our data show that the similar sternum shape in *Ovalipes* and *Portumnus* evolved independently from each other (Fig. A7 in appendix). It was further suggested, that the *Liocarcinus* and *Polybius* type both independently evolved from a non-swimming morphotype that is adapted to effective underwater running (termed "*Unterwasserrenner*" there, our translation) with a rather straight and broad sternum (character states 3(1) and 4(0) herein) and well-developed walking legs. The evolution into the *Liocarcinus*- and/or *Polybius*-type then was simply interpreted as a further "optimization" of underwater running. However, since our analysis recovered underwater runner *Carcinus* and *Chaceon* as derived species within Portunoidea that secondarily lost P5-swimmer character states (Fig. 33, 35), Steudel's assumption here is refused. Spiridonov et al. (2014) also briefly discussed the evolution of the P5-swimmer morphotype, considering the statements of Steudel (1998) and a phylogeny deduced from molecular data, but no morphological characters. In contrast to our view, it was concluded that it most probably evolved three times independently in Carcinidae, Geryonidae and Portunidae, respectively.

Spiridonov (2020) speculated that a broad paddle-like dactylus adapted to burying represented a preadaptation to a P5-swimmer. Several of the species examined by us generally are considered as taxa specialised in a burying mode of life, namely *Ashtoret lunaris*, *Corystes cassivelaunus*, *Calappa granulata*, *Portumnus latipes* and *Thia scutellata* (Garstang 1897a, b, Schäfer 1954, Rees 2001, Türkay & Stecher 2013), perhaps also *Coelocarcinus foliatus* (Ng 2002). However, of these genera, only *Ashtoret*, *Portumnus* and *Coelocarcinus* have a P5 paddle-like dactylus (character state 47(1)), but *Ashtoret* evolved this state probably independently of Portunoidea, and *Portumnus* as well as *Coelocarcinus* are derived portunoids of which a specialisation in a burying existence represents an apomorphy, which evolved *after* P5-swimming (Fig. 35). Based on these data, the assumption by Spiridonov is wrong. As already mentioned, *Varuna litterata*, *Ashtoret lunaris*, and also probably portunoid *Portumnus latipes* (perhaps also *Coelocarcinus foliatus*) are known to be effective swimmers, including morphological features similar to P5-swimmers that facilitate swimming (like the paddle-like dactyli of pereopods), but also some, which are definitely different from those of P5-swimming crabs (like the lack of the P5 anterior coxa muscle origin at the median plate). Especially, typical swimming movements above the carapace thus cannot be performed by these taxa, as was shown by Schmidt et al. (2020).

With regard to axial skeleton features, an interesting aspect of P5-swimming crab evolution refers to the "brachyuran sella turcica" (sensu Guinot et al. 2013), a sella turcica connected to interosternite 7/8. However, in the species examined herein, this connection was only present in outgroup taxa *Sternodromia monodi*, *Medorippe lanata*, *Eriocheir sinensis* and *Varuna litterata* (character state 19(0); Fig. 14 A, B, D, E). In all other taxa, interosternite 7/8 is without a direct connection to the sella turcica (character state 19(1); Fig. 14 G, H, 15 A-D), instead possessing an interosternal process, which sometimes touches interosternite 6/7. This suggests that in the ground pattern of Heterotremata, the direct connection of interosternite 7/8 to the sella turcica (the "brachyuran sella turcica") was secondarily lost. Interestingly, in the taxa examined, a missing connection of interosternite 7/8 to the sella turcica was always associated with a junction plate forming the junction plate cavity, which offers room and attachment sites especially for the large P5 extrinsic musculature of P5-swimmers. We thus interpret this as a preadaptation for the evolution into a P5-swimming crab. This is an apparent explanation, why the P5-swimming crab morphotype could have evolved in Heterotremata only.

6. Declarations

6.1 Ethics approval and consent to participate

Not applicable

6.2 Consent for publication

Not applicable

6.3 Availability of data and materials

Data generated or analysed during this study that are not included in this published article (and its appendix) are available from the corresponding author on reasonable request.

6.4 Competing interests

The authors declare that they have no competing interests.

6.5 Funding

The present project is funded by the Deutsche Forschungsgemeinschaft (DFG RI 837/24-1). The mCT machine was sponsored by the Deutsche Forschungsgemeinschaft (DFG INST 264/38-1 FUGG) and the Land Mecklenburg-Vorpommern.

6.6 Authors' contributions

Dennis Hazerli (DH) and Stefan Richter (SR) created the design of the study. DH performed morphological examinations, analysed and interpreted morphological data, created 3D models, images and further visualisations, with feedback from SR. Christoph Gert Höpel (CH) managed the molecular data set and conducted the phylogenetic analysis. DH wrote the original draft of the manuscript except for the part with regard to the methods concerning molecular data sets and phylogenetic analysis, which was written by CH. A revised version of the manuscript was written by DH with contributions from SR. All authors read and approved the final manuscript.

6.7 Acknowledgements

Our thanks go to our colleagues of the Allgemeine & Spezielle Zoologie of the University of Rostock, Germany, especially to M. Sc. Markus Grams, who helped with the high-speed camera recordings. We further thank Kristin Arnold, Prof. Dr. Angelika Brandt and Bianca Trautwein of the Senckenberg Research Institute and Natural History Museum in Frankfurt, Germany, Dr. Nancy F. Mercado Salas, Kathrin Philipps-Bussa and Petra Wagner of the Zoological Museum of the Center of Natural History in Hamburg, Germany, John D. Slapcinsky of the Florida Museum of Natural History, University of Florida in Gainesville, USA, and Dr. Stephen Keable of the Australian Museum in Sydney, Australia, for providing the voucher material. We are thankful for the comments of anonymous reviewers.

References

1. Ahyong ST, O'Meally D. Phylogeny of the Decapoda Reptantia: Resolution using three molecular loci and morphology. *Raffles B Zool.* 2004;52(2):673–93.
2. Bellwood O. The occurrence, mechanics and significance of burying behaviour in crabs (Crustacea: Brachyura). *J Nat Hist.* 2002;36:1223–38.
3. Brian JV, Fernandes T, Ladle RJ, Todd PA. Patterns of morphological and genetic variability in UK populations of the shore crab, *Carcinus maenas* Linnaeus, 1758 (Crustacea: Decapoda: Brachyura). *J exp mar biol ecol.* 2006;329:47–54.
4. Brösing A, Richter S, Scholtz G. Phylogenetic analysis of the Brachyura (Crustacea, Decapoda) based on characters of the foregut with establishment of a new taxon. *J Zool Syst Evol Res.* 2007;45:20–32. <https://doi.org/10.1111/j.1439-0469.2006.00367.x>.
5. Castelin M, Van Steenkiste N, Pante E, Harbo R, Lowe G, Gilmore SR, Therriault TW, Abbott CL. A new integrative framework for large-scale assessments of biodiversity and community dynamics, using littoral gastropods and crabs of British Columbia, Canada. *Mol Ecol Resour.* 2016;16(6):1322–39. <https://doi.org/10.1111/1755-0998.12534>.
6. Caulier G, Flammang P, Gerbaux P, Eeckhaut I. When a repellent becomes an attractant: harmful saponins are kairomones attracting the symbiotic Harlequin crab. *Sci Rep-UK.* 2013;3:2639. <https://doi.org/10.1038/srep02639>.
7. Cochran DM. The skeletal musculature of the blue crab, *Callinectes sapidus*. *Ratheun Smithson Misc Colls.* 1935;92:1–76.
8. Da Silva JM, Creer S, dos Santos A, Costa AC, Cunha MR, Costa FO, Carvalho GR. Systematic and evolutionary insights derived from mtDNA COI barcode diversity in the Decapoda (Crustacea: Malacostraca). *PLoS ONE.* 2011;6(5):e19449. <https://doi.org/10.1371/journal.pone.0019449>.
9. Davie PJF, Guinot D, Ng PKL. 2015a. Anatomy and functional morphology of Brachyura. *Treatise Zool - Anatomy, Taxon Biol - Crustac to Vol Transl from French Trait Zool 9 (C):* 11–163. https://doi.org/10.1163/9789004190832_004.
10. Davie PJF, Guinot D, Ng PKL. 2015b. Phylogeny of Brachyura. *Treatise Zool - Anatomy, Taxon Biol - Crustac to Vol Transl from French Trait Zool 9 (C):* 921–979. https://doi.org/10.1163/9789004190832_019.
11. Duarte RC, Augusto AR, Flores AV, Queiroga H. Conspecific cues affect stage-specific molting frequency, survival, and claw morphology of early juvenile stages of the shore crab *Carcinus maenas*. *Hydrobiologia.* 2013;724:55–66. <https://doi.org/10.1007/s10750-013-1712-5>.
12. Evans N. Molecular phylogenetics of swimming crabs (Portunoidea Rafinesque, 1815) supports a revised family-level classification and suggests a single derived origin of symbiotic taxa. *PeerJ.* 2018. <https://doi.org/10.7717/peerj.4260>.
13. Garstang W. 1897a. On some modifications of structure subservient to respiration in decapod Crustacea which burrow in sand; with some remarks on the utility of specific characters in the genus *Calappa*, and the description of a new species of *Albunea* *J Cell Sci s2-40 (158):* 211–232. <https://doi.org/10.1242/jcs.s2-40.158.211>.
14. Garstang W. Contributions to marine bionomics: II. The function of antero-lateral denticulations of the carapace in sand-burrowing crabs. *J Mar Biolog Assoc.* 1897b;4(4):396–401. <https://doi.org/10.1017/S002531540000552X>.
15. Göpel T, Wirkner CS. Morphological description, character conceptualization and the reconstruction of ancestral states exemplified by the evolution of arthropod hearts. *PLoS ONE.* 2018;13(9):e0201702. <https://doi.org/10.1371/journal.pone.0201702>.
16. Grant T, Kluge AG. Transformation series as an ideographic character concept. *Cladistics.* 2004;20:23–31. <https://doi.org/10.1111/j.1096-0031.2004.00003.x>.
17. Guinot D, Tavares M, Castro P. Significance of the sexual openings and supplementary structures on the phylogeny of brachyuran crabs (Crustacea, Decapoda, Brachyura), with new nomina for higher-ranked podotreme taxa. *Zootaxa.* 2013;3665:1–414.

18. Hay ME, Pawlik JR, Duffy JE, Fenical W. Seaweed–herbivore–predator interactions: hostplant specialization reduces predation on small herbivores. *Oecologia*. 1989;81(3):418–27. <https://doi.org/10.1007/bf00377093>.
19. Hartnoll RG. The occurrence, methods and significance of swimming in the Brachyura. *Anim Behav*. 1971;19:34–50. [https://doi.org/10.1016/S0003-3472\(71\)80132-X](https://doi.org/10.1016/S0003-3472(71)80132-X).
20. Hazerli D, Richter S. 2020. Why "swimming crabs" are able to swim - The importance of the axial skeleton: A comparison between the "swimming crab" *Liocarcinus depurator* and two other brachyuran crabs (*Cancer pagurus*, *Carcinus maenas*) using μ CT and 3D-reconstruction. *Arthropod Struct Dev* 59. <https://doi.org/10.1016/j.asd.2020.100972>.
21. Hennig W. *Phylogenetic Systematics*. Urbana: University of Illinois Press; 1966.
22. Herter K. Beiträge zur Zentrenfunktion Zehnfüssiger Krebse. *Z f vergl Physiol*. 1932;17:209–66.
23. Jamieson BGM, Tudge CC. Dorippids are Heterotremata: evidence from ultrastructure of the spermatozoa of *Neodorippe astuta* (Dorippidae) and *Portunus pelagicus* (Portunidae) Brachyura: Decapoda. *Mar Biol*. 1990;106:347–54.
24. Karasawa H, Schweitzer CE, Feldmann RM. Revision of Portunoidea Rafinesque, 1815 (Decapoda: Brachyura) with emphasis on the fossil genera and families. *J Crust Biol*. 2008;28:82–127.
25. Kim J-I, Do J-I, Karagozlu TD, Kim MZ, C.-B. Analysis of complete mitochondrial genome of *Matuta planipes* (Decapoda, Brachyura, Matutidae) from South Korea. *T&F*. 2019;4:906–7. <https://doi.org/10.1080/23802359.2019.1579070>.
26. Kühl H. Die Fortbewegung der Schwimmkrabben mit Bezug auf die Plastizität des Nervensystems. *Z vergl Physiol*. 1933;19:489–521.
27. Li G, Xu J, Wang H, Chen X, Xu Y, Zheng Y, Mao X, Yang S. Identification and analysis of the complete mitochondrial genome sequence of *Eriocheir sinensis*. *Mitochondrial DNA A DNA Mapp Seq Anal*. 2016;27(6):3923–4. <https://doi.org/10.3109/19401736.2014.987267>.
28. Lu X, Gong L, Zhang Y, Chen J, Liu L, Jiang L, Lü Z, Liu B, Tong G, Wei X. The complete mitochondrial genome of *Calappa bilineata*: The first representative from the family Calappidae and its phylogenetic position within Brachyura. *Genomics*. 2020;112(3):2516–23. <https://doi.org/10.1016/j.ygeno.2020.02.003>.
29. Meng XL, Jia FL, Liu P, Li J. The complete mitogenome of blue swimming crab *Portunus pelagicus* Linnaeus, 1766 (Crustacea: Decapoda: Portunidae). *Mitochondrial DNA A DNA Mapp Seq Anal*. 2016;27(4):2789–90. <https://doi.org/10.3109/19401736.2015.1053068>.
30. Miller MA, Pfeiffer W, Schwartz T. 2010. Creating the CIPRES Science Gateway for inference of large phylogenetic trees. 2010 Gatew Comput Environ Workshop (GCE): 1–8. <https://doi.org/10.1109/GCE.2010.5676129>.
31. Ng PKL. On the unusual swimming crab, *Coelocarcinus foliatus* Edmondson, 1930, with description of a new species from the Indian Ocean (Decapoda, Brachyura, Portunidae). *Crustaceana*. 2002;75:51–60. <https://doi.org/10.1163/156854002317373519>.
32. Ng PKL, Guinot D, Davie PJF. *Systema Brachyurorum: Part I An annotated checklist of extant brachyuran crabs of the world*. *Raffles B Zool Suppl*. 2008;17:1–286.
33. Place AR, Feng X, Steven CR, Fourcade HM, Boore JL. Genetic markers in blue crabs (*Callinectes sapidus*) II: Complete mitochondrial genome sequence and characterization of genetic variation. *J Exp Mar Biol Ecol*. 2005;319(1–2):15–27. <https://doi.org/10.1016/j.jembe.2004.03.024>.
34. Plagge C, Son NT, Ng PLK, Türkay M, Streit B, Klaus S. *Liocarcinus corrugatus* (Pennant, 1777) (Crustacea: Brachyura: Portunidae): a cosmopolitan brachyuran species? *Raffles B Zool*. 2016;64:374–88. <http://doi.org/10.5281/zenodo.5355780>.
35. Radulovici AE, Sainte-Marie B, Dufresne F. DNA barcoding of marine crustaceans from the Estuary and Gulf of St Lawrence: a regional-scale approach. *Mol Ecol Resour*. 2009;9(S1):181–7. <https://doi.org/10.1111/j.1755-0998.2009.02643.x>.
36. Rambaut A. *FigTree: Tree figure drawing tool version 1.4.2*. Institute of Evolutionary Biology, University of Edinburgh; 2014.
37. Raupach MJ, Barco A, Steinke D, Beermann J, Laakmann S, Mohrbeck I, Neumann H, Kihara TC, Pointner K, Radulovici A, Segelken-Voigt A, Wesse C, Knebelberger T. The Application of DNA barcodes for the identification of marine crustaceans from the North Sea and adjacent regions. *PLoS ONE*. 2015;10(9):E0139421. <https://doi.org/10.1371/journal.pone.0139421>.
38. Rees EIS. Habitat specialization by *Thia scutellata* (Decapoda: Brachyura) off Wales. *J Mar Biol Ass UK*. 2001;81:697–8.
39. Richter S. Homology and synapomorphy-symplesiomorphy—neither synonymous nor equivalent but different perspectives on the same phenomenon. *Cladistics*. 2017;33:540–4. <https://doi.org/10.1111/cla.12180>.
40. Richter S, Wirkner CS. A research program for evolutionary morphology. *J Zool Syst Evol Res*. 2014;52:338–50. <https://doi.org/10.1111/jzs.12061>.
41. Rieppel O. 1999. *Einführung in die computergestützte Kladistik*. Pfeil, München 1999.
42. Ronquist F, Teslenko M, van der Mark P, Ayres DL, Darling A, Höhna S, Larget B, Liu L, Suchard MA, Huelsenbeck JP. MrBayes 3.2: Efficient Bayesian phylogenetic inference and model choice across a large model space. *Syst Biol*. 2012;61(3):539–42. <https://doi.org/10.1093/sysbio/sys029>.
43. Schäfer W. Form und Funktion der Brachyuren-Schere. *Abh Senckenb Naturforsch Ges*. 1954;489:1–65.
44. Schmidt M, Hazerli D, Richter S. Kinematics and morphology: a comparison of 3D-patterns in the 5th pereopod of swimming and non-swimming crab species (Malacostraca, Decapoda, Brachyura). *J Morphol*. 2020;281(12):1547–66. <https://doi.org/10.1002/jmor.21268>.
45. Schubart C, Reuschel S. A proposal for a new classification of Portunoidea and Cancroidea (Brachyura: Heterotremata) based on two independent molecular phylogenies. *Nat Hist*. 2009;18:533–50.
46. Schuh RT. *Biological Systematics: Principles and applications*. Cornell University Press; 2000.
47. Secretan S. Le plan de base du squelette axial d'un Décapode Macroure et sa terminologie. *C r hebd séances Acad sci*. 1980;291:877–80.

48. Secretan S. The sella turcica of crabs and the endophragmal system of decapods. *J Nat Hist.* 1998;32(10–11):1753–67.
49. Secretan S. La lame de jonction, base de l'organisation phragmales des décapodes brachyours. *Crustaceana.* 2002;75(3–4):637–41.
50. Sereno PC. Logical basis for morphological characters in phylogenetics. *Cladistics.* 2007;23:565–87. <https://doi.org/10.1111/j.1096-0031.2007.00161.x>.
51. Sin YW, Lai JCY, Ng PKL, Chu KH. Phylogeny of Dorippoidea (Crustacea: Decapoda: Brachyura) inferred from three mitochondrial genes. *Invertebr Syst.* 2009;23(3):223–30. <https://doi.org/10.1071/IS09020>.
52. Sotelo G, Posada D, Moran P. Low-mitochondrial diversity and lack of structure in the velvet swimming crab *Necora puber* along the Galician coast. *Mar Biol.* 2009;156:1039–48. <https://doi.org/10.1007/s00227-009-1148-7>.
53. Spiridonov VA. Results of the Rumphius biohistorical expedition to Ambon (1990). *Zool Med Leiden.* 1999;73(4):63–97.
54. Spiridonov VA, Neretina TV, Schepetov D. Morphological characterization and molecular phylogeny of Portunoidea Rafinesque, 1815 (Crustacea Brachyura): Implications for understanding evolution of swimming capacity and revision of the family-level classification. *Zool Anz.* 2014;253:404–29. <https://doi.org/10.1016/j.jcz.2014.03.003>.
55. Spiridonov VA. An update of phylogenetic reconstructions, classification and morphological characters of extant Portunoidea Rafinesque, 1815 (Decapoda, Brachyura, Heterotremata), with a discussion of their relevance to fossil material. *Geologija.* 2020;63:133–66. <https://doi.org/10.5474/geologija.2020.014>.
56. Spirito CP. An analysis of swimming behavior in the portunid crab *Callinectes sapidus*. *Mar Behav Physiol.* 1972;1:261–76. <https://doi.org/10.1080/10236247209386902>.
57. Stephenson W, Rees M. The endeavour and other Australian Museum collections of portunid crabs (Crustacea, Decapoda, Portunidae). *Rec Aust Mus.* 1968;27(13):285–98. <https://doi.org/10.3853/j.0067-1975.27.1968.447>.
58. Steudel SC. 1998. Über Schwimmkrabben und Krabbenschwimmen. Dissertation zur Erlangung des Doktorgrades der Naturwissenschaften. Johann WolfgangGoethe-Universität, 1–183.
59. Swofford D, Maddison W. Parsimony, character-state reconstructions, and evolutionary inferences. *Systematics; 1992. Historical Ecology, and North American Freshwater Fishes,* 186–223.
60. Szucsich N, Wirkner CS. Homology: A synthetic concept of evolutionary robustness of patterns. *Zoolog Scr.* 2007;36(3):281–28. <https://doi.org/10.1111/j.1463-6409.2007.00275.x>.
61. Tan MH, Gan HM, Lee YP, Austin CM. 2014. The complete mitogenome of the moon crab *Ashtoret lunaris* (Forskål, 1775), (Crustacea; Decapoda; Matutidae). *Mitochondrial DNA Part A,* 27(2): 1313–4. <http://dx.doi.org/10.3109/19401736.2014.945572>.
62. Tsang LM, Schubart CD, Ahyong ST, Lai JCY, Au EYC, Chan T-Y, Ng PKL, Chu KH. Evolutionary history of true crabs (Crustacea: Decapoda: Brachyura) and the origin of freshwater crabs. *Mol Biol Evol.* 2014;31(5):1173–87. <https://doi.org/10.1093/molbev/msu068>.
63. Türkay M, Stecher J. Occurrence of Pennant's swimming crab, *Portumnus latipes*, along the German North Sea coast. *Mar Biodiv.* 2013;43:199–204.
64. Wagner GP. *Homology, Genes, and Evolutionary Innovation.* Princeton: Princeton University Press; 2014.
65. Wang Q, Wang J, Wu Q, Xu X, Wang P, Wang Z. Insights into the evolution of Brachyura (Crustacea: Decapoda) from mitochondrial sequences and gene order rearrangements. *Int J Biol Macromol.* 2021;170:717–27. <https://doi.org/10.1016/j.ijbiomac.2020.12.210>.
66. Wirkner CS, Richter S. Evolutionary morphology of the circulatory system in Peracarida (Malacostraca; Crustacea). *Cladistics.* 2010;26:143–67. <https://doi.org/10.1111/j.1096-0031.2009.00278.x>.
67. Yang M, He Y, Liu H. Characterization of complete mitochondrial genome of Japanese sponge crab *Lauridromia dehaani* (Rathbun, 1923). *Mitochondrial DNA B Resour.* 2020;5(2):1496–7. <https://doi.org/10.1080/23802359.2020.1742611>.

Figures

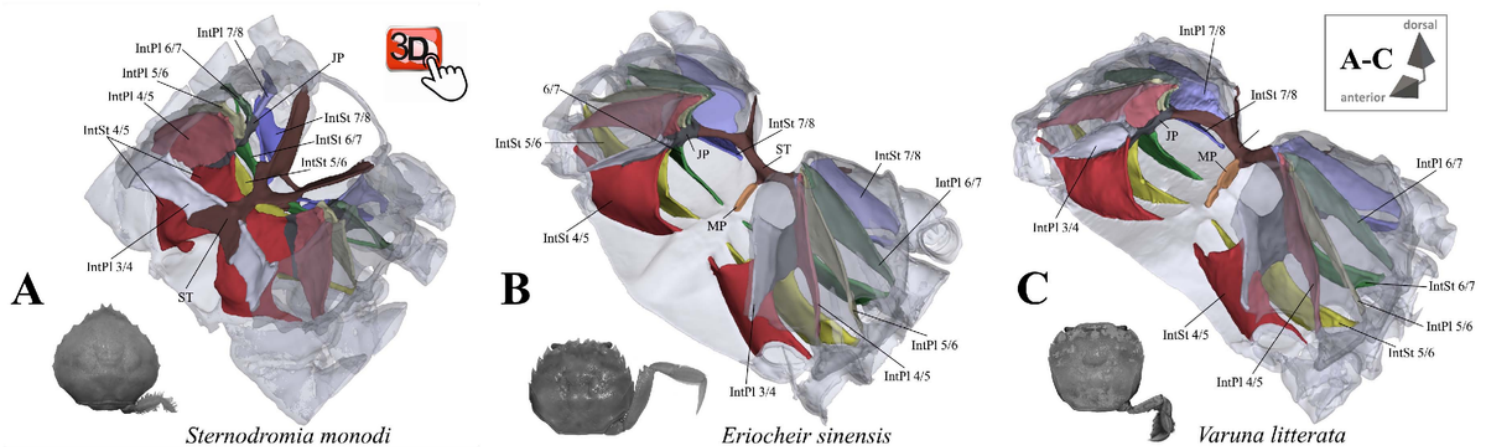


Figure 1

Representations of three-dimensional (3D) data from the axial skeletons of outgroup taxa of Podotremata and Thoracotremata. **A** Dromiidae (Podotremata). **B, C** Varunidae (Thoracotremata). Each taxon is also represented by an image, showing the cephalothorax with right 5th pereiopod from dorsal view. **IntPI** Interpleurite (with pair of numbers indicating between which thoracomeres it is situated). **IntSt** Interosternite (with pair of numbers indicating between which thoracomeres it is situated). **JP** Junction plate. **ST** Sella turcica.

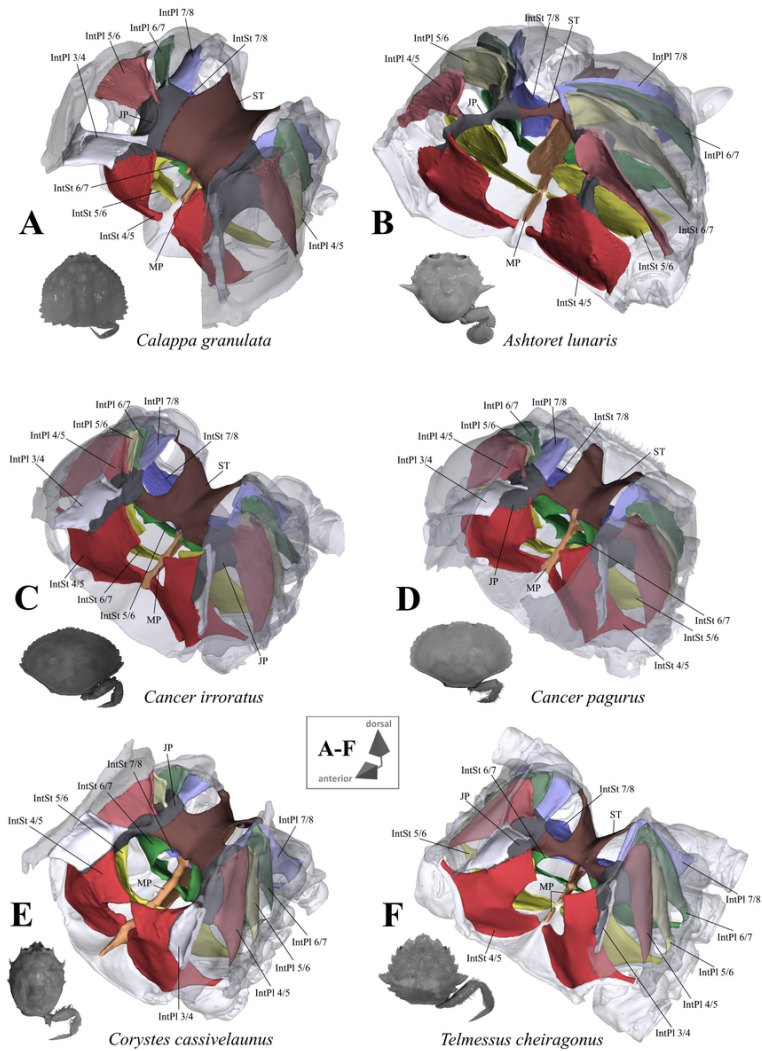


Figure 2

Representations of three-dimensional (3D) data from the axial skeletons of outgroup taxa of Heterotremata. **A** Calappidae (Calappoidea). **B** Matutidae (Calappoidea) **C, D** Cancridae (Cancroidea). **E** Corystidae (Corystoidea). **F** Cheiragonidae (Cheiragonoidea). Each taxon is also represented by an image, showing the cephalothorax with right 5th pereiopod from dorsal view. **IntPI** Interpleurite (with pair of numbers indicating between which thoracomeres it is situated). **IntSt** Interosternite (with pair of numbers indicating between which thoracomeres it is situated). **JP** Junction plate. **ST** Sella turcica.

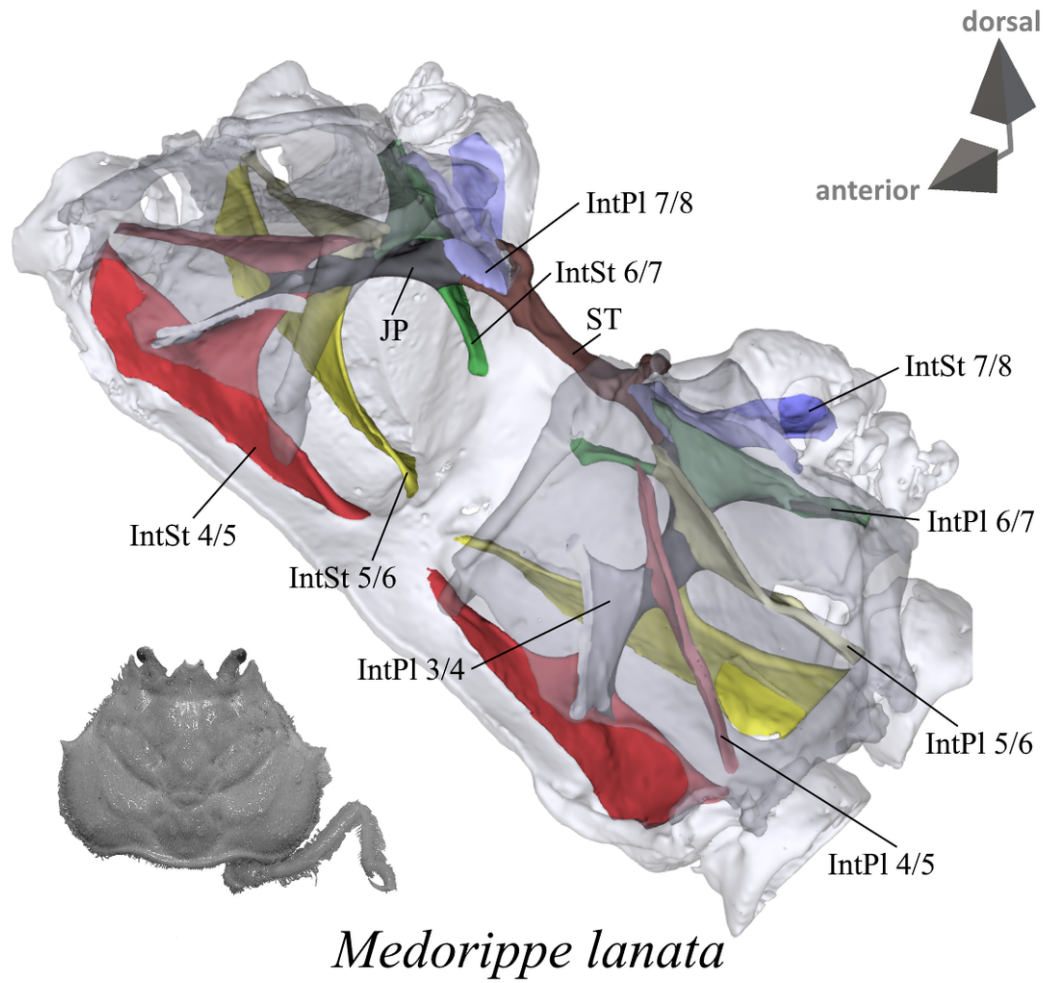


Figure 3

Representations of three-dimensional (3D) data from the axial skeleton of outgroup taxon *Medorippe lanata*. The species is also represented by an image, showing the cephalothorax with right 5th pereopod from dorsal view. **IntPl** Interpleurite (with pair of numbers indicating between which thoracomeres it is situated). **IntSt** Interosternite (with pair of numbers indicating between which thoracomeres it is situated). **JP** Junction plate. **ST** Sella turcica.

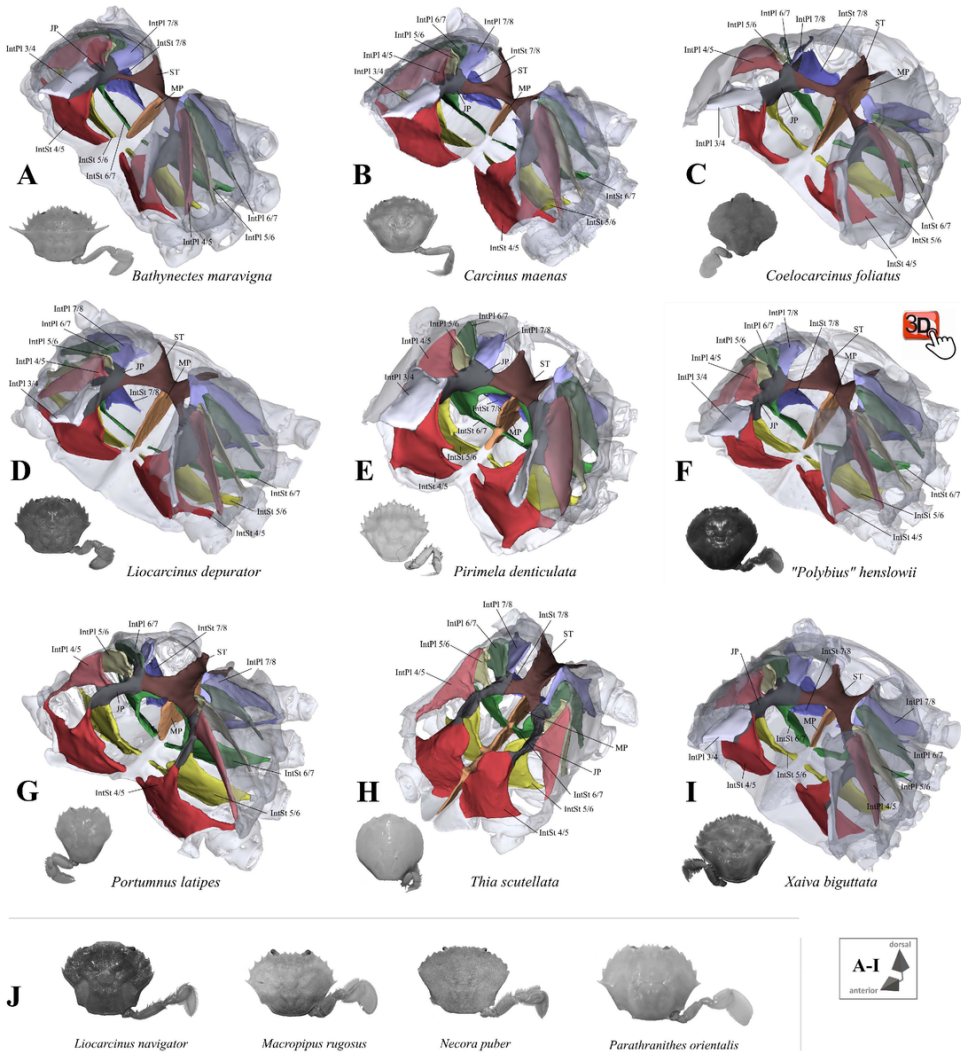


Figure 4
 Portunoid taxa assigned to Carcinidae based on Evans (2018). **A-I** Representations of three-dimensional (3D) data from the axial skeletons together with an image of each species, showing the cephalothorax with right or left 5th pereopod from dorsal view. **J** Images of species (showing the cephalothorax with right 5th pereopod from dorsal view) of which the axial skeleton was examined in this study, but without a complete three-dimensional (3D) model being created. **IntPI** Interpleurite (with pair of numbers indicating between which thoracomeres it is situated). **IntSt** Interosternite (with pair of numbers indicating between which thoracomeres it is situated). **JP** Junction plate. **ST** Sella turcica.

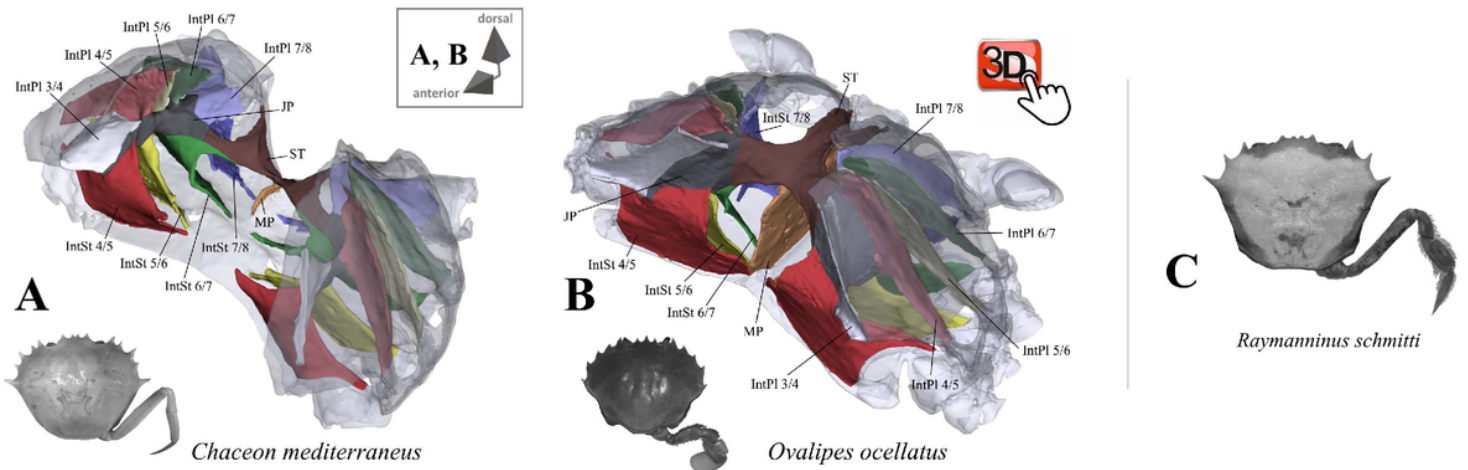


Figure 5

Portunoid taxa assigned to Geryonidae based on Evans (2018). **A, B** Representations of three-dimensional (3D) data from the axial skeletons together with an image of each species, showing the cephalothorax with right or left 5th pereiopod from dorsal view. **C** Image of *Raymanninus schmitti* of which the axial skeleton was examined in this study, but without a complete three-dimensional (3D) model being created (showing the cephalothorax with right 5th pereiopod from dorsal view). **IntPl** Interpleurite (with pair of numbers indicating between which thoracomeres it is situated). **IntSt** Interosternite (with pair of numbers indicating between which thoracomeres it is situated). **JP** Junction plate. **ST** Sella turcica

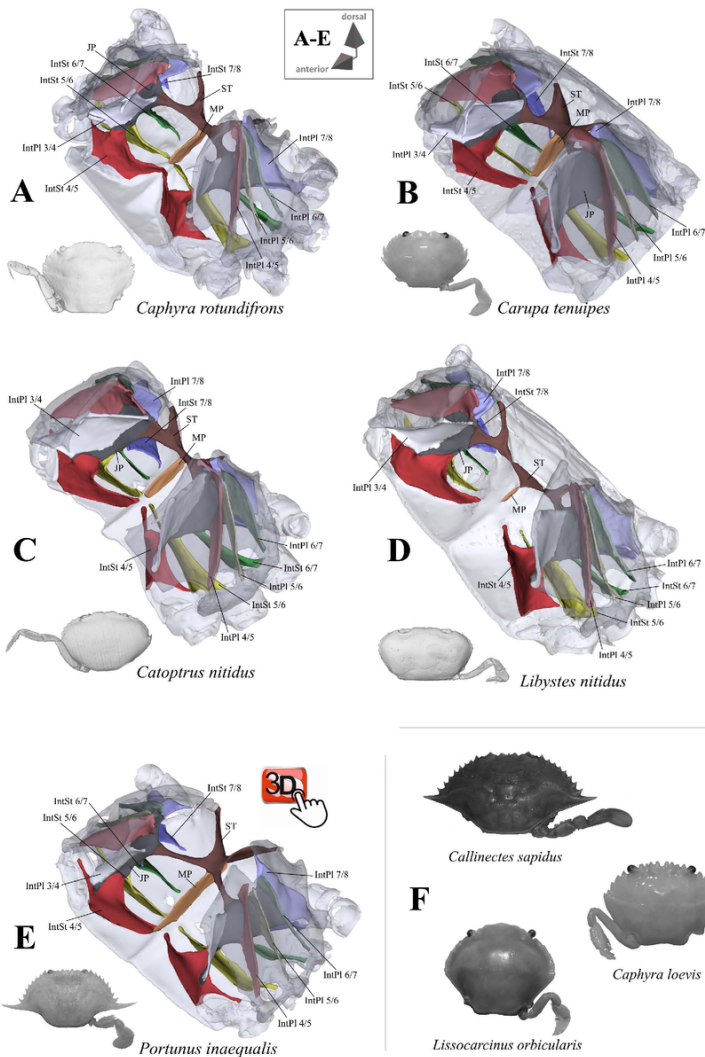


Figure 6

Portunoid taxa assigned to Portunidae based on Evans (2018). **A-E** Representations of three-dimensional (3D) data from the axial skeletons together with an image of each species, showing the cephalothorax with right or left 5th pereiopod from dorsal view. **F** Images of species (showing the cephalothorax with right 5th pereiopod from dorsal view) of which the axial skeleton was examined in this study, but without a complete three-dimensional (3D) model being created. **IntPl** Interpleurite (with pair of numbers indicating between which thoracomeres it is situated). **IntSt** Interosternite (with pair of numbers indicating between which thoracomeres it is situated). **JP** Junction plate. **ST** Sella turcica.

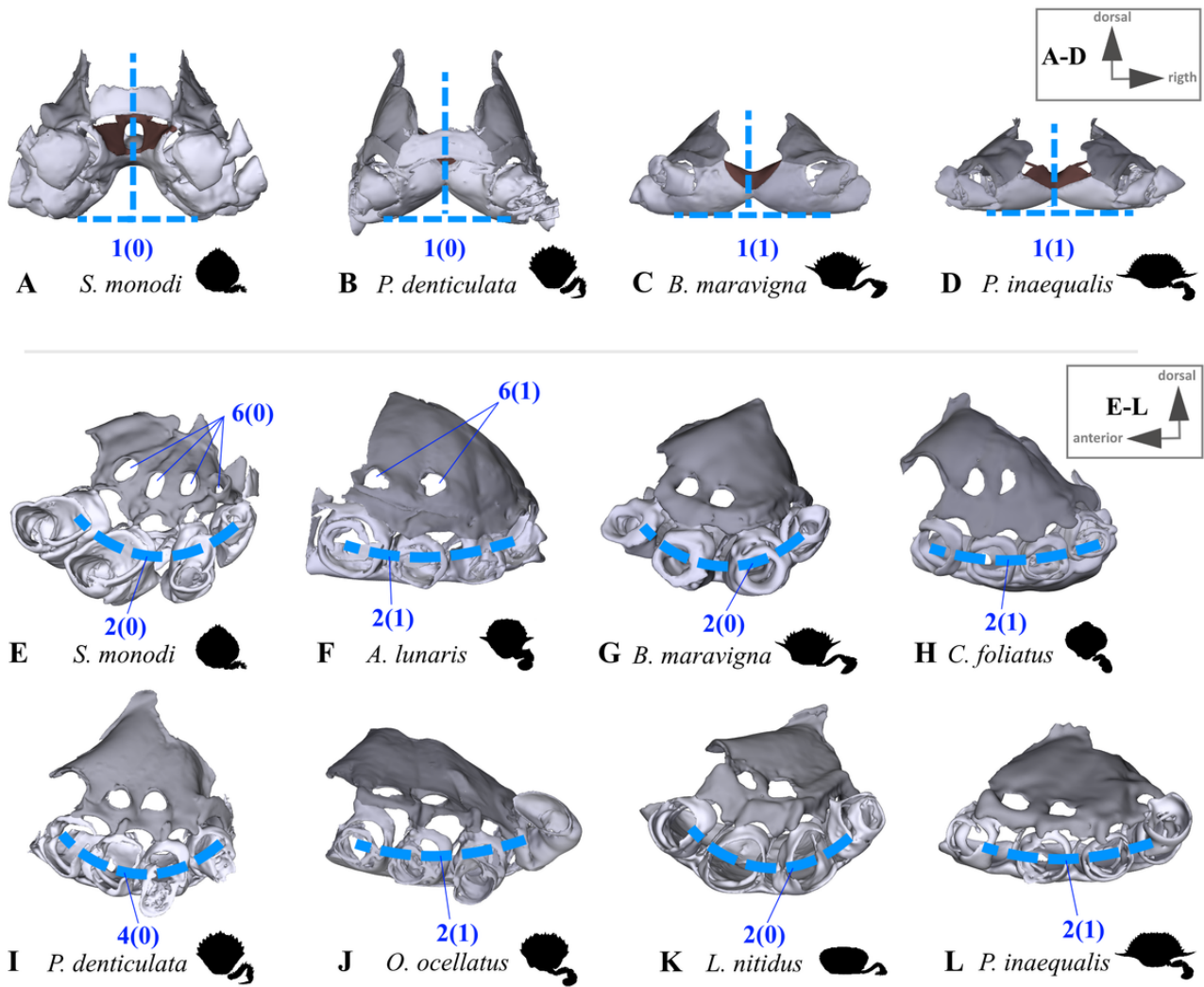


Figure 7

Examples showing character states concerning axial skeleton shape and axial skeleton proportion. **A-D** Posterior view indicating sternum width in relation to axial skeleton height (character 1). **E-L** Lateral view indicating degree of sternum curving (character 2) and number of gill openings (character 6).

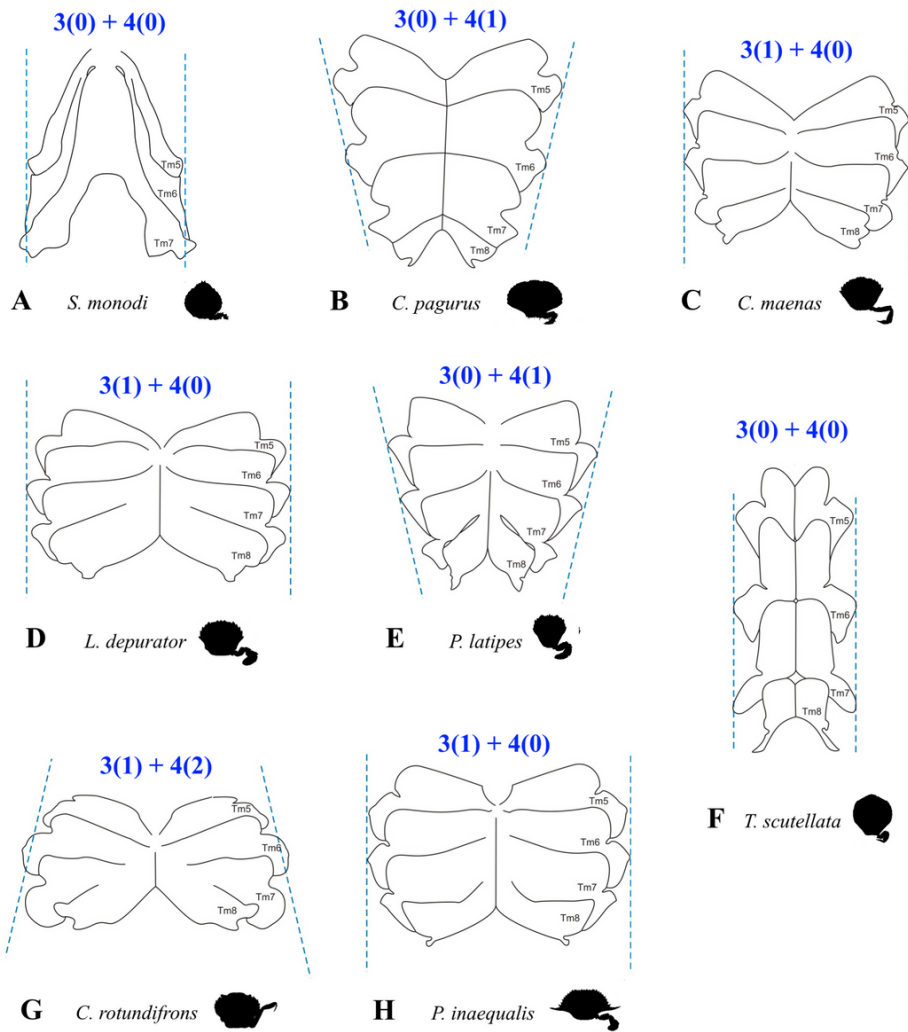


Figure 8

Drawings showing the variability in sternum shape seen from ventral, with character states concerning sternum proportion (character 3) and sternum shape (character 4). **Tm** Thoracomere (with number).

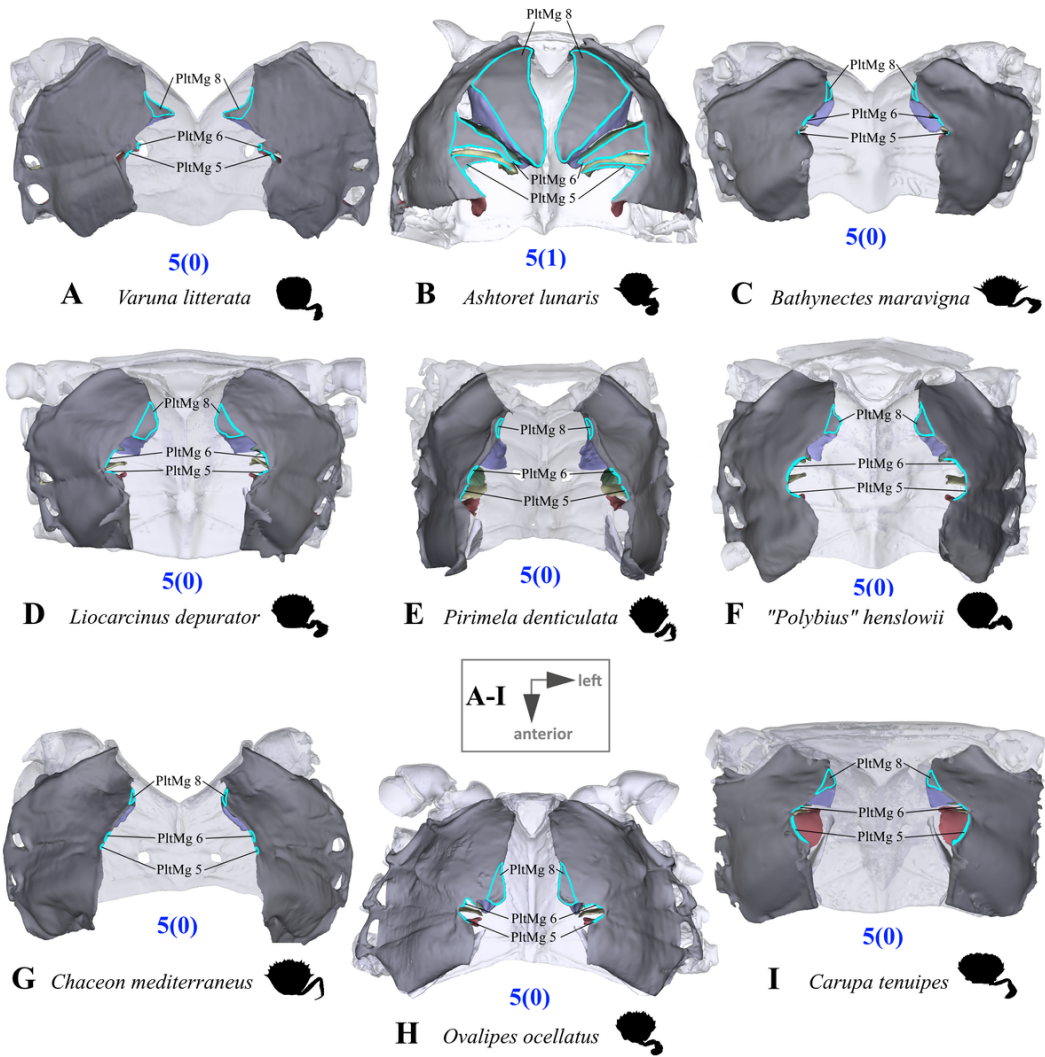


Figure 9
 Examples showing the variability in pleural medial margins of thoracomerites 5-6 and 8 (character 5) seen from dorsal. Note the prominent pleural expansions in *Ashtoret lunaris* (B). **PltMg** Pleural medial margin (with number indicating thoracomerite).

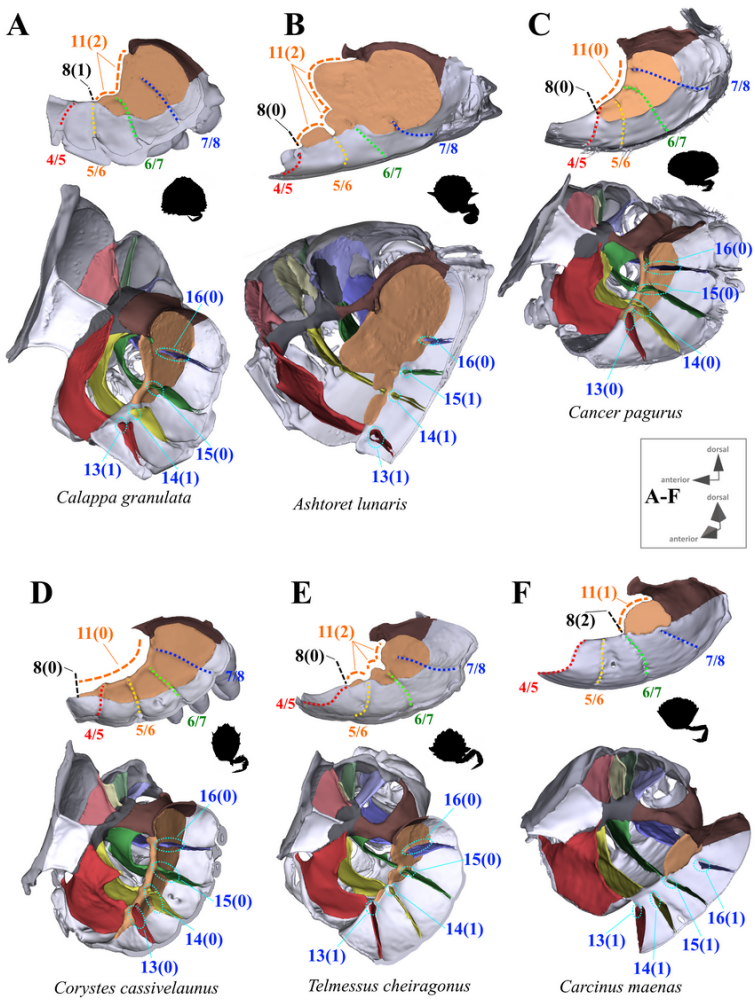


Figure 10

Examples showing characters referring to anterior median plate extension (character 8), shape of dorsal median plate margin (character 11) and the absence or presence in connections of interosternites to the median plate (characters 13-16) in axial skeletons seen from lateral (respective upper image) and from antero-dorsal (respective lower image). In sideview, pair of numbers separated by backslash indicate between which thoracomeres the respective interosternite is situated.

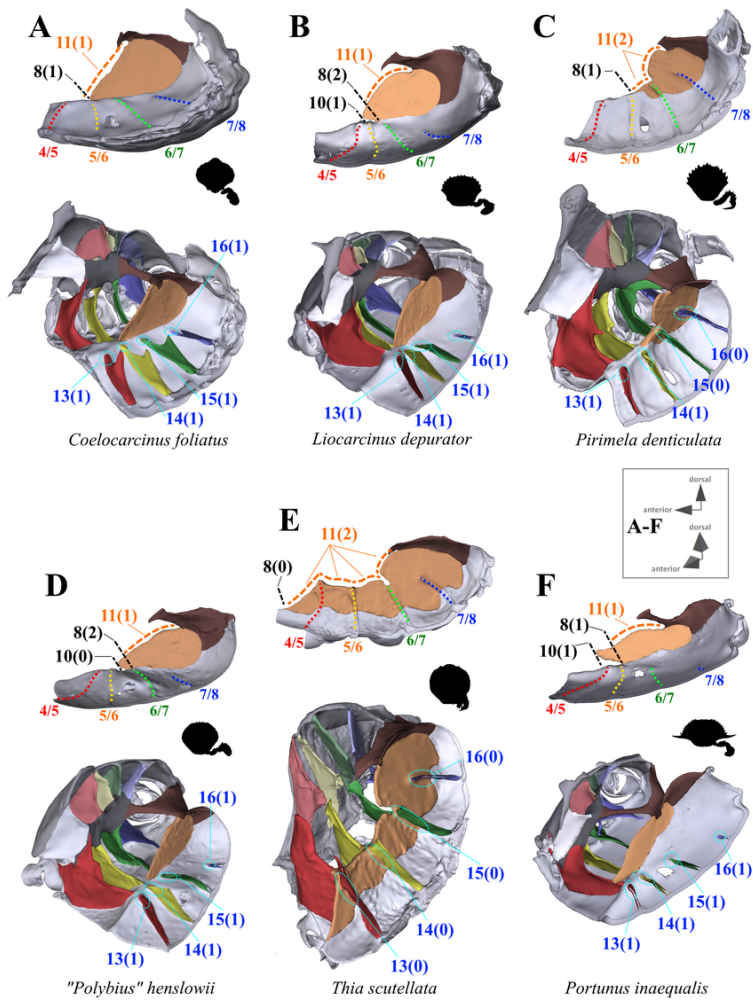


Figure 11

Examples showing characters referring to anterior median plate extension (character 8), length of median plate anterior process (if present; character 10), shape of dorsal median plate margin (character 11) and the absence or presence of connections of interosternites to the median plate (characters 13-16) in axial skeletons seen from lateral (respective upper image) and from antero-dorsal (respective lower image). Pair of numbers separated by backslash in sideview indicate between which thoracomeres the respective interosternite is situated.

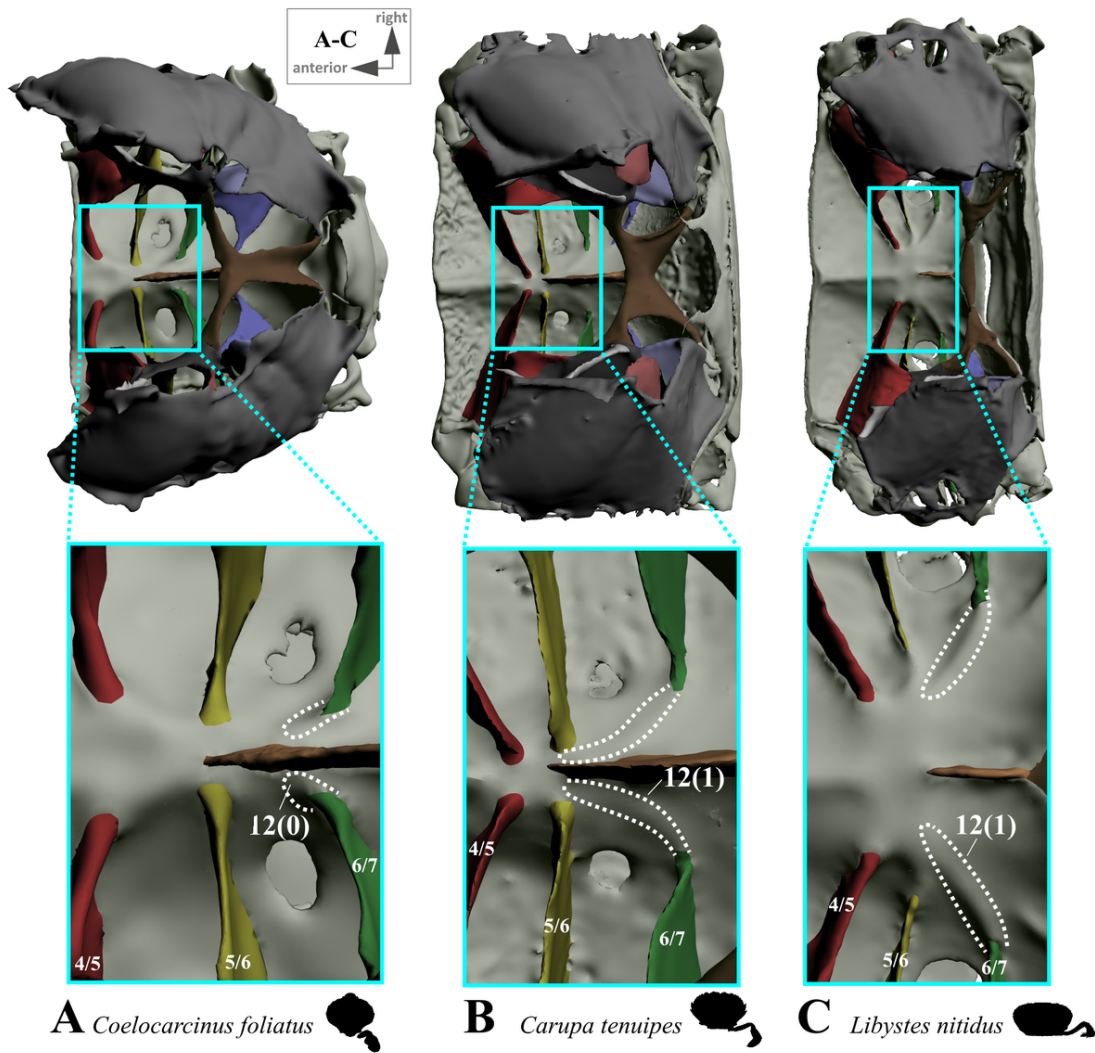


Figure 12

Examples showing characters referring to the absence or presence of a transverse sternal ridge from interosternite 6/7 to anterior end of median plate (character 12) in axial skeletons seen from dorsal. Pair of numbers separated by backslash indicate between which thoracomeres the respective interosternite is situated

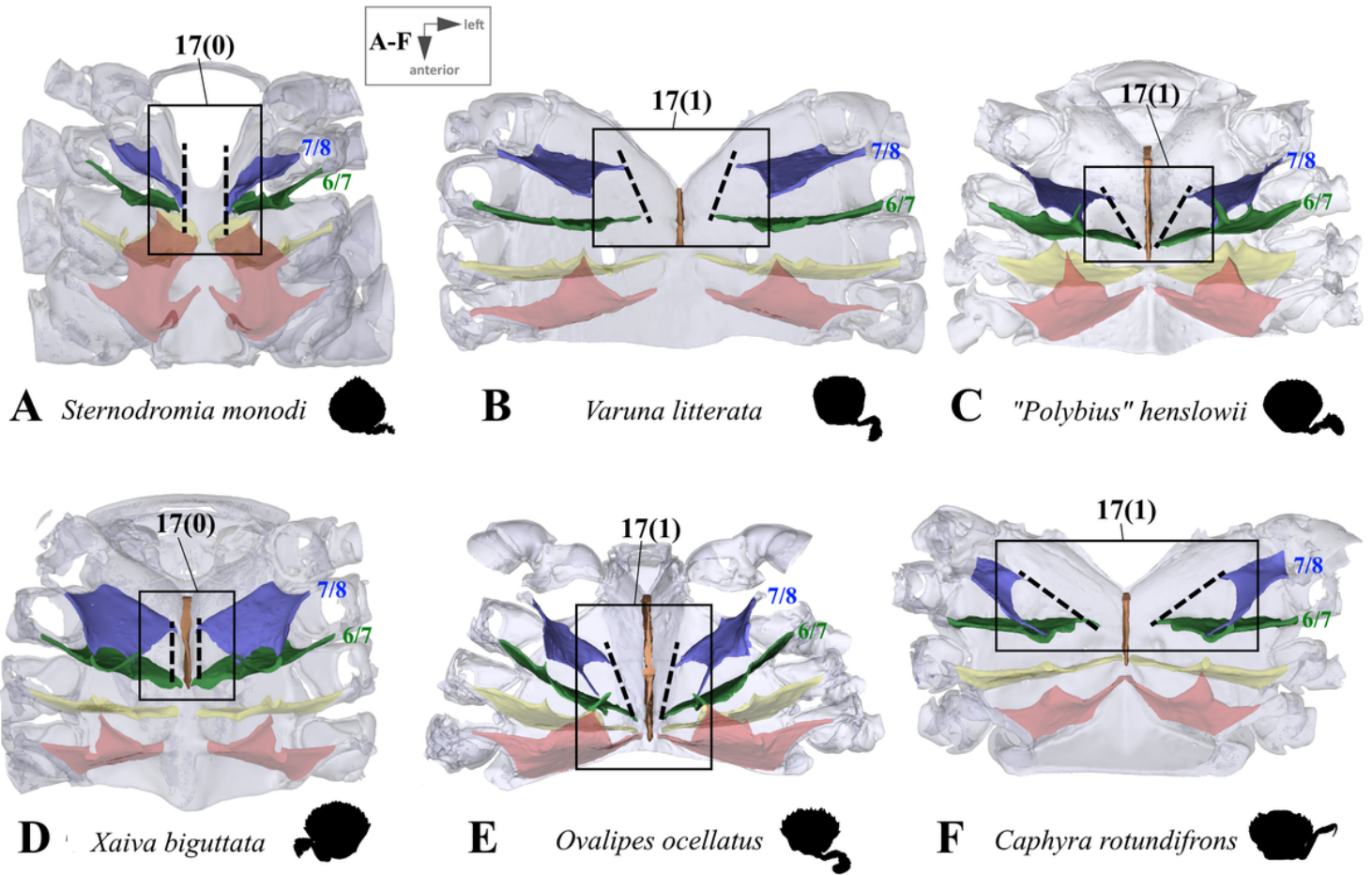


Figure 13

Examples showing characters referring to distance of medial edge to median plane in intersternite 6/7 compared to intersternite 7/8 (character 17) in axial skeletons seen from dorsal. Pair of numbers separated by backslash indicate between which thoracomeres the respective intersternite is situated.

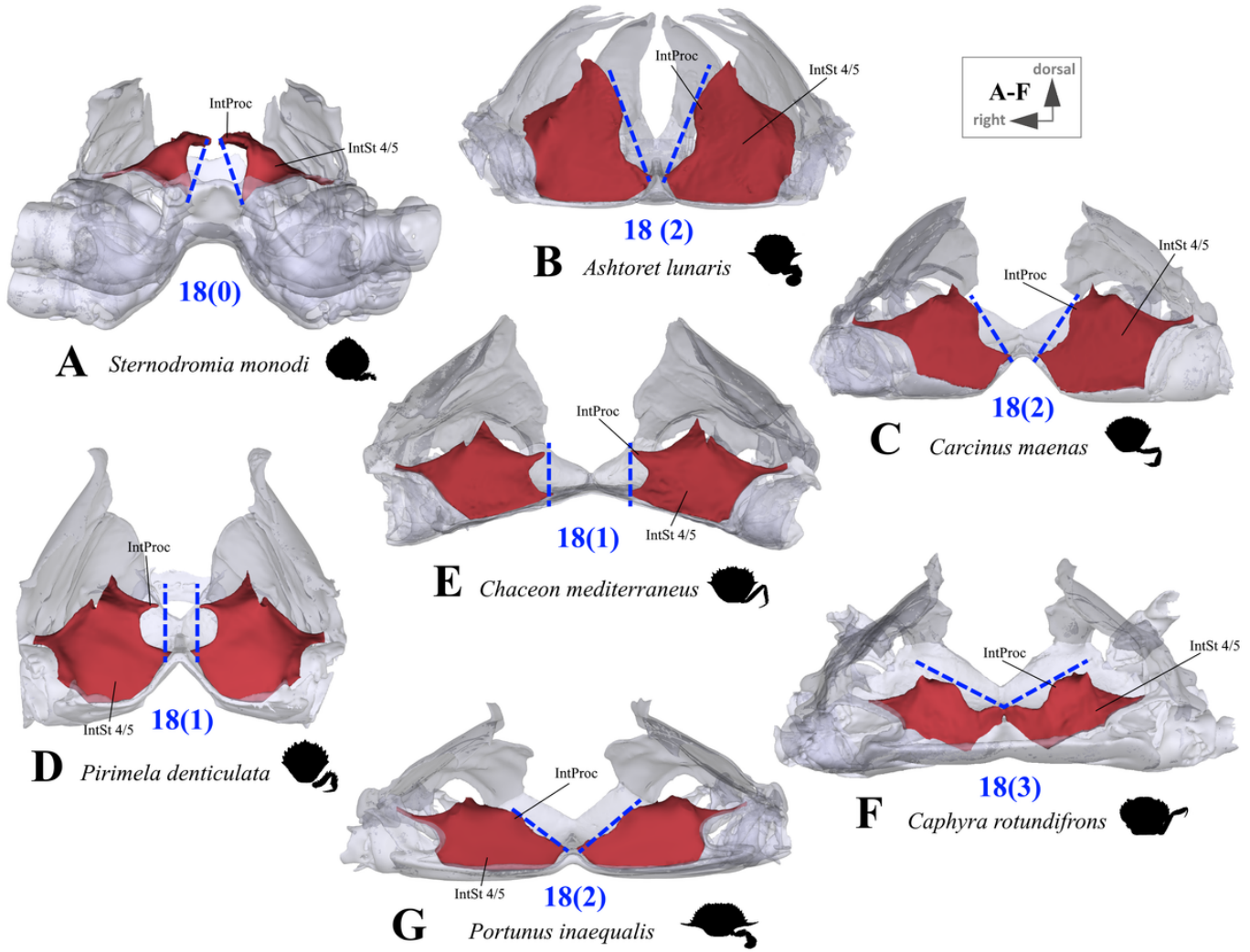


Figure 14

Examples showing character 18 referring to the shape of interosternite 4/5 medial margin seen from anterior. **IntProc** Interosternal process. **IntSt 4/5** Interosternite between thoracomeres 4 and 5.

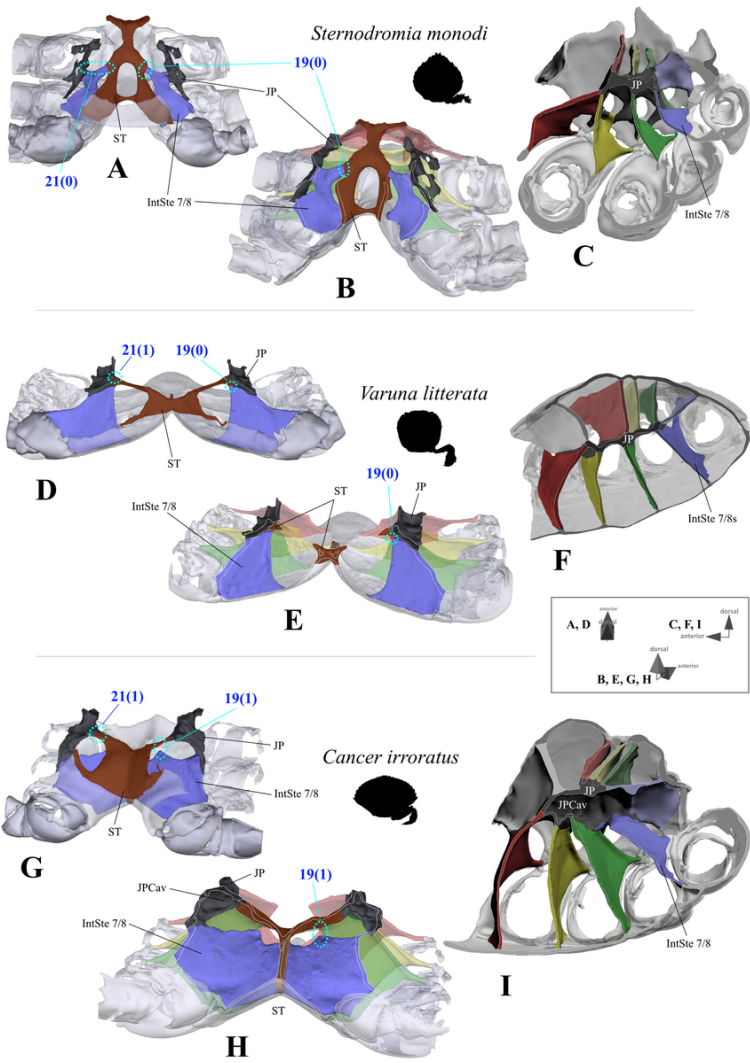


Figure 15

Examples showing character states concerning the absence or presence of the connection of interosternite 7/8 to sella turcica (character 19) and the absence or presence of a connection of junction plate to sella turcica (character 21) in the axial skeleton seen from posterior (**A, B, D, E, G, H**). Note that in the species with interosternite 7/8 being connected to the sella turcica (character state 19(0); **B, E**), the junction plate does not form a cavity while in the species without a connection (character state 19(1); **G, H**), a junction plate cavity is present (**I**). **JP** Junction plate. **JPCav** Junction plate cavity. **IntSt 7/8** Interosternite between thoracomeres 7 and 8. **ST** Sella turcica.

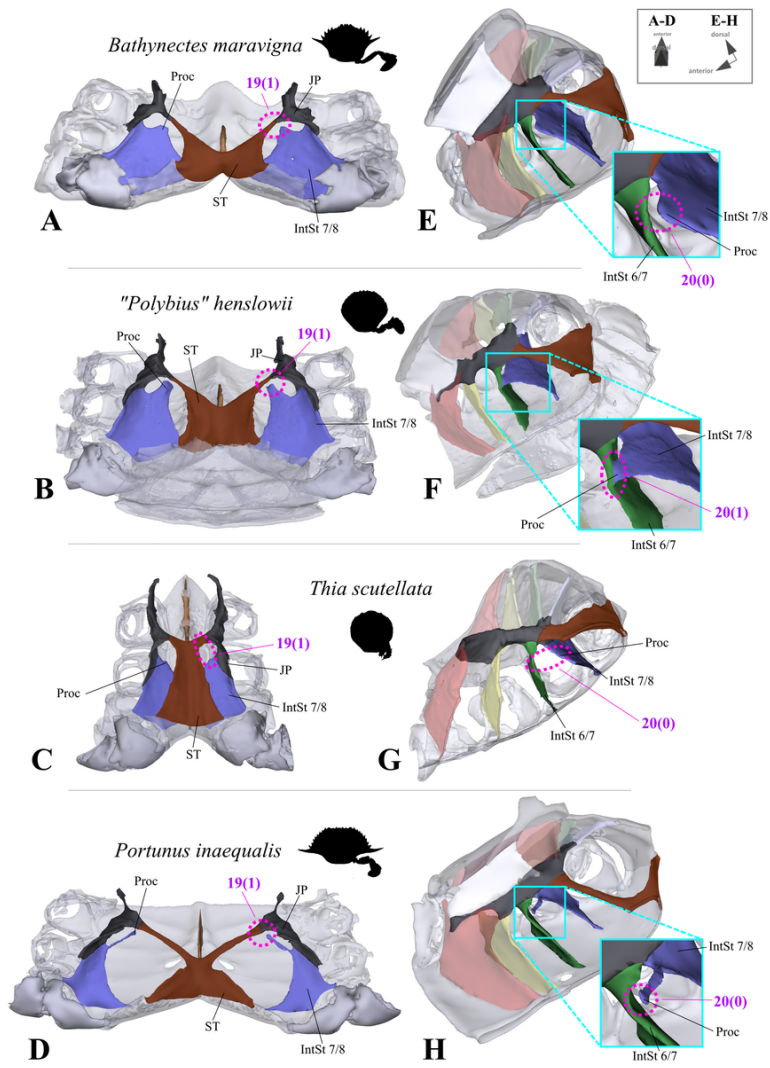


Figure 16

Variability in the shape of the interosternite 7/8 process. **A-D** Examples showing character states concerning the absence or presence of the connection of interosternite 7/8 to sella turcica (character 19) in the axial skeleton seen from postero-dorsal. **E-H** Examples showing character states concerning the absence or presence of a connection of interosternite 7/8 process to interosternite 6/7 (character 20) in the axial skeleton seen from left side.

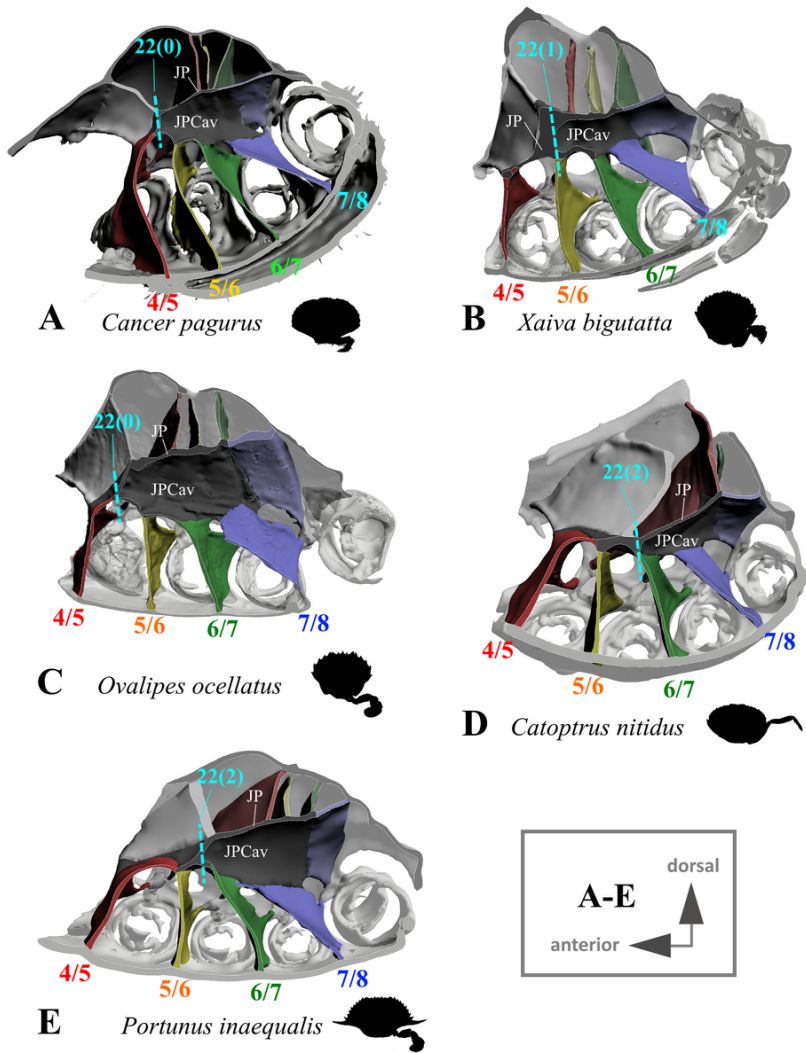


Figure 17

Variability in the shape of the junction plate cavity with examples showing character states concerning the anterior extension of the junction plate (character 22). Pair of numbers separated by backslash indicate between which thoracomeres the respective interosternite is situated. **JP** Junction plate. **JPCav** Junction plate cavity.

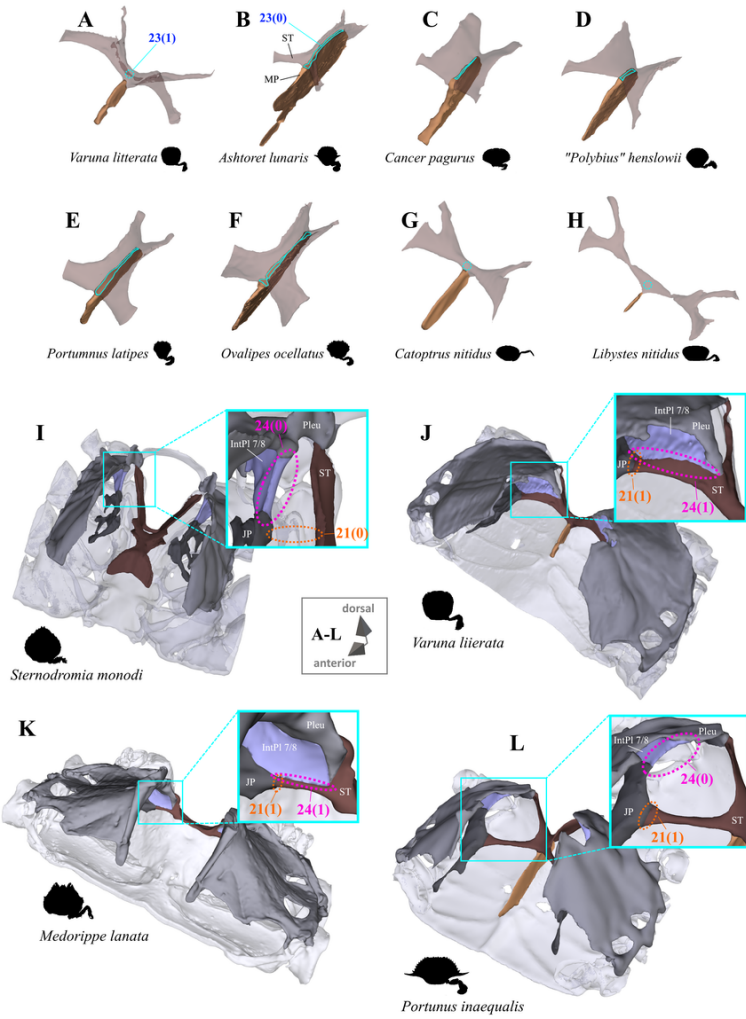


Figure 18

Variability in the shape of the sella turcica and in its connection to interpleurite 7/8 and the junction plate. **A-H** Examples showing character states concerning the covering of dorsal median plate margin by the sella turcica (character 23). **I-L** Examples showing character states concerning the presence or absence of a connection of the junction plate to the sella turcica (character 21) and character states concerning the degree of connection of interosternite 7/8 to the sella turcica (character 24). **IntPI 7/8** Interpleurite between thoracomeres 7 and 8. **JP** Junction plate. **MP** Median plate. **Pleu** Pleurum. **ST** Sella turcica.

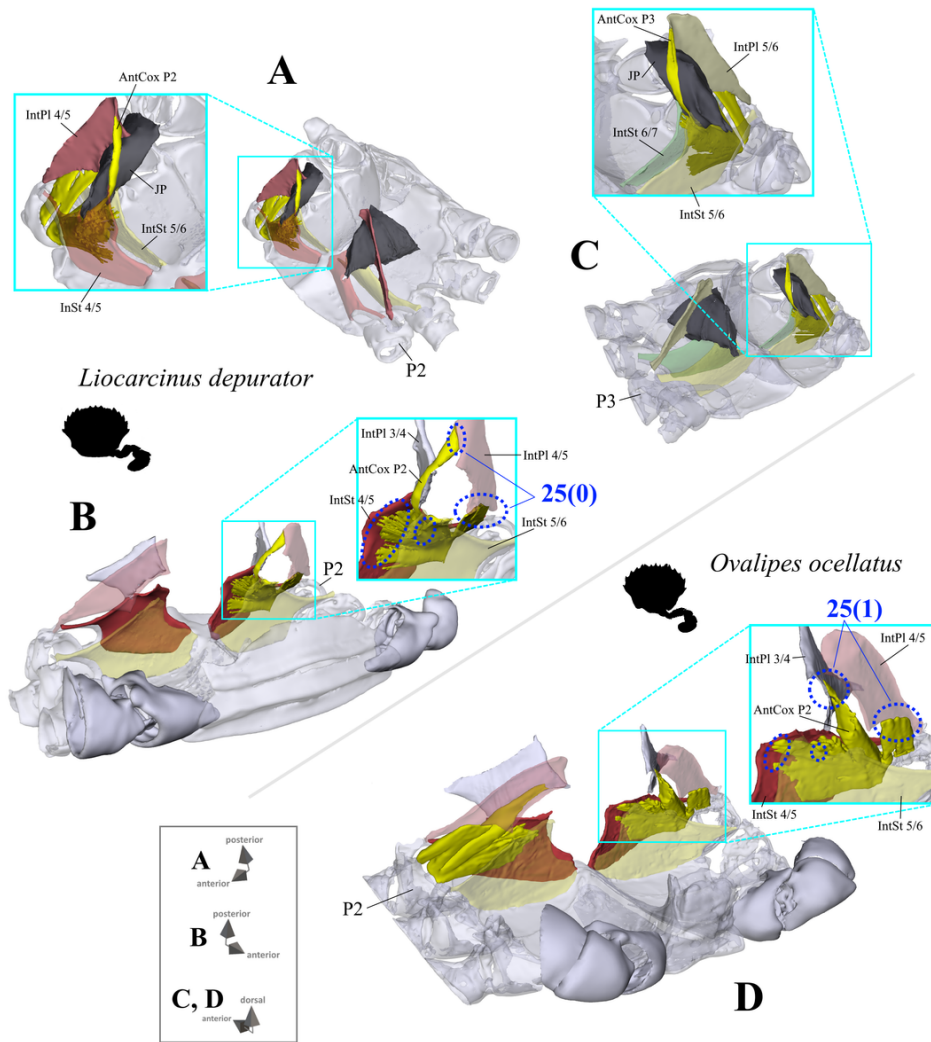


Figure 19

Examples showing character states concerning the origin of 2nd pereopod anterior coxa muscle (character 25; **A, B, D**) as well as the shape of 3rd pereopod anterior coxa muscle (**C**) in axial skeletons seen from different perspectives. Note that for example in *Liocarcinus depurator*, both muscles have a branch running along, but not attaching at the medial side of the junction plate and originating at interpleurite 4/5 and 5/6, respectively (**A, C**). **AntCox P2** 2nd pereopod anterior coxa muscle. **AntCox P3** 3rd pereopod anterior coxa muscle. **IntPl** Interpleurite (with pair of numbers indicating between which thoracomeres it is situated) **IntSt** Interosternite (with pair of numbers indicating between which thoracomeres it is situated) **JP** Junction plate. **MP** Median plate. **P2** proximal 2nd pereopod podomeres **P3** proximal 3rd pereopod podomeres. **ST** Sella turcica.

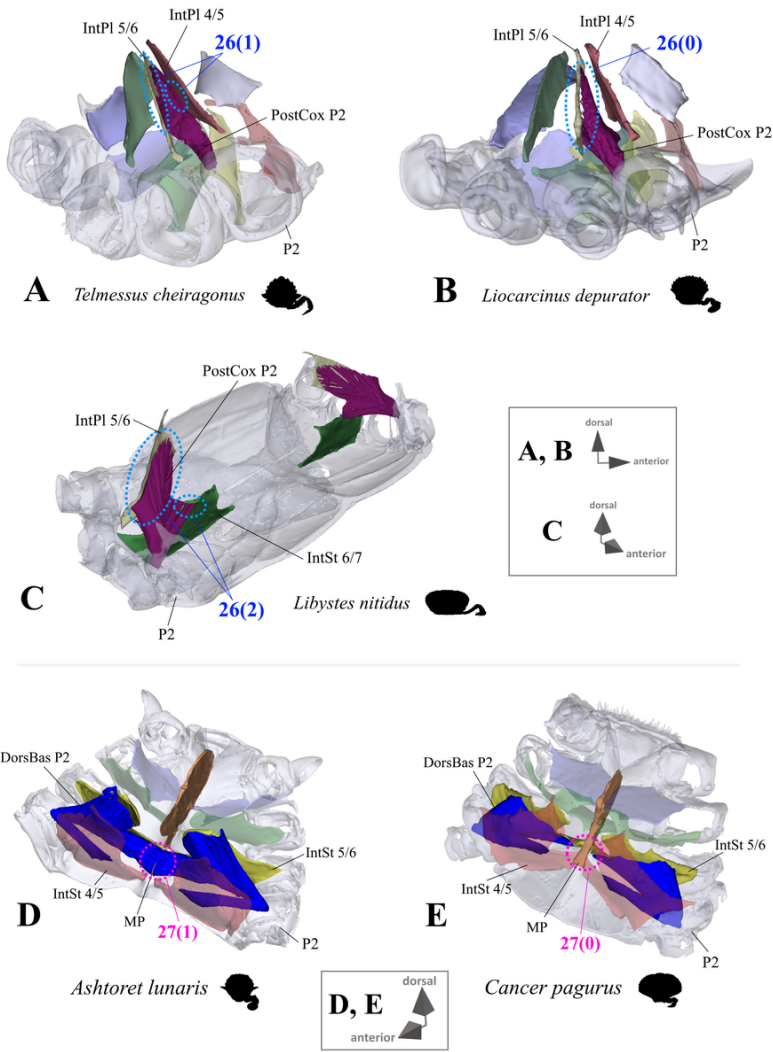


Figure 20

Examples showing character states concerning the origin of 2nd pereopod posterior coxa muscle (character 26; **A-C**) and 2nd pereopod dorsal basi-ischium muscle (character 27; **D, E**). **DorsBas P2** 2nd pereopod dorsal basi-ischium muscle. **IntPl** Interpleurite (with pair of numbers indicating between which thoracomeres it is situated). **IntSt** Interosternite (with pair of numbers indicating between which thoracomeres it is situated). **MP** Median plate. **P2** proximal 2nd pereopod podomeres. **PostCox P2** 2nd pereopod posterior coxa muscle. **ST** Sella turcica.

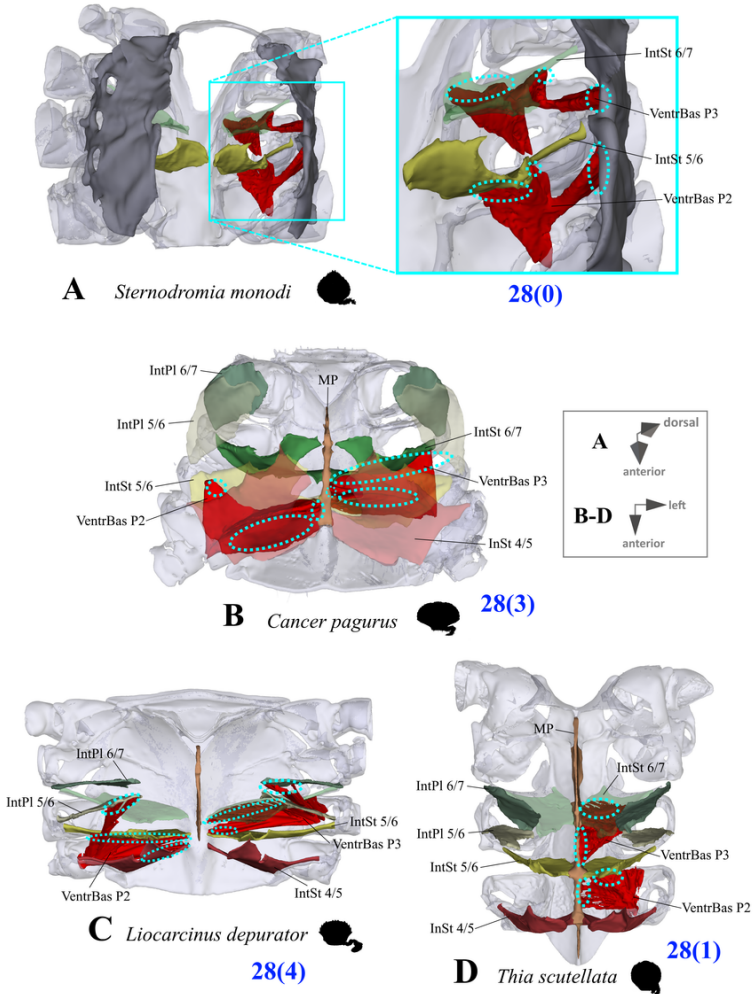


Figure 21

Examples showing character states concerning the origin of 2nd pereopod and 3rd pereopod ventral basi-ischium muscles (character 28) in axial skeletons seen from different perspectives. **IntPl** Interpleurite (with pair of numbers indicating between which thoracomeres it is situated). **IntSt** Interosternite (with pair of numbers indicating between which thoracomeres it is situated). **MP** Median plate. **VentrBas P2** 2nd pereopod ventral basi-ischium muscles. **VentrBas P3** 3rd pereopod ventral basi-ischium muscles.

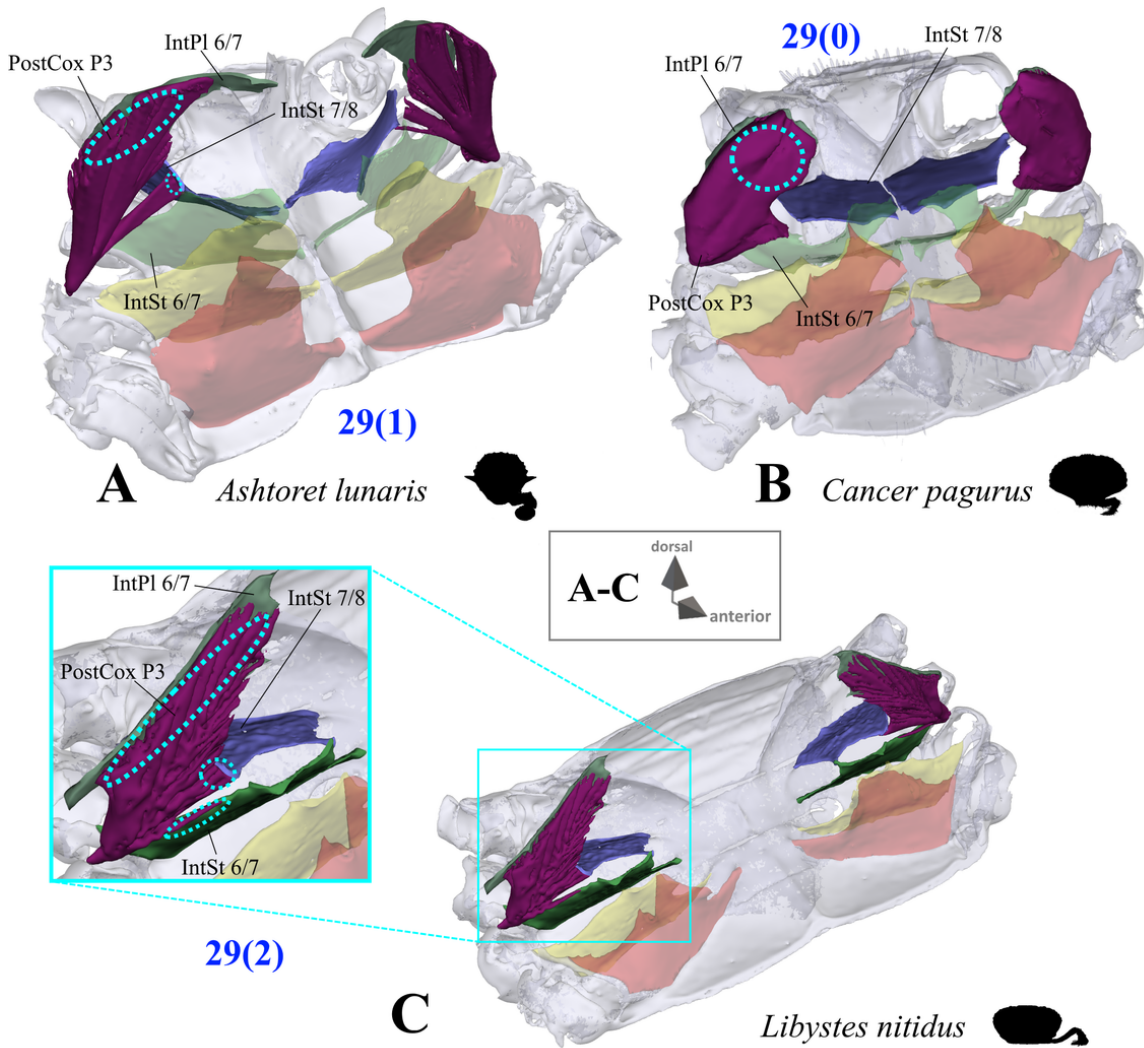


Figure 22

Examples showing character states concerning the origin of 3rd pereopod posterior coxa muscle (character 29) in axial skeletons seen antero-dorsal. **IntPl 6/7** Interpleurite between thoracomeres 6 and 7. **IntSt** Interosternite (with pair of numbers indicating between which thoracomeres it is situated). **PostCox P3** 3rd pereopod posterior coxa muscle.

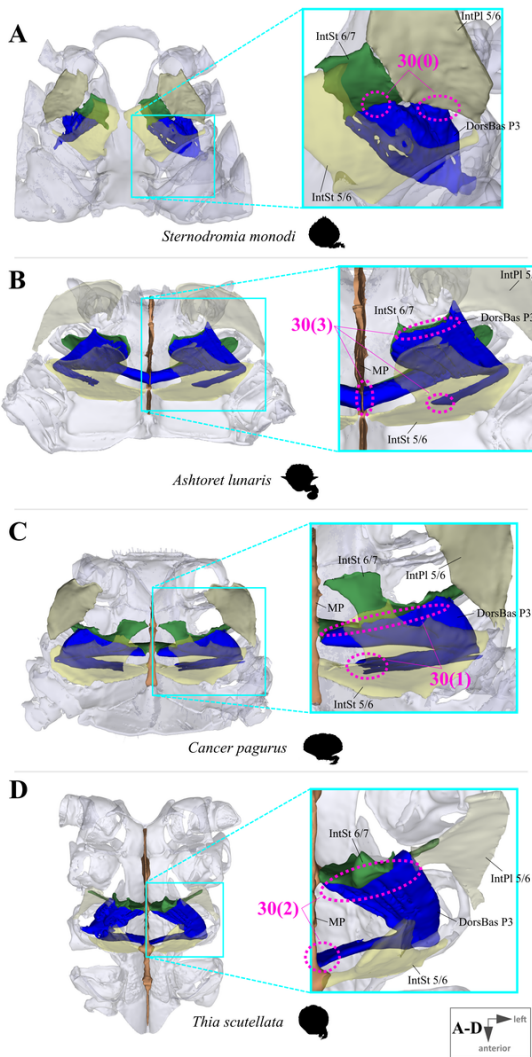


Figure 23

Examples showing character states concerning the origin of 3rd pereopod dorsal basi-ischium muscle (character 30). **DorsBas P3** 3rd pereopod dorsal basi-ischium muscle. **IntPI 6/7** Interpleurite between thoracomeres 6 and 7. **IntSt** Interosternite (with pair of numbers indicating between which thoracomeres it is situated). **MP** Median plate.

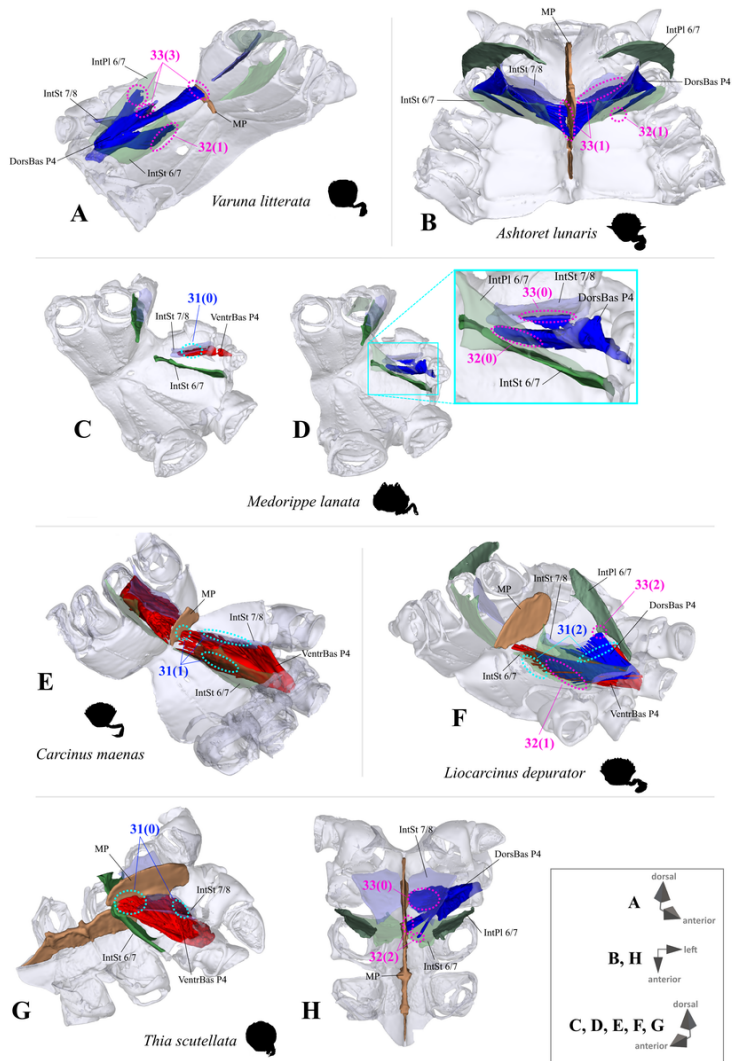


Figure 24

Examples showing character states concerning the origin of 4th pereiopod dorsal and ventral basi-ischium muscle (character 28) in axial skeletons seen from different perspectives. **DorsBas P4** 4th pereiopod ventral basi-ischium muscles. **IntPI 6/7** Interopleurite between thoracomeres 6 and 7. **IntSt** Interosternite (with pair of numbers indicating between which thoracomeres it is situated). **MP** Median plate. **VentrBas P4** 4th pereiopod ventral basi-ischium muscles.

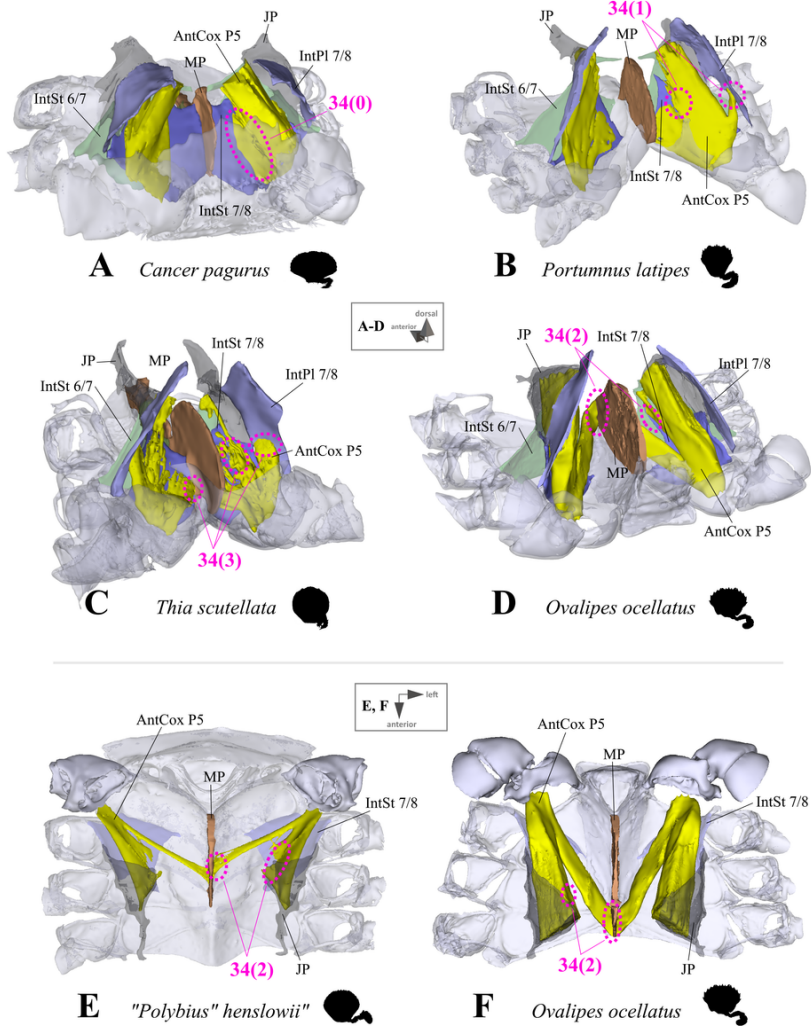


Figure 25

Examples showing character states concerning the origin of 2nd pereopod anterior coxa muscle (character 34) in axial skeletons seen from posterior-dorsal (A-D) and from dorsal (E, F). Note that in the P5-swimmers (E, F), long muscle fibres originate at the median plate, and that there are also shorter fibres originating at the median plate in *Thia* (C). **AntCox P5** 5th pereopod anterior coxa muscle. **IntPI 7/8** Interpleurite between thoracomeres 7 and 8. **IntSt** Interosternite (with pair of numbers indicating between which thoracomeres it is situated) **JP** Junction plate. **MP** Median plate.

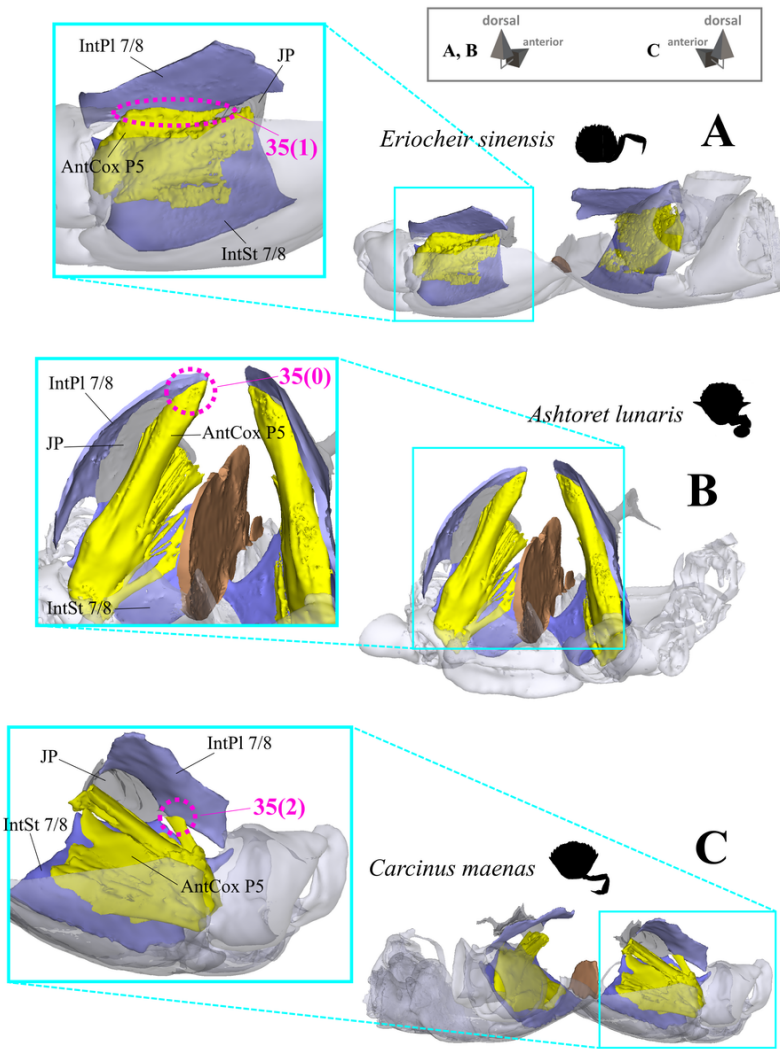


Figure 26

Examples showing character states concerning the position of the origin of the 5th pereopod anterior coxa muscle origin (character 35) in axial skeletons seen from different perspectives. **AntCox P5** 5th pereopod anterior coxa muscle. **IntPl 7/8** Interpleurite between thoracomeres 7 and 8. **IntSt 7/8** Interosternite between thoracomeres 7 and 8. **JP** Junction plate.

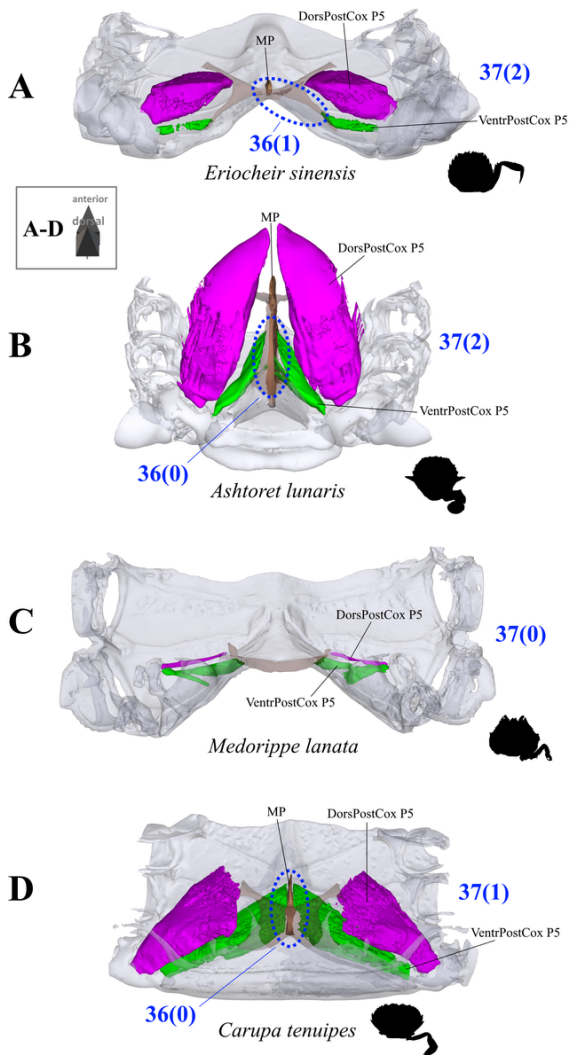


Figure 27

Examples showing character states concerning the origin of 5th pereiopod ventral posterior coxa muscle (character 36) and the relative volume of the of 5th pereiopod dorsal compared to ventral posterior coxa muscle in axial skeletons seen from postero-dorsal. **DorsPostCox P5** 5th pereiopod dorsal posterior coxa muscle. **MP** Median plate. **VentrPostCox P5** 5th pereiopod ventral posterior coxa muscle.

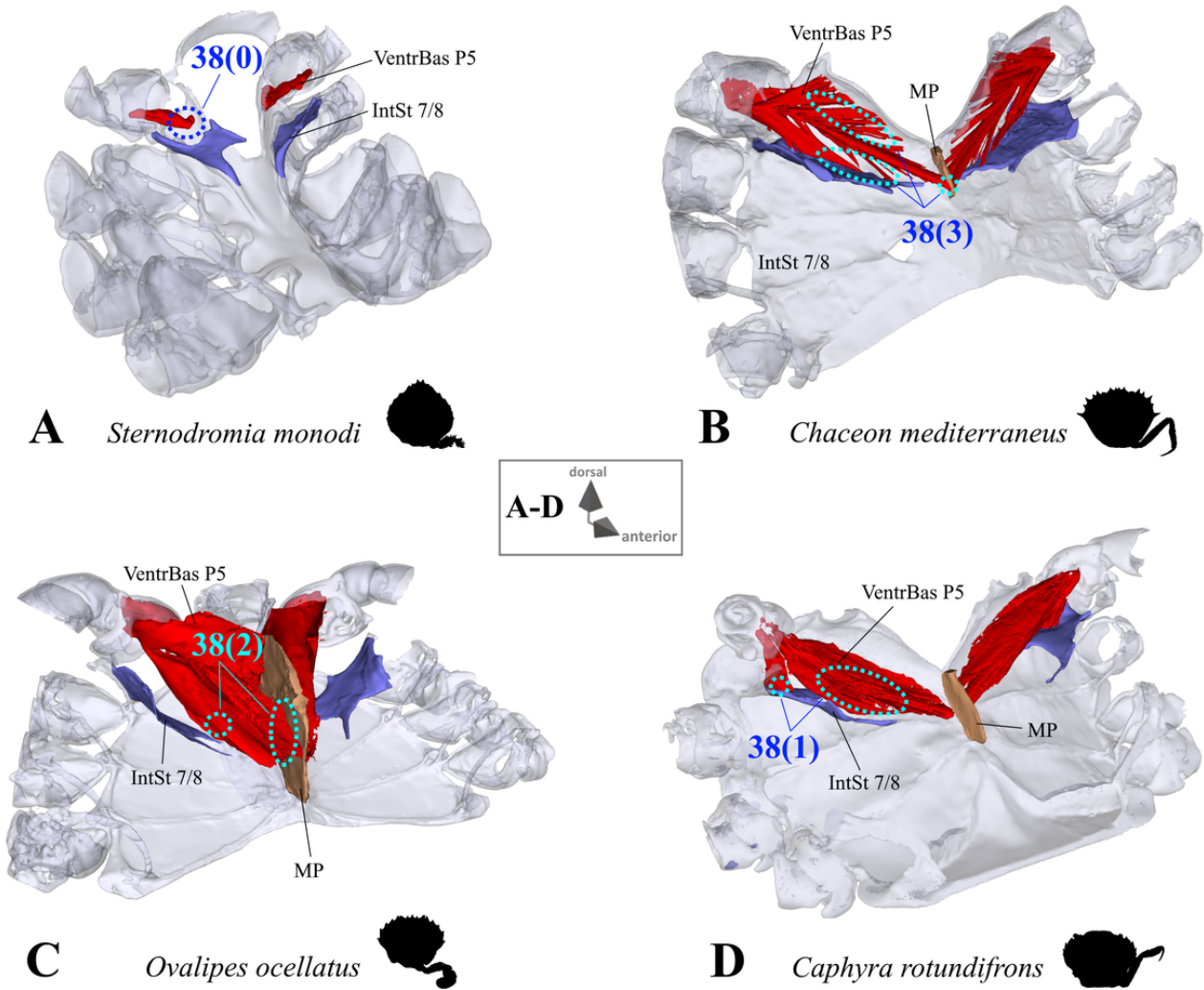


Figure 28

Examples showing character states concerning the origin of 5th pereiopod ventral basi-ischium muscle (character 38) in axial skeletons seen from antero-dorsal. **IntSt 7/8** Interosternite between thoracomeres 7 and 8. **MP** Median plate. **VentrBas P5** 5th pereiopod ventral basi-ischium muscle.

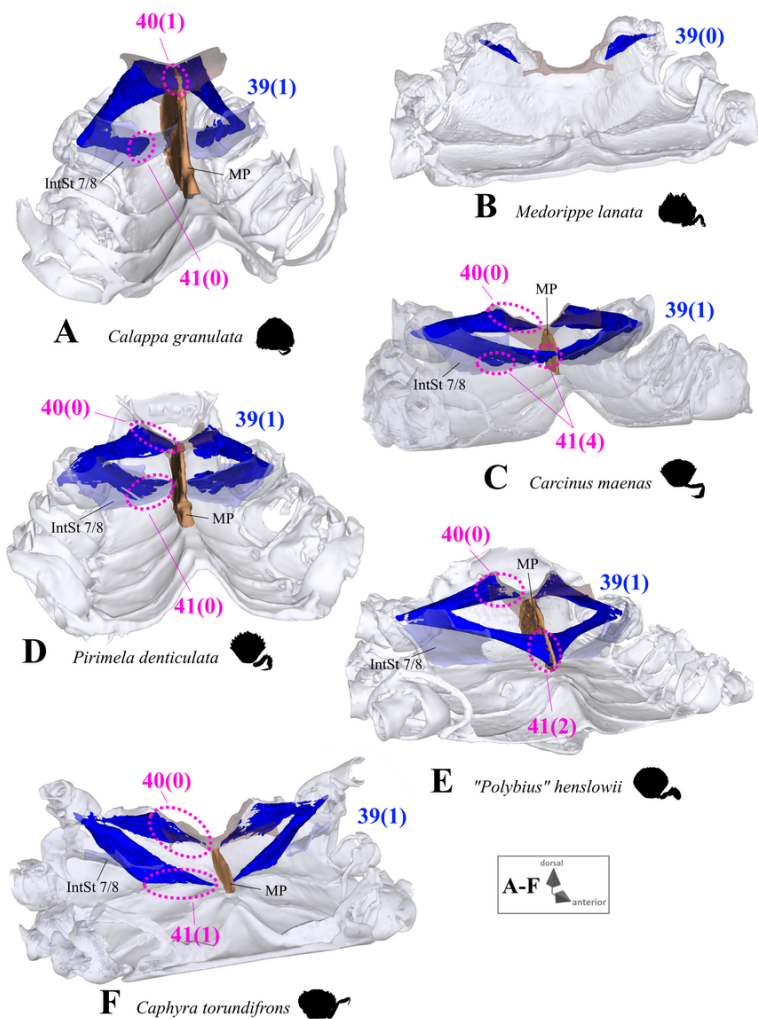


Figure 29

Examples showing character states concerning the configuration of 5th pereopod ventral basi-ischium muscle (character 39), as well as the origin of its dorsal (character 40) and ventral (character 41) branch (if present) in axial skeletons seen from antero-dorsal. **DorsalBas P5** 5th pereopod dorsal basi-ischium muscle. **IntSt 7/8** Interosternite between thoracomeres 7 and 8. **MP** Median plate.

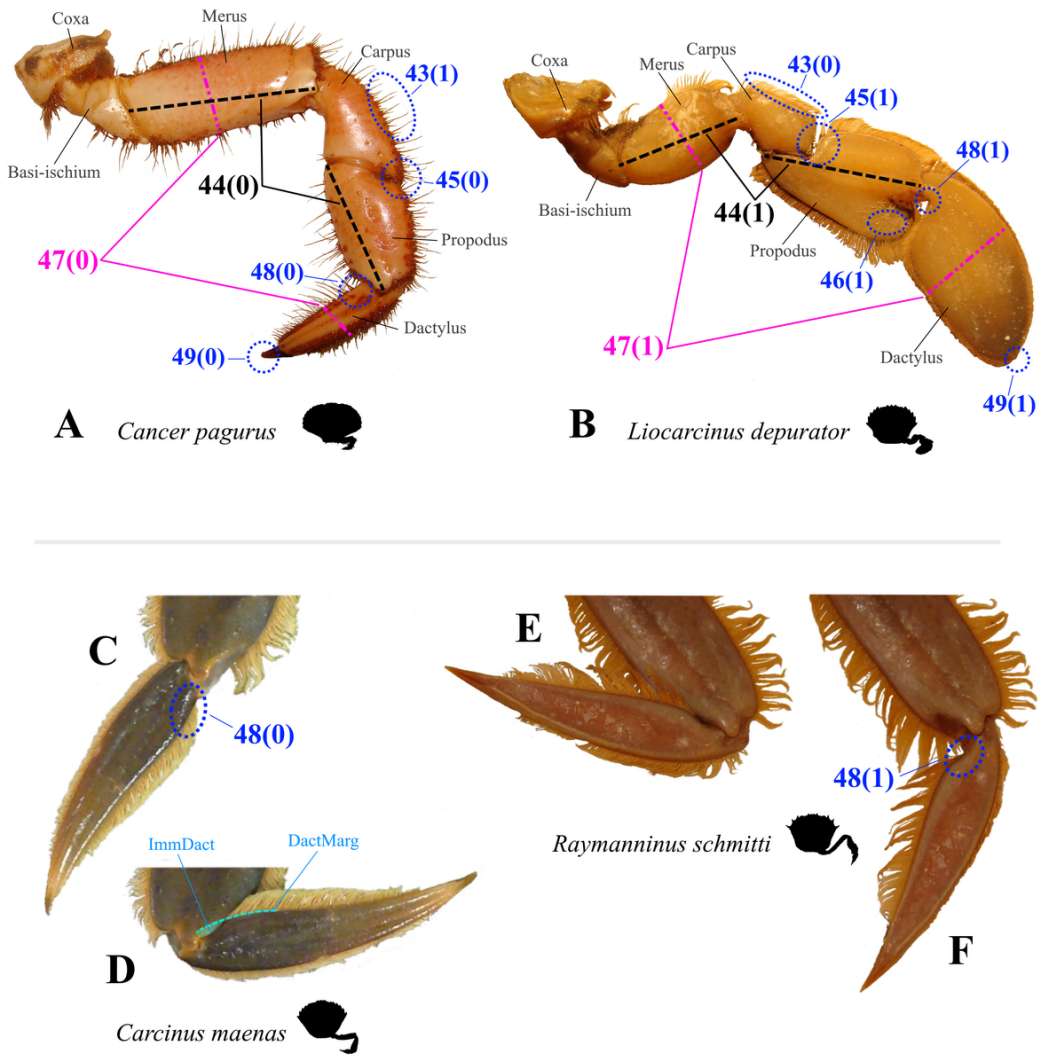


Figure 30

Examples showing character states concerning 5th pereiopod's exterior. **A, B** Comparison of the 5th pereiopod having the shape of a walking leg (**A**) and swimming leg (**B**). Note that character state 43(1) concerning arrangement of long setae shown here are not necessarily typical for a walking leg, and those concerning merus length (44(1)) and shape of the dactylus tip (49(1)) are not necessarily typical for a swimming leg (see also Fig. 34 and 35). **C-F** Examples showing character states concerning 5th pereiopod proximo-ventral dactylus margin shape (character 48). Note that when the dactylus is adducted (**D, E**), in a convex (or straight) proximo-ventral dactylus margin (**C**), it is partly immersed in propodus arthroal cavity (**D**), while it is not immersed (**E**) if proximo-ventral dactylus margin is concave (**F**). **DactMarg** Proximo-ventral dactylus margin. **ImmDact** Area of the dactylus that is immersed in propodus arthroal cavity when dactylus is adducted.

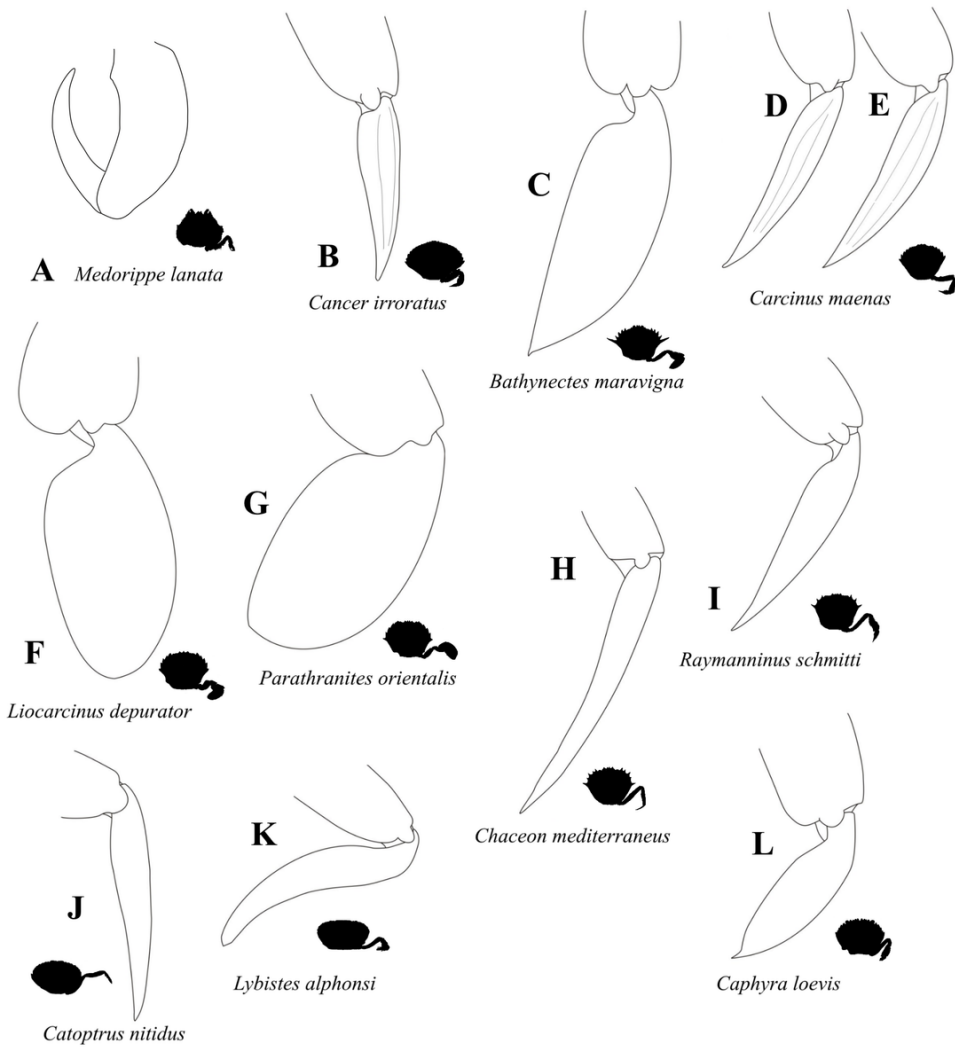
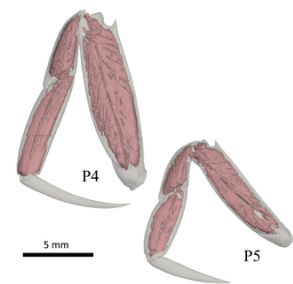
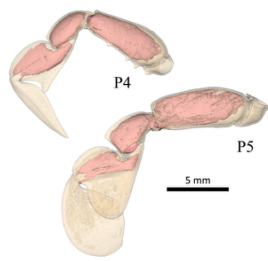


Figure 31

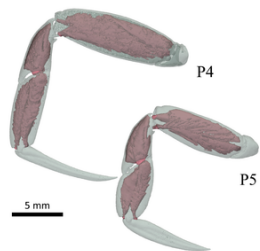
Drawings showing the variability in the shape of the right 5th pereiopod dactylus.



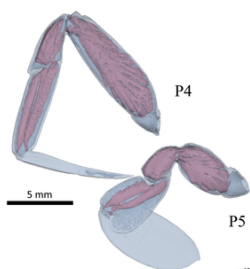
A *Eriocheir sinensis*



B *Ashtoret lunaris*



C *Carcinus maenas*



D *Liocarcinus depurator*



E *Portunus latipes*

Figure 32

Representations of three-dimensional (3D) data showing the variability in the shape of the left 4th (P4) and 5th (P5) pereiopod and its intrinsic musculature. Representations of three-dimensional (3D) data showing the variability in the shape of the left 4th (P4) and 5th (P5) pereiopod and its intrinsic musculature.

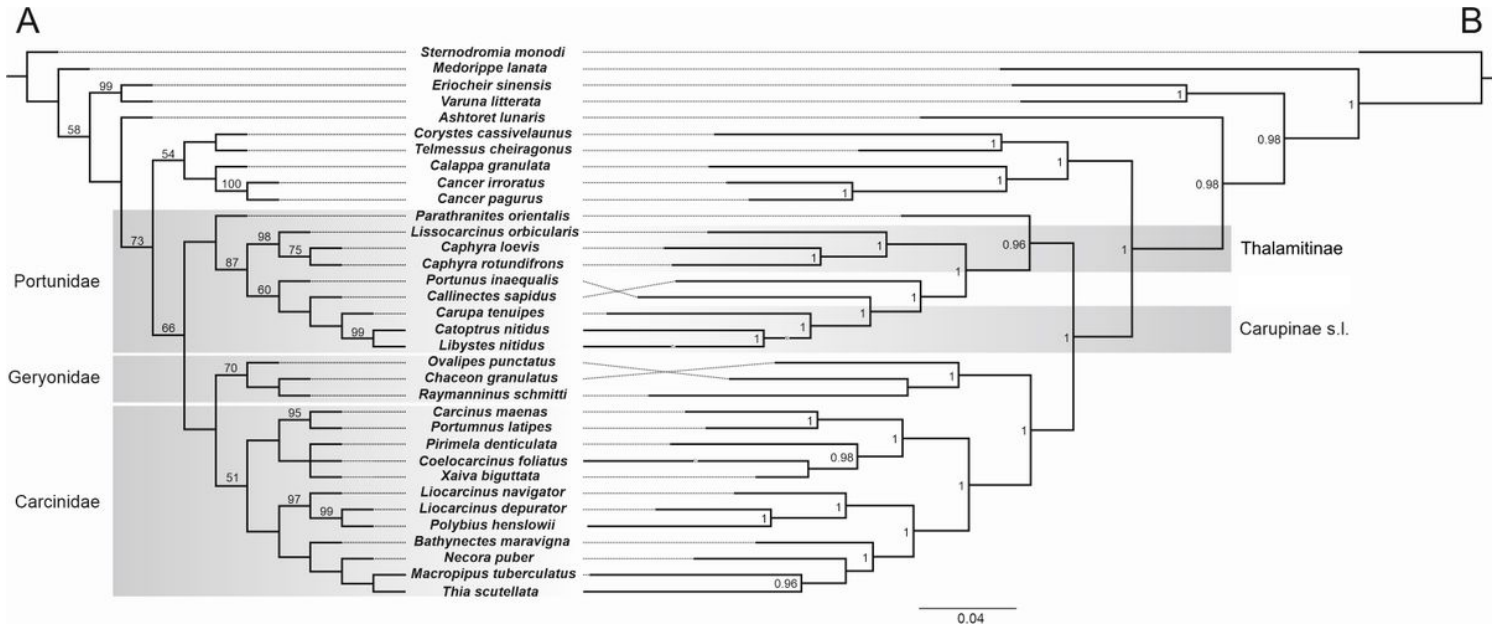


Figure 33

Phylograms of the combined data set of the 34 OTUs with higher classification and *Sternodromia monodi* set as outgroup. **A** Maximum Parsimony (MP) phylogram calculated with TNT 1.5; strict consensus of the two most parsimonious trees; tree length: 6029; Bootstrap values over 50 (1000 Bootstrap replicates) are shown on the respective branch. **B** Bayesian inference (BI) phylogram calculated with MrBayes 3.2.7a; posterior probabilities >0.95 are shown for the respective branches.

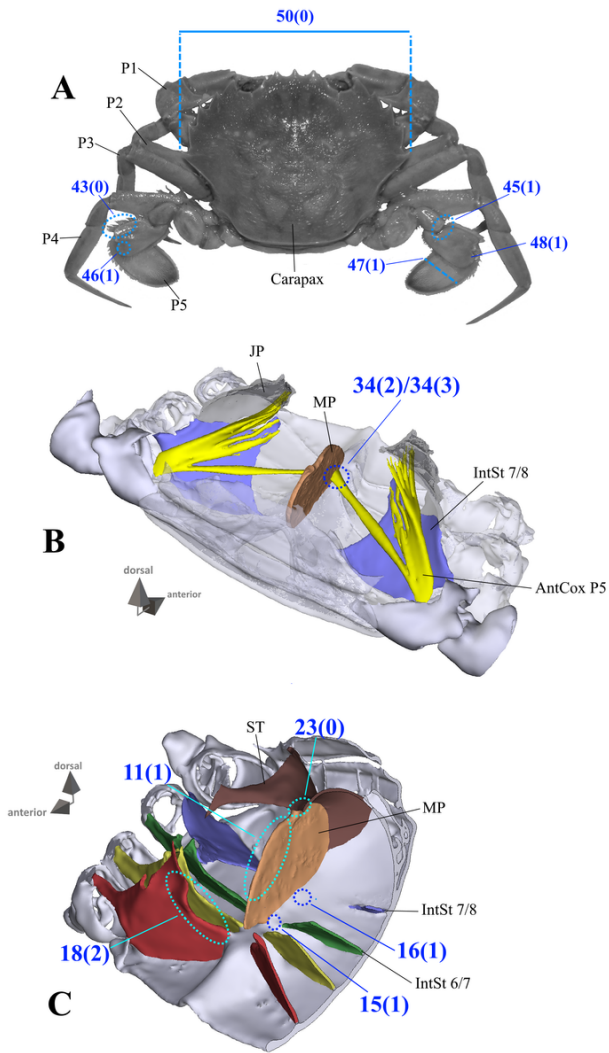


Figure 34

Character states that were found in all examined P5-swimming crabs, exemplified by *Liocarcinus depurator*. **A** Dorsal view of whole body. **B** Anterior view of three-dimensional (3D) data representation showing axial skeleton. **C** Antero-lateral view of three-dimensional (3D) data representation showing axial skeleton. **AntCox P5** 5th pereiopod anterior coxa muscle. **IntPl 6/7** Interpleurite between thoracomeres 6 and 7. **IntSt** Interosternite (with pair of numbers indicating between which thoracomeres it is situated). **MP** Median plate.

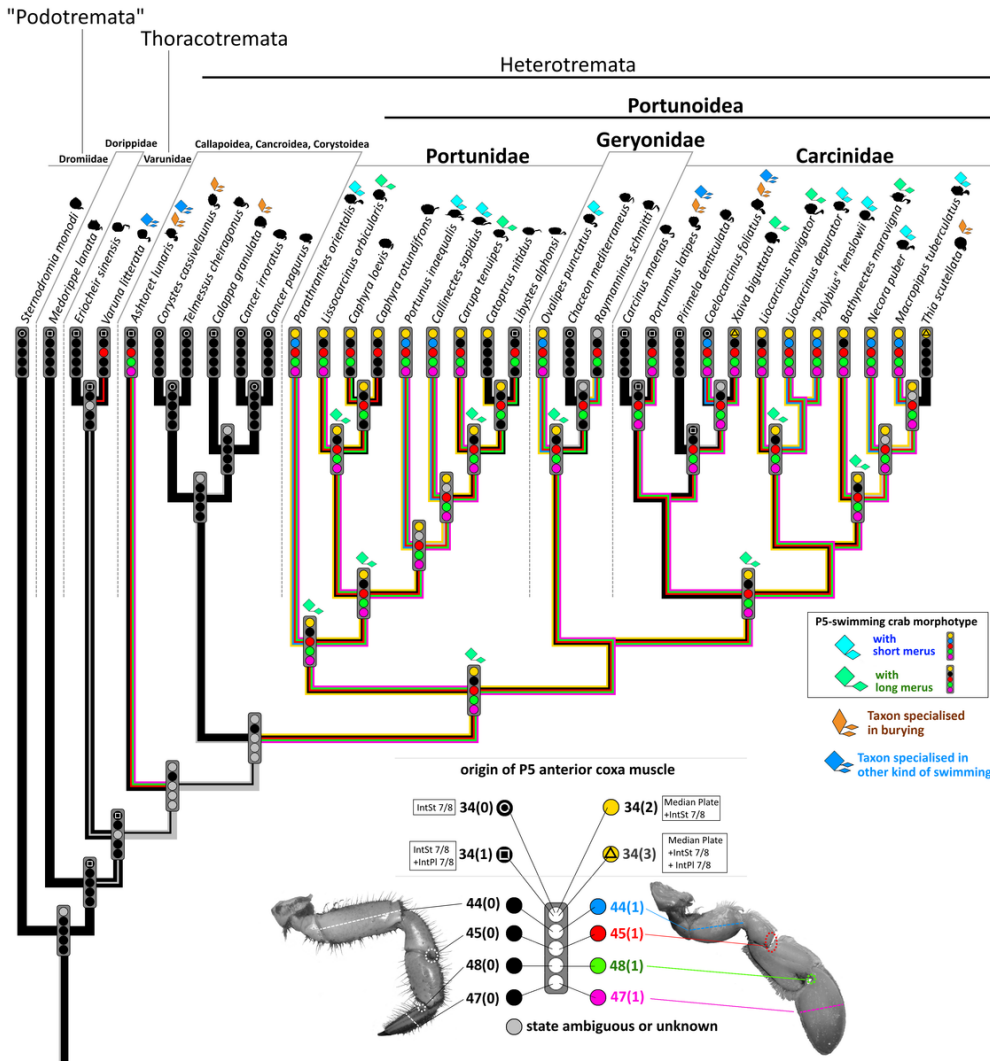


Figure 35

Character states and ancestral state reconstructions of states that unambiguously show if a taxon is a P5-swimming crab. Character state combinations of each extant species and several ancestral stem species are indicated by dots in a colour palette, with a distinct dot position representing a character and a distinct colour (sometimes with symbol) in each dot position representing a state. Note that symbols indicate if an extant species or reconstructed stem species is assigned to the P5-swimming crab morphotype or if it is considered as being specialised in burying and/or swimming that is different from P5-swimming.

Supplementary Files

This is a list of supplementary files associated with this preprint. Click to download.

- [Ashtoretlunaris3Dmodel.pdf](#)
- [Bathynectesmaravigna3Dmodel.pdf](#)
- [Calappagranulata3Dmodel.pdf](#)
- [Cancerirroratus3Dmodel.pdf](#)
- [Cancerpagurus3Dmodel.pdf](#)
- [Caphyarotundifrons3Dmodel.pdf](#)
- [Carcinusmaenas3Dmodel.pdf](#)
- [Carapatenuipes3Dmodel.pdf](#)
- [Catoptrusnitidus3Dmodel.pdf](#)
- [Chaceonmediterraneus3Dmodel.pdf](#)

- Charactermatrix.xlsx
- Coelocarcinusfoliatus3Dmodel.pdf
- Corystescassivelaunus3Dmodel.pdf
- Eriocheirsinensis3Dmodel.pdf
- FigureA1.png
- FigureA2.png
- FigureA3.png
- FigureA4.png
- FigureA5.png
- FigureA6.png
- FigureA7.png
- Libystesalphonsi3Dmodel.pdf
- Liocarcinusdepurator3Dmodel.pdf
- Medorippelanata3Dmodel.pdf
- M
- Pirimeladenticulata3Dmodel.pdf
- Polybiushenslowii3Dmodel.pdf
- Portumnuslatipes3Dmodel.pdf
- Portunusinaequalis3Dmodel.pdf
- Sternodromiamonodi3Dmodel.pdf
- Telmessuscheiragonus3Dmodel.pdf
- Thiascutellata3Dmodel.pdf
- Varunalitterata3Dmodel.pdf
- Video1Liocarcinusdepurator1000FPS.mp4
- Video2Liocarcinusdepurator1000FPS.avi
- Video3Liocarcinuspusillus1000FPS.mp4
- Xaivabiguttata3Dmodel.pdf